ENERGY MANAGEMENT STRATEGIES FOR HYBRID ELECTRIC VEHICLES WITH HYBRID POWERTRAIN SPECIFIC ENGINES

ENERGY MANAGEMENT STRATEGIES FOR HYBRID ELECTRIC VEHICLES WITH HYBRID POWERTRAIN SPECIFIC ENGINES

BY

YUE WANG, M.Sc., B.Sc.

A THESIS

SUBMITTED TO THE DEPARTMENT OF MECHANICAL ENGINEERING

AND THE SCHOOL OF GRADUATE STUDIES

OF MCMASTER UNIVERSITY

IN PARTIAL FULFILMENT OF THE REQUIREMENTS

FOR THE DEGREE OF

DOCTOR OF PHILOSOPHY

Doctor of Philosophy (2022) McMaster University

(Mechanical Engineering) Hamilton, Ontario, Canada

TITLE:	Energy Management Strategies for Hybrid Electric Vehicles with Hybrid Powertrain Specific Engines
AUTHOR:	Yue Wang M.Sc. Mechanical Engineering Tianjin University, Tianjin, China
SUPERVISOR:	Professor Ali Emadi Professor Zahra Keshavarz-Motamed
NUMBER OF PAGES:	xxiv, 218

Abstract

Energy-efficient powertrain components and advanced vehicle control strategies are two effective methods to promote the potential of hybrid electric vehicles (HEVs). Aiming at hybrid system efficiency improvement, this thesis presents a comprehensive review of energy-efficient hybrid powertrain specific engines and proposes three improved energy management strategies (EMSs), from a basic non-adaptive real-time approach to a state-of-the-art learning-based intelligent approach.

To evaluate the potential of energy-efficient powertrain components in HEV efficiency improvement, a detailed discussion of hybrid powertrain specific engines is presented. Four technological solutions, i.e., over-expansion cycle, low temperature combustion mode, alternative fuels, and waste heat recovery techniques, are reviewed thoroughly and explicitly. Benefits and challenges of each application are identified, followed by specific recommendations for future work. Opportunities to simplify hybrid-optimized engines based on cost-effective trade-offs are also investigated.

To improve the practicality of HEV EMS, a real-time equivalent consumption minimization strategy (ECMS)-based HEV control scheme is proposed by incorporating

powertrain inertial dynamics. Compared to the baseline ECMS without such considerations, the proposed control strategy improves the vehicle drivability and provides a more accurate prediction of fuel economy. As an improvement of the baseline ECMS, the proposed dynamic ECMS offers a more convincing and better optimal solution for practical HEV control.

To address the online implementation difficulty faced by ECMS due to the equivalence factor (EF) tuning, a predictive adaptive ECMS (A-ECMS) with online EF calculation and instantaneous power distribution is proposed. With a real-time self-updating EF profile, control dependency on drive cycles is reduced, and the requirement for manual tuning is also eliminated. The proposed A-ECMS exhibits great charge sustaining capabilities on all studied drive cycles with only slight increases in fuel consumption compared to the basic non-adaptive ECMS, presenting great improvement in real-time applicability and adaptability.

To take advantage of machine learning techniques for HEV EMS improvement, a deep reinforcement learning (DRL)-based intelligent EMS featuring the state-of-the-art asynchronous advantage actor-critic (A3C) algorithm is proposed. After introducing the fundamentals of reinforcement learning, formulation of the A3C-based EMS is explained in detail. The proposed algorithm is trained successfully with reasonable convergence. Training results indicate the great learning ability of the proposed strategy with excellent charge sustenance and good fuel optimality. A generalization test is also conducted to test its adaptability, and results are compared with an A-ECMS. By showing better charge sustaining performance and fuel economy, the proposed A3C-based EMS proves its potential in real-time HEV control.

To the memory of my grandpa

Zhenguo Guan

Acknowledgements

Foremost, I would like to express my deepest gratitude to my supervisors, Prof. Ali Emadi and Prof. Zahra Keshavarz-Motamed, for their constant guidance and support throughout my time at McMaster. The completion of this thesis could not have been accomplished without their supervision. The enthusiasm, dedication, patience, and wisdom I see in them have inspired me in not only my research but also my life.

I would like to extend my sincere thanks to my supervisory committee, Prof. Saeid Habibi and Prof. Fengjun Yan, for their invaluable advice and guidance at every stage of my research.

My special thanks go to Dr. Atriya Biswas, who has been a great research partner and an amazing friend. Many thanks to Dr. Jianbin Liang, who has always been willing and enthusiastic to help in any way he could. I am grateful to have the pleasure of working with the electrified powertrain team: Joel Roeleveld, Lucas Bruck, Dr. Pier Giuseppe Anselma, Aashit Rathore, Adam Lempert, Jack Toller, Fabricio Machado, and Saeed Amirfarhangi Bonab. I would also like to thank all my colleagues and friends at McMaster Automotive Resource Centre (MARC) for their friendship and assistance.

It is impossible to express enough thanks to my parents for their unconditional love and support over the years. My heartfelt thanks go to my grandparents for their unwavering belief in me. Finally, my endless gratitude to Jiandong Sun, FSA, FCIA, who is always by my side through the good times and the bad.

This research was undertaken, in part, thanks to funding from the Canada Research Chair in Transportation Electrification and Smart Mobility and the Natural Sciences and Engineering Research Council of Canada (NSERC).

Contents

List of Figures

List of Tables

Nomenclature

Abbreviations

A3C	Asynchronous advantage actor-critic
A-ECMS	Adaptive equivalent consumption minimization strategy
AF	Alternative fueled
AI	Artificial intelligence
APU	Auxiliary power unit
BEV	Battery electric vehicle
BSFC	Brake specific fuel consumption
CI	Compression ignition
CS	Charge sustaining
DL	Deep learning
DOF	Degrees of freedom

DP	Dynamic programming
DRL	Deep reinforcement learning
ECMS	Equivalent consumption minimization strategy
EF	Equivalence factor
EM	Electric motor
EMS	Energy management strategy
EV	Electric vehicle
HCCI	Homogeneous charge compression ignition
HEV	Hybrid electric vehicle
HIL	Hardware-in-the-loop
HWFET	Highway Fuel Economy Test
ICE	Internal combustion engine
ICEV	Internal combustion engine vehicle
LHV	Lower heating value
LIVC	Late intake valve closing
LTC	Low temperature combustion
ML	Machine learning
MVEM	Mean value engine model

NEDC	New European Driving Cycle
ORC	Organic Rankine cycle
PCCI	Premixed charge compression ignition
PG	Planetary gear
PHEV	Plug-in hybrid electric vehicle
RCCI	Reactivity-controlled compression ignition
REEV	Range-extended electric vehicle
RL	Reinforcement learning
SI	Spark ignition
SIL	Software-in-the-loop
SOC	State-of-charge
TEG	Thermoelectric generator
UDDS	Urban Dynamometer Driving Schedule
VVT	Variable valve timing
WHR	Waste heat recovery
WLTP	Worldwide Harmonized Light Vehicles Test Procedure

Symbols

acc_{veh}	Vehicle acceleration
$\alpha_{\text{EV\_HEV}}$	Penalty from EV to HEV mode
$\alpha_{\text{HEV\_EV}}$	Penalty from HEV to EV mode
α_{μ}	Learning rate for critic network
α_{θ}	Learning rate for actor network
β	Gear ratio of Ring/Sun
fd	Final drive ratio
Γ	A large weighting factor
γ	Discount factor
η	Coulombic efficiency of battery
η_{ICE}	Efficiency of engine
η_m	Efficiency of electric motors
I_{batt}	Battery current
J	Mass moment of inertia
LHV_{fuel}	Lower heating value of fuel
λ	Equivalence factor

m_{equiv}	Equivalent mass of vehicle
$\dot{m}_{fuel}$	Fuel mass flow rate
μ_1,μ_2,μ_3	Road load coefficients
ω	Rotational speed
P_{APU}	APU power
P_{batt}	Battery power
$P_{elec,m}$	Motor electrical power
P_{ICE}	Engine power
Q_{batt}	Battery capacity
R	Battery internal resistance
R_{wh}	Wheel radius
SOC_{ref}	Battery SOC reference
T	Torque
$\ddot{\theta}$	Rotational acceleration
V_{oc}	Battery open circuit voltage
V_t	Battery terminal voltage
v_{veh}	Vehicle speed

Chapter 1

Introduction

1.1 Motivation

The gradual decline of global fossil resources and severe greenhouse gas emission issues have brought significant challenges such as increasing fuel prices and stringent emission regulations faced by public and automotive manufacturers [1]. According to the International Energy Agency, extending recent trends in energy use to 2050 yields 70% and 60% growth in global energy demand and emissions, respectively, compared to 2011 [2]. In response to the growing public concern over the environment and people's livelihoods attributed to the transportation sector, scientific groups and industries have exerted great effort in seeking renewable and efficient solutions to replace conventional petroleum-based vehicles [3].

Recent research activities and projects have proven powertrain electrification a promising long-term solution, and technological advancements have promoted the development and popularization of electrified vehicles [4]. Ever since the emergence of electrified vehicles, the automotive industry has witnessed remarkable improvements in fuel economy and emission reductions [5].

Electric vehicles (EVs) and hybrid electric vehicles (HEVs), which are no or less dependent on fossil fuels, respectively, are the two variants of electrified vehicles. EVs with higher energy efficiency and zero tailpipe emissions are considered the foreseeable future of the automobile industry. However, issues associated with safety, cost, durability, and range anxiety concerns are the biggest challenge for their market penetration and expansion [6]. As another major portion of electrified vehicles, HEVs have attracted wide research attention around the globe.

With less energy consumption, lower emissions, and higher mileage, HEVs present a midterm solution by combining the benefits of internal combustion engine vehicles (ICEVs) and EVs [7]. Compared to ICEVs, HEVs provide more flexibility in engine operation by introducing an additional propulsion system. In addition to an engine, a typical hybrid electric powertrain also includes an energy storage system and one/more electric motors (EMs) [8]. The multiple energy sources of HEVs allow various available patterns of power flow to meet vehicle load requirements through different powertrain topologies [9].

Although HEVs present higher fuel efficiency and lower emissions than conventional vehicles, further performance improvements are still demanded. Energy-efficient powertrain components are a feasible approach to further explore the potential of HEV systems. Along with the development of HEVs, engines as a crucial power source have been continually evolving over the years [10–12]. Researchers have been creating, evaluating, and choosing new technological solutions for engines to apply to HEVs. The combination of energy-efficient engines with the hybrid-electric concept has been proven as an effective way to improve vehicle performance [13].

Apart from powertrain components, the ability of HEV to maximize its overall hybrid system efficiency is also indelibly associated with the vehicle energy management strategy (EMS) [14]. Therefore, developing dedicated and efficient EMSs is another promising method to further exploit the potential of HEVs.

On this account, this thesis aims to investigate enhanced hybrid electric vehicles through the pursuit of energy-efficient engines and improved energy management strategies.

1.2 Contributions

The thesis has several original contributions, which can be summarized as follows:

(1) A comprehensive review of hybrid powertrain specific engines is provided. Current research status is identified, and the viewpoints from discussions provide insights on future research opportunities.

(2) An improved equivalent consumption minimization strategy (ECMS) incorporating powertrain inertial dynamics is proposed. With the proposed strategy, vehicle drivability can be improved, a more accurate prediction of fuel economy can be made for real-world driving tasks, and novel hybrid powertrain configurations can be evaluated more realistically and critically. The proposed methodology can be extended to other optimal control strategies and powertrain configurations.

(3) A predictive adaptive equivalent consumption minimization strategy (A-ECMS) with online equivalence factor (EF) calculation and instantaneous power splitting is proposed to improve the real-time applicability of HEV EMS. With a real-time self-updating EF profile, the control dependency of HEV EMS on drive cycles is reduced, and the need for manual tuning of the EF is eliminated. The proposed A-ECMS can be implemented on various hybrid architectures.

(4) A deep reinforcement learning (DRL)-based EMS featuring state-of-the-art asynchronous advantage actor-critic (A3C) algorithm is developed to further improve the intelligence and real-time capabilities of HEV EMS. With the proposed

EMS, control dependency on drive cycles can be completely relieved while maintaining good charge sustaining performance and fuel economy. The proposed approach can be applied to different electrified powertrain configurations.

1.3 Thesis Outline

The rest of the thesis is organized as follows:

Chapter 2 introduces the fundamentals of HEVs, engines in HEVs, and HEV EMSs. Different HEV variants are identified and compared, and the potential for efficiency improvement is investigated. Engines in different HEV configurations are described, and the hybrid engine modeling techniques are thoroughly explained. The existing HEV EMSs are categorized, and the advantages and disadvantages of each category are briefly discussed.

Chapter 3 provides an in-depth review of four technology pathways to energy-efficient hybrid powertrain specific engines: over-expansion cycle, low temperature combustion (LTC) concept, alternative fuels, and waste heat recovery (WHR) techniques. Working principles, influencing factors, benefit potentials, advantages, and disadvantages of each technological solution are discussed in detail. Challenges are specified, and recommendations are given accordingly. Opportunities for simplification from a hybrid-optimized engine standpoint are identified.

Chapter 4 presents a real-time ECMS incorporating powertrain inertial dynamics. An inertial-based dynamic vehicle model of a power-split HEV is constructed, which

is numerically verified by an energy balance analysis and experimentally validated by comparing with disclosed testing results. A comparative study is performed between the proposed strategy and a baseline steady-state ECMS without inertial considerations. Simulation results are compared and discussed in terms of battery state-of-charge (SOC), vehicle mode shifts, powertrain dynamics, engine operations, and fuel consumption.

Chapter 5 proposes a predictive A-ECMS for a multi-mode hybrid powertrain architecture. A control-oriented HEV model is constructed with primary powertrain component modeling. Based on the HEV model, the optimal control problem is described, and the formulation of the proposed A-ECMS is explained thoroughly. A basic non-adaptive ECMS is also implemented for comparison. Simulation results of the two ECMS are compared and discussed in detail.

Chapter 6 develops a DRL-based HEV EMS with A3C algorithm. Fundamentals of reinforcement learning (RL) is presented, including key concepts and algorithms. A control-oriented HEV model of a series configuration is introduced as the simulation platform, based on which the optimal control problem is identified. Formulation of the A3C-based EMS is explained thoroughly and explicitly. The proposed algorithm is then trained on a typical drive cycle, and training results are compared with dynamic programming (DP) benchmark and an A-ECMS. The trained EMS is also tested on a different long drive cycle to verify its generalization and adaptability.

Chapter 7 summarizes the conclusions and future work.

Chapter 2

Fundamentals of Hybrid Electric Vehicles

As a brief introduction to the research background of the thesis, this chapter presents the fundamentals of HEVs. To further explore the potential of HEV systems, powertrain components and HEV EMS are two effective pathways that should be comprehensively investigated. As a result, this chapter provides a detailed description of hybrid engines and HEV EMS. The discussions in this chapter lay the foundation for the following research work.

2.1 Hybrid Electric Vehicles

Owing to the improved fuel economy and emission performance, HEVs have received wide research attention from industry and academics alike and are sharing an increasing percentage of vehicles in the market. Over the years, there have been a large number of vehicles in the market with a broad spectrum of hybridization ratios, from the simplest start-stop systems to full hybrid vehicles [15]. In the meantime, different HEV variants have also been developed.

For example, as the most eco-friendly HEV variant, plug-in hybrid electric vehicles (PHEVs) can travel a long distance solely on battery power due to the larger battery size and the ability to charge externally from the electric grid [16]. Another type of HEVs is called range-extended electric vehicles (REEVs), also known as series HEVs or series PHEVs, depending on whether it can be charged externally. REEVs mostly operate like EVs since only battery power is used for propulsion. When the battery level is low, a range extender, which is an internal combustion engine (ICE) that drives a generator, begins to charge the battery and enables extended range [17]. A

comparison of conventional HEVs, PHEVs, and REEVs is given in Table 2.1.

Table 2.1: Comparison of conventional HEV, PHEV, and REEV.

Type	Conventional HEV	PHEV	REEV
Powertrain	ICE & Electric motor	ICE & Electric motor	ICE & Electric motor
Battery charging	On-board by ICE Regenerative braking	On-board by ICE Regenerative braking Electricity from grid	On-board by ICE Regenerative braking Electricity from grid (for plug-in REEV)
Battery size	Small/Medium	Medium	Medium
Electric driving range	Small/Medium	Large	Medium/Large (for plug-in REEV)
ICE size	Small/Medium	Small/Medium	Small/Medium
Fuel consumption	Medium	Low	Medium/Low (for plug-in REEV)

HEVs possess the ability to improve fuel economy and exhaust emissions due to the following factors. Firstly, HEVs are equipped with electric motors with higher efficiency and improved torque characteristics compared to ICEs. Secondly, HEVs recapture braking energy instead of losing it to friction and heat. Thirdly, it is possible to shut down the engine or operate it at peak efficiencies due to the multiple power sources. Besides, HEVs enable engine downsizing since the traction motor will share part of the maximum power demand, so the engine only needs to fulfill average loads. Last but not least, HEVs can benefit from energy-efficient engines specific to electrified powertrains. The combination of these capabilities results in a significant increase in efficiency for HEVs.

2.2 Engines in Hybrid Electric Vehicles

As a crucial propulsion component in HEVs, engines significantly affect vehicle performance in terms of fuel economy, emissions, drivability, etc. Therefore, energy-efficient engines offer the opportunity to further improve HEV efficiency. In this regard, this section gives a brief introduction of engines in HEVs, based on which technology pathways to energy-efficient hybrid engines will be presented in Chapter 3.

2.2.1 Engines in Various HEV Configurations

According to the power flow from source to load, existing HEV configurations can be fundamentally divided into three types: series, parallel, and power-split, as shown in Fig. 2.1.

In series configurations, the engine can operate independently of the vehicle power demand and consistently at peak efficiencies since no mechanical connection exists between the engine and driving wheels, as shown in Fig. 2.1a. Generally, engines in series HEVs are smaller than those in conventional ICEVs, presenting excellent potential in engine downsizing [18]. As a result, the engine only accounts for a minority of the power demand in series HEVs. Although the commercial application of series HEVs is still limited to heavy-duty vehicles and buses [4], automotive manufacturers are making efforts to expand the market.

In parallel HEVs, the ICE and the EM provide traction power individually or together, and the torque contributions are combined. According to the position of EMs in the

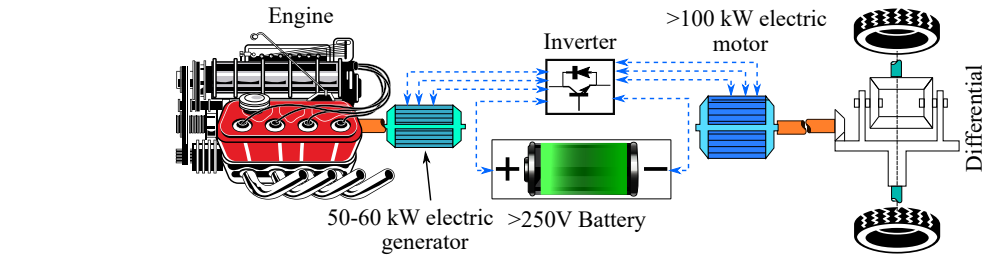

(a)

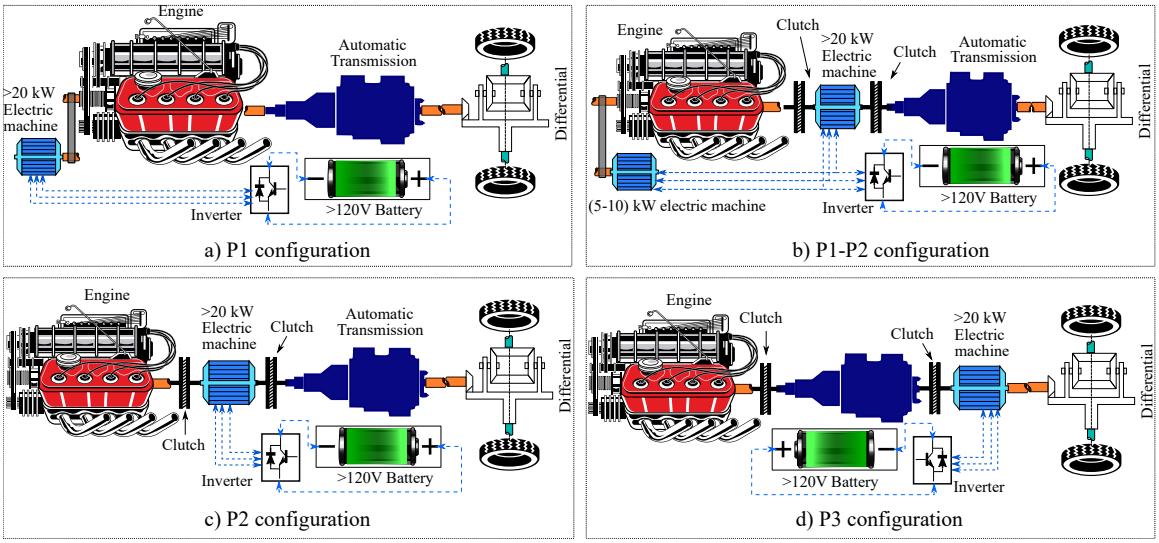

(b)

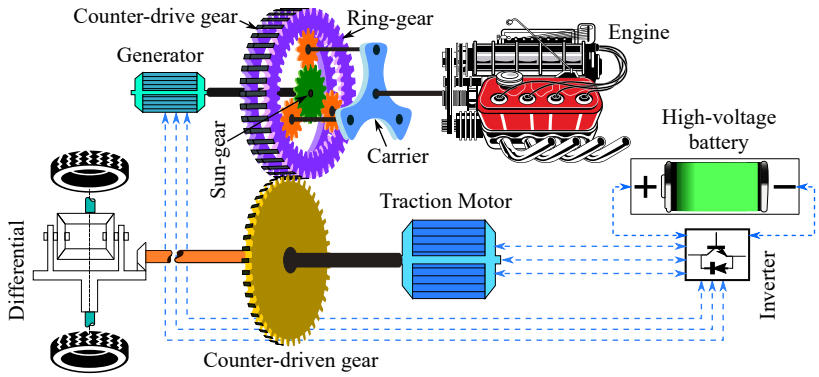

(c)

Figure 2.1: HEV configurations: (a) Series; (b) Parallel; (c) Power-split.

drivetrain, parallel HEVs with a single motor can be sub-categorized into P0, P1, P2, P3, and P4. Similarly, dual-motor architectures can be sub-categorized as P1-P2, P2-P4, etc. [19]. Some examples of these configurations are depicted in Fig. 2.1b.

Although engine speed is constrained by vehicle speed in parallel HEVs, the power distribution between the engine and EM can be varied so that engine runs at peak efficiency at each speed of operation. Such a target leads to a growing body of literature on vehicle supervisory control algorithms. Offline control strategies such as DP [20], as well as online control strategies such as ECMS [21] and model predictive control (MPC) [22], have been widely researched for parallel architectures. In most cases, the engine works as the primary power source, and the traction motor assists in vehicle propelling during accelerations. As a result, engines in parallel configurations are usually bigger than those in series configurations. Due to the higher flexibility in powertrain design, parallel configurations receive more research attention and are primarily used in light-duty vehicles over recent years [18].

Power-split or series-parallel HEV integrates series and parallel configurations with a power-split device, i.e., planetary gear set, as shown in Fig. 2.1c. It combines the advantages of both series and parallel architectures, offering the possibility of all-electric and hybrid-electric driving with high-efficiency engine operations. Engine operation in such configurations is less steady than series configurations but less transient than parallel configurations [8]. However, this architecture suffers from the drawback of higher power losses in path mechanical-to-electrical, which need to be mitigated through proper energy management.

Engine characteristics of these three configurations are listed and compared in Table

2.2.

Table 2.2: Comparison of engines in series, parallel, and power-split configurations.

Features	Series	Parallel	Power-split
Size	Small	Large	Medium
Power source	Secondary	Primary	-
Coupled to wheels	No	Yes	No
Controllability of speed and torque	Speed & torque	Torque	Speed & torque
Transient	Low	High	Medium
Zero-emission operation	Possible	Possible	Possible

In recent years, multi-mode power-split powertrains have been proposed, such as the intelligent multi-mode drive (iMMD) of Honda [23], the two-mode electric variable transmission (EVT) of General Motors Company [24], and the single-input electrically variable transmission (SiEVT) of Chrysler (now Stellantis N.V.) with three electrified modes [25]. Schematic diagrams of the SiEVT layout and its operation modes are illustrated in Fig.2.2. Multiple modes are commonly realized by adding clutches or brakes to the transmission and are expected to improve both fuel economy and drivability. Since the design process is more complex than single-mode power-split configuration, significant efforts have been made on powertrain topology selection and control development [26].

2.2.2 Modeling Techniques for Hybrid Engines

HEV is a complex multidisciplinary system. Research and development of HEVs requires a fairly deep knowledge of various academic subjects, such as mechanical

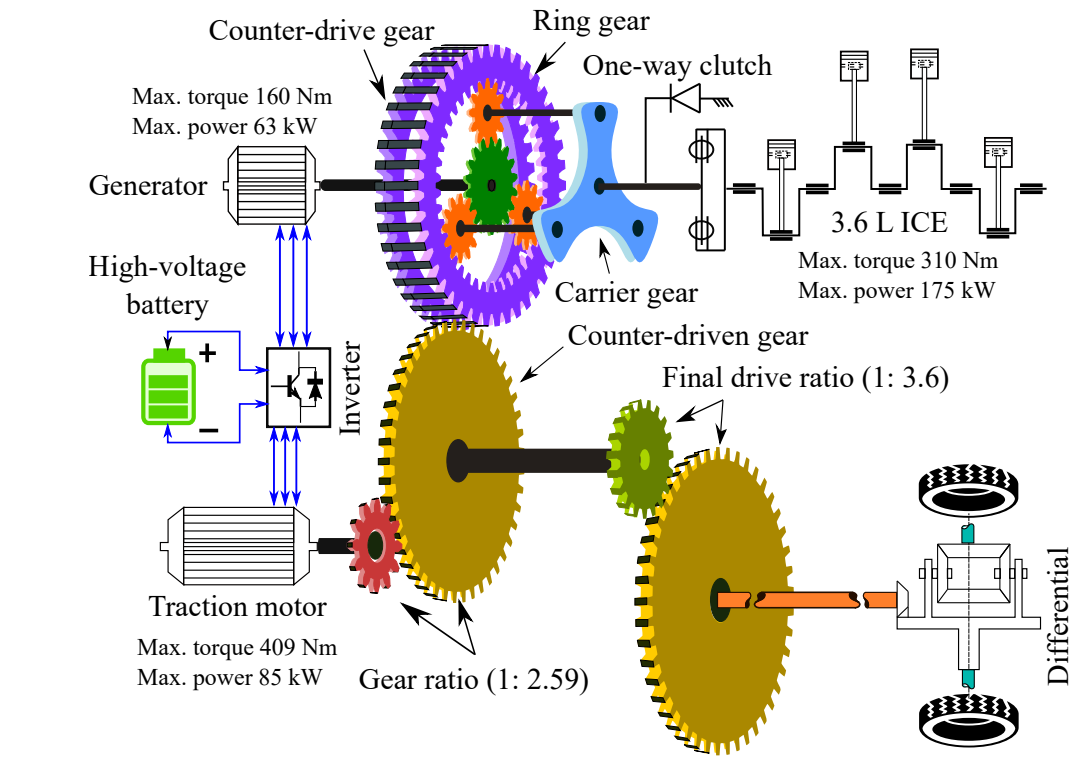

(a)

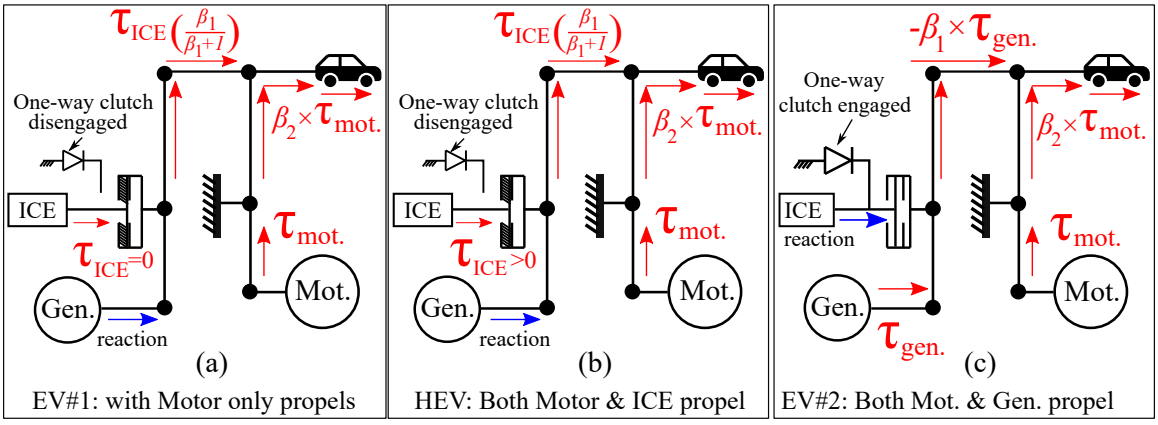

(b)

Figure 2.2: Schematic diagrams of: (a) SiEVT architecture; (b) operating modes.

design, electronic control units, etc., and is thus time-consuming. By developing virtual prototypes of vehicle designs before investing in physical prototypes, designers can obtain great insight into the vehicle behavior and substantially reduce time and cost. Therefore, computational models are an effective tool for HEV development.

Modeling of a physical system aims for different purposes. Detailed modeling, software-in-the-loop (SIL) modeling, and hardware-in-the-loop (HIL) modeling should be adopted at different stages of the HEV development cycle [18]. In general, detailed modeling is employed at an early stage, focusing on detailed information of individual powertrain components such as engines and EMs. Engine models at this stage require higher fidelity and computational loads. SIL modeling is widely adopted in HEV control system development, and engine models at this stage are less accurate but more computationally efficient.

Therefore, hybrid engine modeling can be low-fidelity that only give steady-state characteristics, medium-fidelity where detailed modeling at certain locations is provided, or high-fidelity where most engine dynamics are captured and presented. In this section, widely-used engine modeling techniques for hybrid applications are introduced in the order of increasing fidelity and complexity.

Quasi-static Map Model

In most situations, engine models for HEV development are control-oriented, and detailed modeling of the physical process inside engines is unnecessary. Quasi-static map models are sufficient and efficient when studies focus on a system level, such as

vehicle supervisory control development, where engines are only seen as one of the powertrain components. Most studies on HEV control strategy designs employ this approach [27].

In quasi-static map models, engines are assumed to be perfect actuators responding instantly to commands. Generally, there are two inputs to such models, i.e., a torque command given by the upper-layer controller and a speed signal resulting from the coupling of the engine with other powertrain components. The outputs of such engine models are usually effective torque, fuel consumption, and possible emissions. Such model structure can be described in Fig. 2.3. Inside the model, the feasible operating range is limited by physical speed and torque constraints, as expressed in Eq. (2.2.1):

$$\omega_{eng,min} \leq \omega_{eng}(t) \leq \omega_{eng,max} \tag{2.2.1a}$$

$$T_{eng,min} \leq T_{eng}(t) \leq T_{eng,max}(\omega_{eng}(t)) \tag{2.2.1b}$$

where the upper torque limit varies with engine speed. To calculate fuel consumption, brake specific fuel consumption (BSFC) maps are commonly used. Such maps are usually obtained from steady-state engine tests and are therefore only valid for warm engine operations or where thermal effects can be neglected. If warm-up losses are to be addressed, the model can be extended by introducing a correction factor which is a function of coolant temperature, to account for additional fuel use [28]. Fig. 2.4 shows a typical engine map with BSFC contour and maximum torque curve.

Although dynamics are not directly modeled in such models, some can be added to

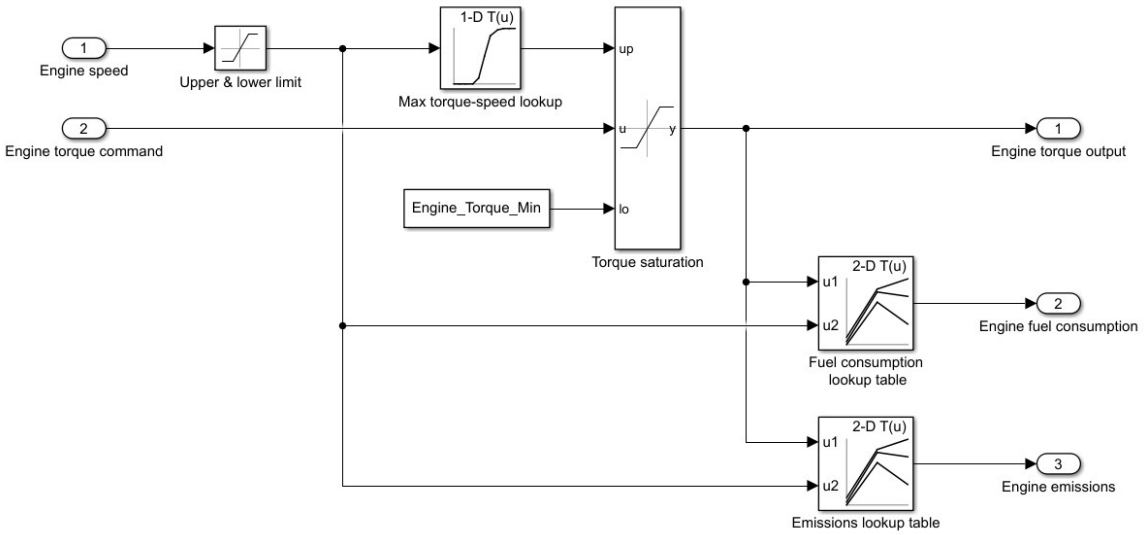

Figure 2.3: Schematic of a quasi-static map engine model in Simulink®.

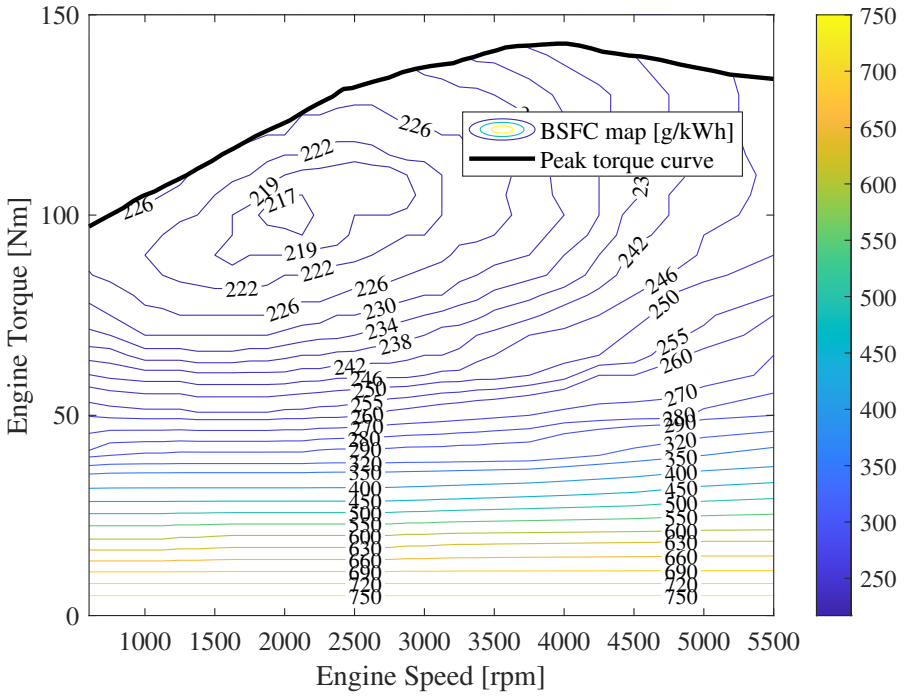

Figure 2.4: A typical engine BSFC map with maximum torque curve.

the torque calculation. For instance, the air/fuel dynamics can be represented as a delay between torque command and actual torque output by coupling with a transfer function; the crankshaft dynamics can be reflected as inertia [29].

Mean Value Model

Sometimes, however, the transient performance of specific engine parts needs to be captured. Quasi-static map models are no longer sufficient at these locations, and detailed modeling is required. Detailed engine models can be analytical or mathematical models derived from basic principles of physics such as thermodynamic laws and conservation of mass and energy. Theoretically, a fully dynamic model should include all the physics behind the engine. However, the intense computational load makes it extremely tough to derive such a model. Therefore, proper assumptions should be made to simplify the model by neglecting less irrelevant dynamics based on research purposes.

Mean value engine models (MVEMs) are employed in hybrid engine modeling when particular dynamics inside engines are of interest while computational efficiency is also required. Such model designs are not unique, depending on the designer's experience and research focus. In MVEMs, parameters and variables are averaged over one or several engine cycles [30]. Gas is assumed to be ideal with constant specific heat capacity. Basic principles of physics and fluid flow equations are applied to model engine subsystems, including the throttle system, intake manifold system, and combustion system, as illustrated in Fig. 2.5. The model input is the throttle position that gives the air mass flow. Engine speed, torque, fuel consumption, and emissions

are taken as the model outputs. Since spatial dimensions are not included, MVEM is a kind of zero-dimensional model.

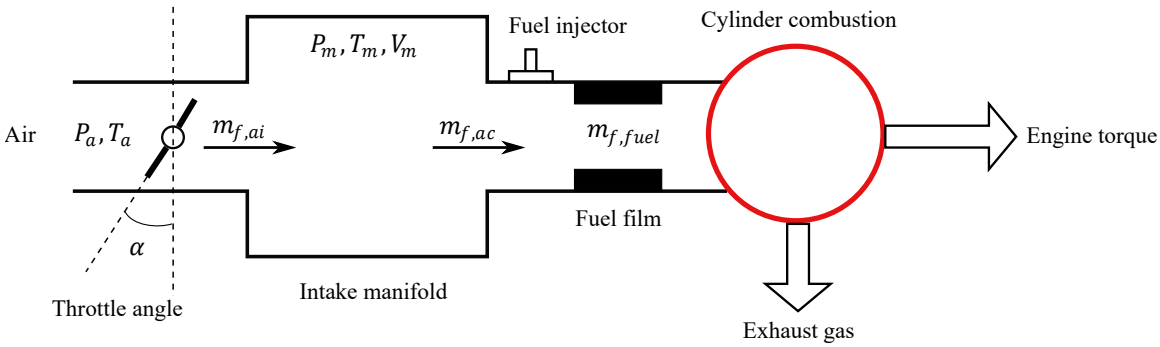

Figure 2.5: Illustration of a mean value engine model.

Fluid Dynamic Model

Fluid dynamic models are another type of analytical model based on conservation laws and flow equations. They can describe the unsteady combustion and heat transfer process and the non-uniform pressure and temperature distributions in manifolds and cylinders, thus giving a more accurate description of engines. But also, they are computationally intensive and thus not preferable for control-oriented modeling [31].

The most common fluid dynamic model for hybrid engines is the 1-D simulation model employing engine simulation software, e.g., GT-POWER [32] and Simcenter Amesim [33]. Such models come with higher accuracy and computational loads, thus preferred in studies where engine dynamics are greatly important. Fig. 2.6 presents an example of a Simcenter Amesim model for a naturally-aspirated four-cylinder engine.

Apart from the discussed methods, there are other types of models for hybrid engine modeling, such as black-box models. In real practice, most engine models combine

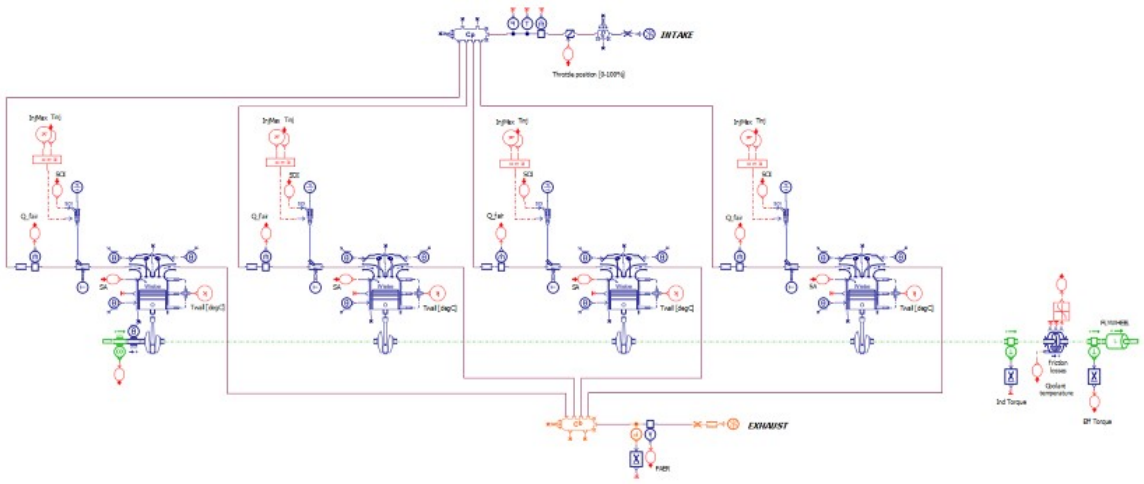

Figure 2.6: A typical engine model built in Simcenter Amesim.

several modeling approaches to different degrees to meet reasonable accuracy with acceptable computational demands.

2.3 Energy Management Strategies in Hybrid Electric Vehicles

As indicated in Section 2.1, the flexibility in ICE operation provides HEVs with additional degrees of freedom (DOF) to efficiently control the power distribution between power sources. Since the effectiveness of EMS has great and direct influences on HEV performance, developing efficient EMS is another effective method to further exploit the potential of HEVs. Recently, HEV EMS has been extensively explored with different objectives such as fuel consumption minimization [34, 35], emission reduction [36, 37], battery lifetime [38, 39], etc.

Generally, the existing EMSs can be classified into rule-based, optimization-based, and learning-based control strategies [40], details of which are presented in the following.

2.3.1 Rule-based Control Strategies

Rule-based control strategies are designed based on the engineer's experience and expertise through either deterministic or fuzzy rules [41]. Examples of deterministic and fuzzy rules used in rule-based control strategies are given in Fig. 2.7.

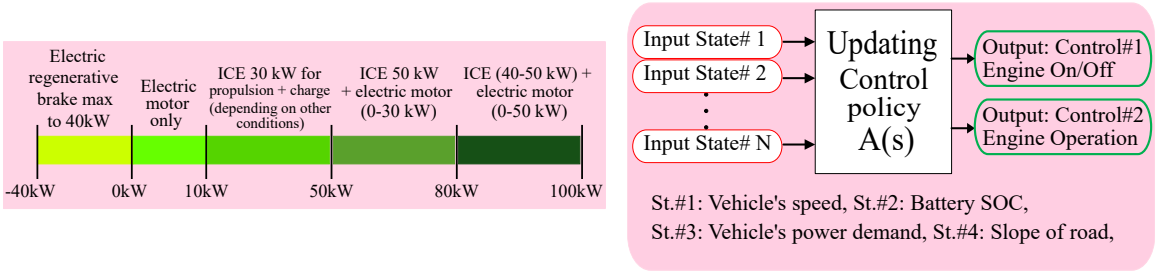

(a)

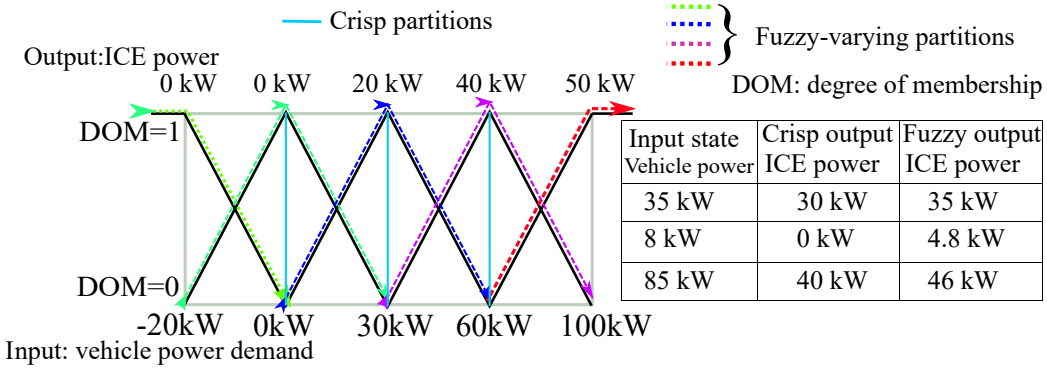

Input state Vehicle power	Crisp output ICE power	Fuzzy output ICE power
35 kW	30 kW	35 kW
8 kW	0 kW	4.8 kW
85 kW	40 kW	46 kW

(b)

Figure 2.7: Rule-based control strategies with (a) deterministic and (b) fuzzy rules.

Generally, control parameters for main powertrain components, i.e., ICE, EMs, and the battery, are calibrated through tests and then designed into a set of look-up

tables to be used in the controller, as illustrated in Fig. 2.8. Although such control strategies are simple and easy to implement, they suffer from drawbacks such as significant calibration efforts, lack of optimality, and poor adaptability to powertrain architectures and drive cycles [42].

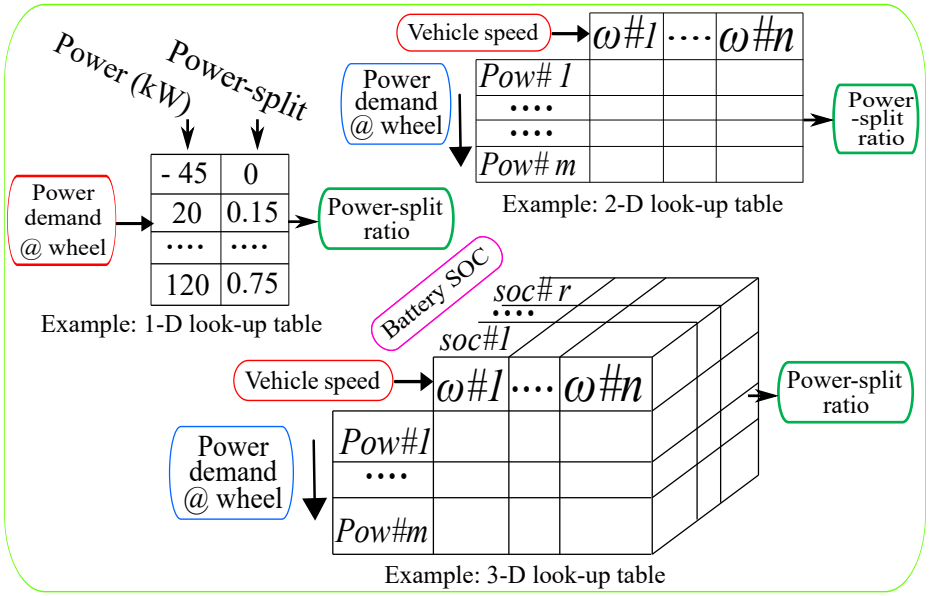

Figure 2.8: Examples of look-up tables used in rule-based control strategies.

2.3.2 Optimization-based Control Strategies

Optimization-based control strategies deal with HEV energy management as an optimal control problem, which relies on optimization algorithms to solve [43]. They can be further divided into off-line and online strategies based on the requirement for a prior knowledge of the drive cycle [7].

Off-line strategies can find the global optimal control sequence, but they are heavily dependent on the entire drive cycle and thus not real-time implementable. In addition,

the high computational loads of global optimization approaches also make off-line strategies hard to apply in real-time controls [18]. Representatives of off-line control algorithms are DP [44], Pontryagin's minimum principle (PMP) [45], particle swarm optimization (PSO) [46], genetic algorithm (GA) [47], linear programming (LP) [48], quadratic programming (QP) [49], slope-weighted energy-based rapid control analysis (SERCA) [50], etc.

In contrast, online strategies provide higher adaptability to drive cycles with near-global optimal solutions. Vehicle states are updated in real-time, and the local optimal solution is derived by instantaneously minimizing the predefined cost function [51]. Among existing online strategies, ECMS and MPC are two well-known candidates that have been widely investigated and used.

ECMS originates from PMP, where metrics of interest such as fuel consumption, battery electrical energy, exhaust emissions, etc., are converted into an equivalent amount of fuel consumption through an EF [52]. By tuning the EF, the equivalent fuel consumption can be minimized instantaneously, arriving at a near-global optimal control sequence [53]. Fig. 2.9 illustrates the working principle of ECMS for HEVs.

MPC relies on the future information provided by the prediction models to optimize control solutions. By minimizing a predefined cost function over the prediction horizon, MPC can achieve similar performance to DP if the prediction method is accurate [54].

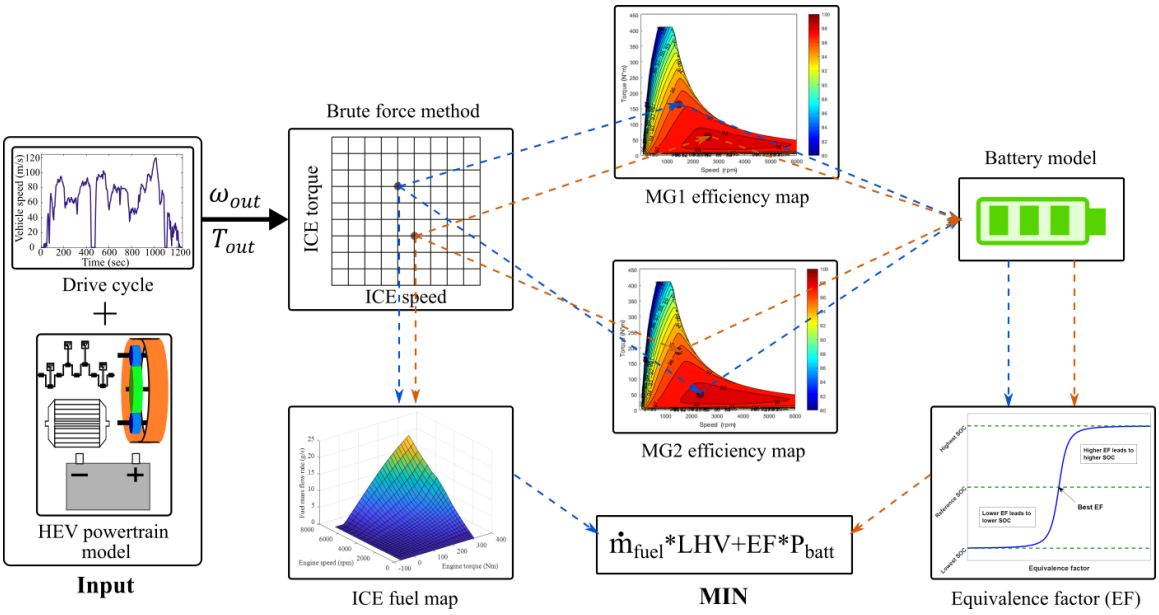

Figure 2.9: Illustration of ECMS for HEVs.

2.3.3 Learning-based Control Strategies

As the artificial intelligence (AI) technique penetrates our daily lives deeper and deeper, the automotive industry starts to explore learning-based control strategies for HEVs to keep up with the pace. Learning-based EMS relies on data mining algorithms and learns from historical data such as previous driving information for online training. Based on their learning algorithms, learning-based EMSs can be further categorized into RL, DRL, supervised learning, unsupervised learning, deep learning (DL), etc [55].

As a representative of learning-based strategies, RL derives the optimal control law on a trial-and-error basis. During state transitions, the learning agent receives an observation (or state) of the environment along with an immediate reward that measures the success of the training and then gives an action (or control) to the environment

for the following state. Through continuous interactions between the agent and the environment, an optimal control policy can be obtained after sufficient training [56]. An illustration of RL-based HEV EMS is given in Fig. 2.10.

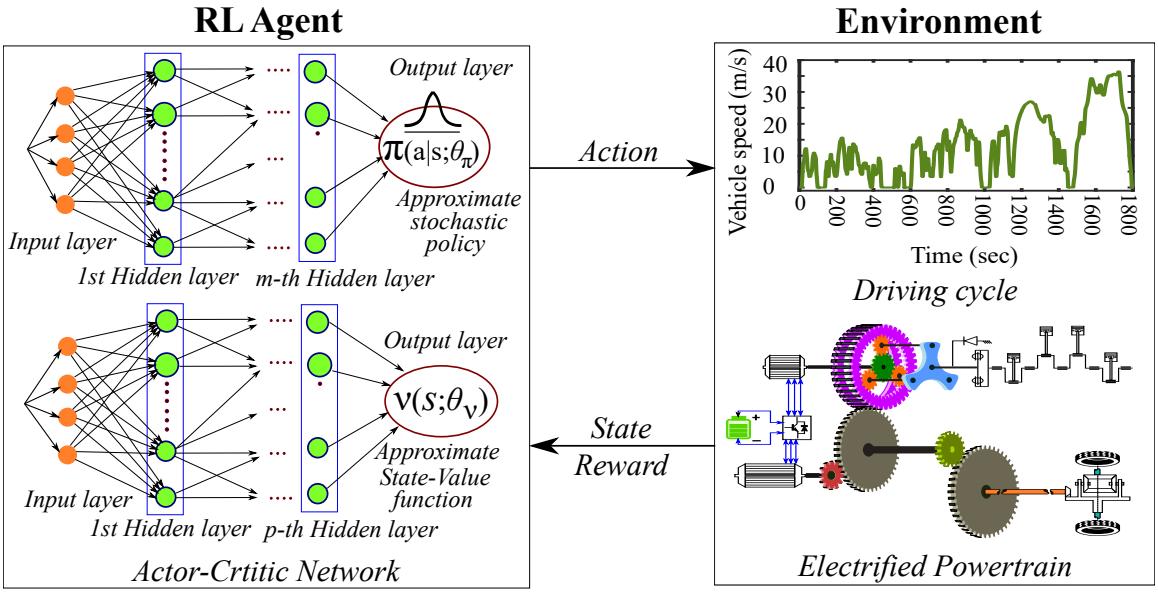

Figure 2.10: Illustration of RL-based EMS for HEVs.

RL-based EMSs present several advantages over the control strategies discussed above, namely:

- Higher optimality than rule-based EMSs
- Lighter computational burden and the capability of using online as opposed to off-line global optimization-based EMSs
- Less dependency on drive cycle information compared to online optimization-based EMSs

Due to these benefits, RL-based EMSs have been extensively explored in recent years

on a variety of hybrid architectures, such as series HEV [57], parallel HEV [58], power-split HEV [59], PHEV [60], etc.

2.4 Summary

This chapter provides a detailed description of HEVs, engines in HEVs, and HEV EMS. The improved efficiency of HEVs is a result of multiple contributing factors. Thanks to them, HEVs and their variants are taking up an increasing portion of the automotive market. Further efficiency improvement of HEVs can be achieved through energy-efficient engines and efficient vehicle control strategies. Therefore, engines in various HEV configurations and hybrid engine modeling techniques are introduced. The existing HEV EMSs are categorized, and the advantages and disadvantages of each category are briefly discussed. The fundamentals presented in this chapter will be the basis of the discussions and analyses in this thesis.

Chapter 3

Hybrid Electric Vehicle Specific Engines

This chapter provides a comprehensive review of energy-efficient hybrid electric vehicle specific engines through discussions on the following four aspects (bolded).

- The amount of useful work that can be extracted from fuel combustion depends on the operating cycle being used. A higher expansion ratio, which generally leads to more useful work, is restricted in conventional Otto-cycle engines due to knock limit [61]. Hence, **adopting alternative operating cycles or making modifications to the existing Otto cycle** is a feasible technology pathway to realize higher engine efficiency.

- ICEs are heat engines where the combustion of fuels transforms chemical energy into kinetic energy through thermodynamic cycles. The combustion process, by which the engine emissions are formed, is especially important as it affects not only emission characteristics but also fuel efficiency. Therefore, energy-efficient engines can be achieved by developing clean and efficient combustion approaches, among which **advanced combustion concepts** and **alternative fuels** are most widely recognized [62].

- Of the chemical energy that is not converted into useful work, a huge majority is wasted as heat via hot exhaust gases and coolant. **Recovering the waste heat of engines** can bring about a significant improvement in engine efficiency and therefore has the potential to make major advances in engine development [63].

3.1 Over-expansion Cycle

The Otto cycle is the most common thermodynamic cycle in automobile engines and has dominated the market since the beginning of automobile manufacturing. However, in Otto-cycle engines where the compression ratio equals the expansion ratio, the expansion ratio (compression ratio) cannot be significantly enhanced due to the knock limit [64]. Therefore, the actual thermal efficiency of Otto engines is generally low. Efforts have been made to explore alternative thermodynamic cycles to improve engine thermal efficiency, and the over-expansion cycle is proposed.

3.1.1 Overview of Over-expansion Cycle

Over-expansion cycle is a modified Otto cycle designed to improve efficiency by enabling a higher expansion ratio than the compression ratio [65]. Modern over-expansion engines are often realized by variable valve timing (VVT) technology. Philosophies of VVT are thoroughly explained in [66]. Fig. 3.1 depicts a P-V diagram of an Otto cycle and an over-expansion cycle implemented with late intake valve closing (LIVC). In the over-expansion cycle, the working charge expands beyond the point where compression begins, allowing more mechanical work to be converted from thermal energy and thus achieving higher thermal efficiency.

There are two famous representatives of over-expansion cycles, i.e., the Atkinson cycle and the Miller cycle. Both Atkinson and Miller cycles typically have a higher geometric compression ratio (GCR) to differentiate themselves from their VVT cousins. The Atkinson cycle is mostly defined as the implementation of LIVC plus increased

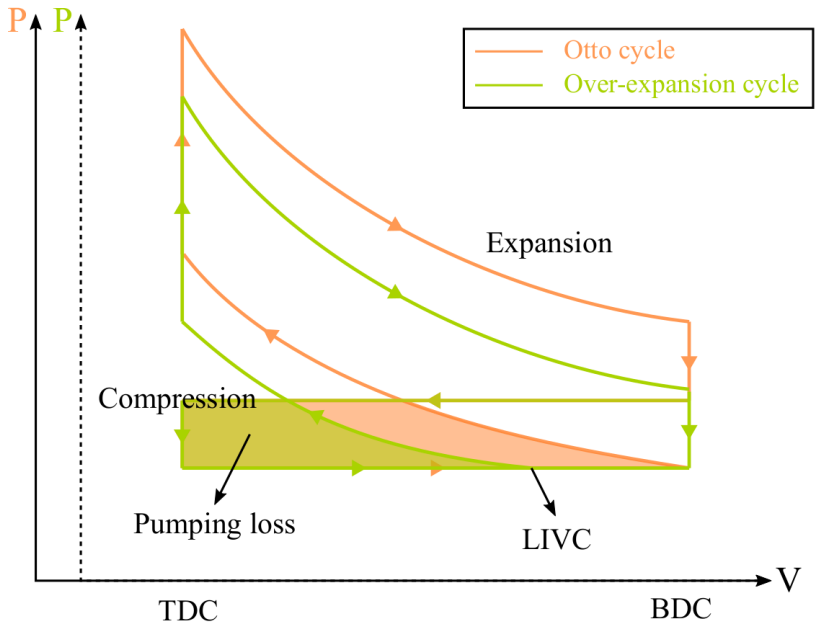

Figure 3.1: P-V diagram of Otto cycle vs. over-expansion cycle with LIVC.

GCR, and the Miller cycle is defined as the implementation of early intake valve closing (EIVC) plus increased GCR. In another definition, the Miller cycle is defined as a variant of the Atkinson cycle with intake boosted by turbochargers or superchargers, which can be seen as an extension of the original Atkinson cycle to boosted engines [61]. Sometimes these two terms are used interchangeably. Therefore, the term Atkinson cycle is used for both within this chapter for the sake of simplicity.

Fig. 3.2 compares the BSFC of an Atkinson engine (Toyota's TNGA 2.5L engine) and an Otto engine (Ricardo's 2.4L engine, initially used in the 2007 Toyota Camry). Engine data is obtained from the Advanced Light-Duty Powertrain and Hybrid Analysis (ALPHA) tool by U.S. Environmental Protection Agency (EPA) [67]. It can be seen that the Atkinson engine presents higher fuel efficiency than the Otto engine. As predicted by EPA, adopting Atkinson cycle can reduce carbon dioxide (CO_2) emissions

by 3-8% if effects of exhaust gas recirculation (EGR) and high compression ratio are included. Recent progress in engine technologies suggests this benefit to be higher, up to 10-14% [68]. Moreover, fuel savings from the Atkinson cycle are projected to be 8-10.3%, and manufacturers are on track to meet and even exceed this number [69].

3.1.2 Atkinson Cycle in HEVs

Recent years have witnessed the widespread use of Atkinson-cycle engines in HEVs among major automotive manufacturers such as Toyota, Ford, and Honda. Almost all HEVs and PHEVs in the US market are equipped with Atkinson-cycle engines [70], e.g., Toyota Prius, Camry Hybrid, Ford Fusion Hybrid, Honda Accord Hybrid, and Chevrolet Volt.

In the 2018 Camry Hybrid, Toyota's A25A-FXS engine, which is a naturally aspirated Atkinson-cycle engine with a compression ratio of 14:1, is used and equipped with VVT and cooled EGR. Although details of this specific engine are not found, a similar engine (A25A-FKS) calibrated for use in the non-hybrid 2018 Camry has been studied [71, 72]. The peak engine brake thermal efficiency (BTE) is reported to be 40%, and CO_2 emissions are reduced by 18.6% compared to the engine in MY 2015 without Atkinson and EGR features. However, as other improvements are involved in the model upgrade, the numbers may exaggerate the contribution of the Atkinson cycle alone. Similarly, Toyota's 2ZR-FXE engine used in the third-generation Prius and Lexus CT200h combines the Atkinson cycle, cooled EGR, and port fuel injection (PFI), claiming the same peak BTE of 40% [73].

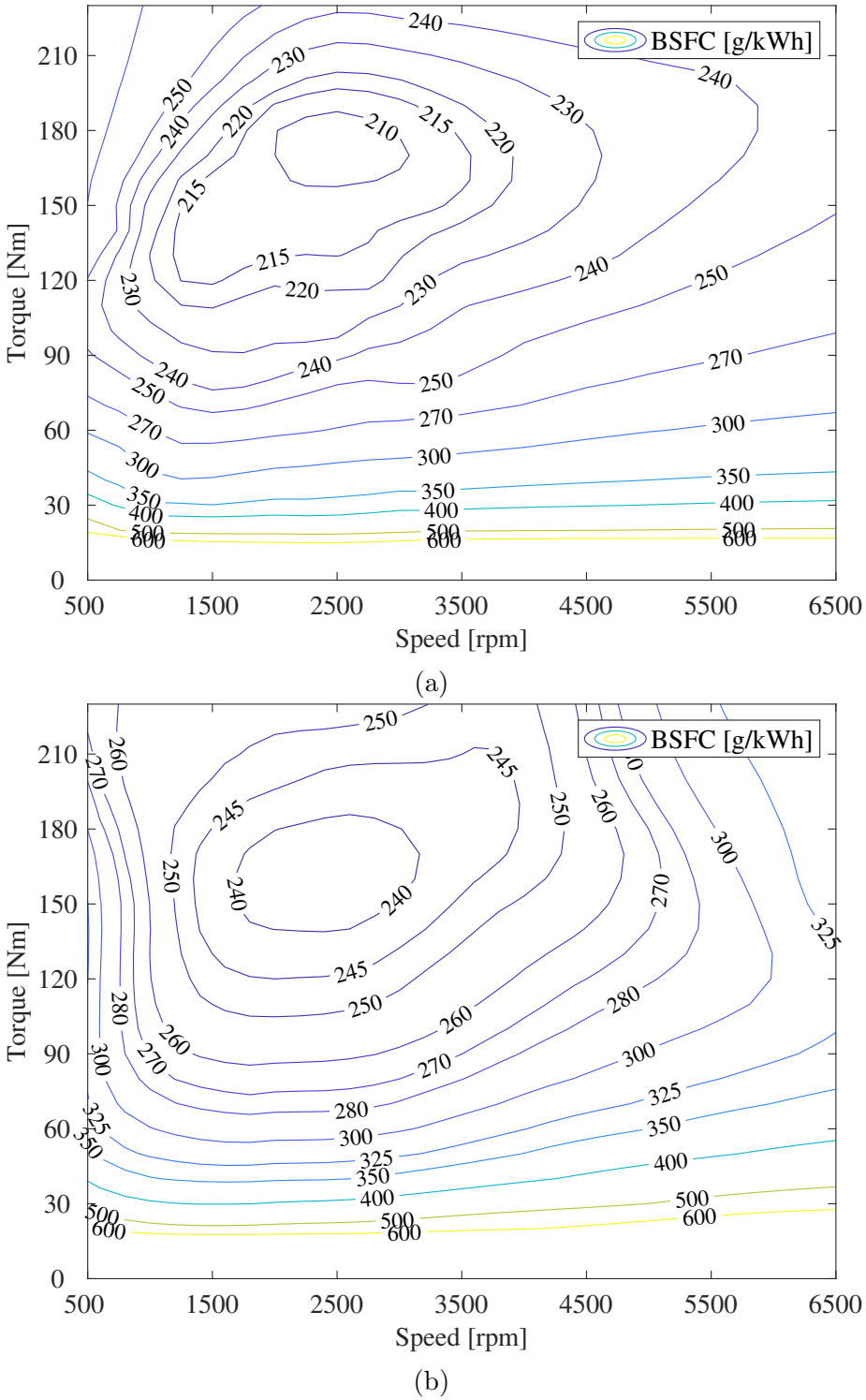

Figure 3.2: Comparison of BSFC between (a) Atkinson and (b) Otto engine.

Apart from manufacturers' data, Li Y et al. explored the fuel-saving potential of an Atkinson gasoline engine on a series HEV [74]. The cumulative fuel consumption was reduced by 4.58% compared with the original Otto engine, and oxides of nitrogen (NO_x) and CO_2 emissions were reduced by 46.1% and 18.37%, respectively. In another study, four range extenders, including an Atkinson-cycle engine, were tested and compared on a REEV platform [75]. Results indicated that the Atkinson-cycle engine was the most efficient solution under a combined urban-highway drive cycle, achieving a 6% reduction in energy consumption and 9% in well-to-wheel CO_2 emissions than the baseline Otto-cycle engine.

Atkinson engines are opening up new possibilities to achieve better fuel economy and emission performance in HEVs. It is estimated that 20-30% of the fuel improvement brought by HEVs is attributed to the Atkinson cycle [73]. However, it also has drawbacks. The major challenge of Atkinson and Miller cycles in hybrid applications is the reduced power density due to the charge backflow in the Atkinson cycle and the reduced valve period in the Miller cycle.

One possible solution is to implement VVT with variable compression ratio (VCR) to switch between Otto operation at high loads and Atkinson operation at low/medium loads. At low/medium loads, the engine operates on the Atkinson cycle, aiming for higher fuel efficiency. When high loads are required, a smaller compression ratio is enabled by VCR so that the engine can run on the Otto cycle without causing knock. Such a method improves the fuel efficiency through the Atkinson effect while satisfying the peak power requirement by Otto operation. Another solution is to use the Miller cycle with boosting to get back to the desired power density, which also

brings additional costs.

3.2 Low Temperature Combustion

Compression ignition (CI) and spark ignition (SI) engines are two traditional combustion systems that have evolved over decades. However, both combustion concepts still have limitations. CI engines with conventional diesel combustion (CDC) are known to have higher thermal efficiency but significant emissions. On the contrary, SI engines have lower emissions but are relatively less efficient [76]. In such a scenario, advanced combustion concepts which can achieve clean and efficient combustion modes are highly demanded.

For this reason, a variety of innovative combustion concepts such as gasoline direct injection (GDI), gasoline compression ignition (GCI), and partially premixed combustion (PPC) have been developed over the years [77]. Interestingly, the vast majority of these new technologies share the common feature of a premixed lean combustion pattern that leads to a lower temperature environment. The LTC concept is thereby proposed and has become mainstream of existing advanced combustion technologies.

3.2.1 Fundamentals of LTC

LTC is an advanced combustion concept with flameless fuel burning and a lower combustion temperature than conventional engine combustion. The flameless, lower

temperature combustion results from the dilution effect enabled by either lean combustion (excess air) or EGR and sufficient energy to drive the chemical reactions. A comparison of SI, CI, and LTC is given in Fig. 3.3, and the working principle of a four-stroke LTC engine is depicted in Fig. 3.4.

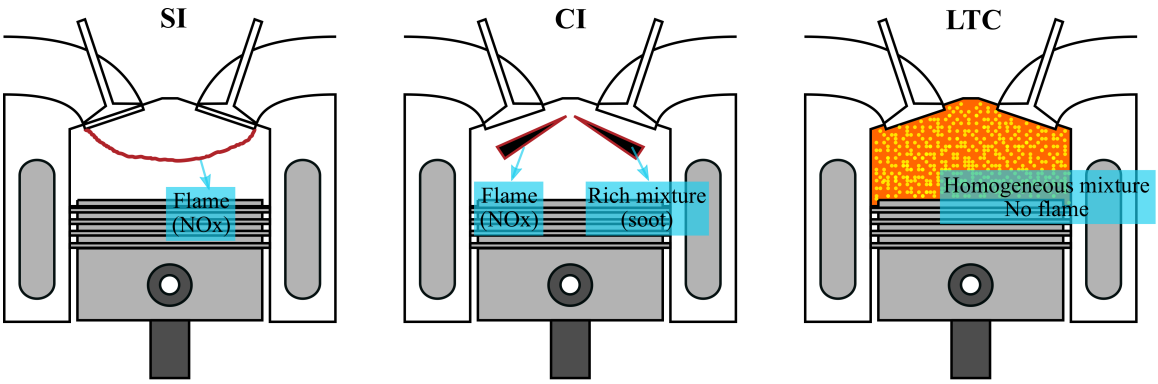

Figure 3.3: Comparison of SI, CI, and LTC.

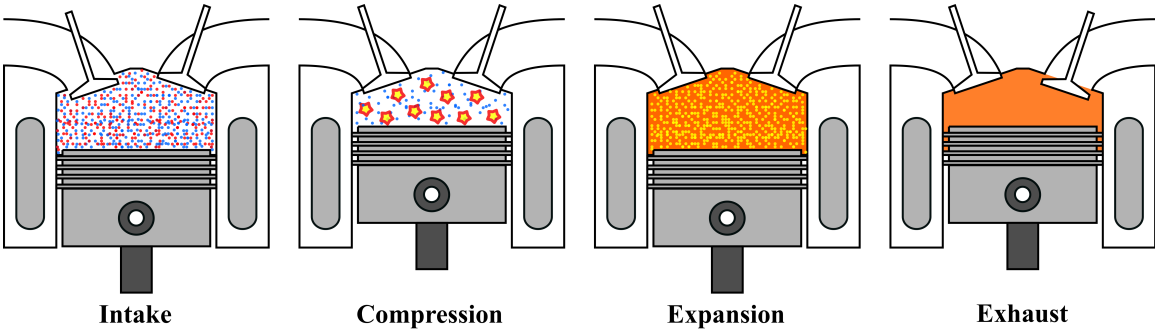

Figure 3.4: Working principle of a four-stroke LTC engine.

On the one hand, LTC presents higher fuel efficiency than SI due to the lower temperature, higher compression ratio, and lean combustion. On the other hand, LTC enables simultaneously ultra-low emissions of NO_x and soot compared to CI, reducing the aftertreatment requirements. However, LTC suffers from higher hydrocarbon (HC) emissions and a narrow operating range located at low-to-medium engine loads [78].

3.2.2 Classification of LTC

Over the decades, different LTC strategies have been developed and classified in literature [79]. Based on degrees of charge premixing, there are mainly two categories: homogeneous charge compression ignition (HCCI) and premixed charge compression ignition (PCCI). HCCI is an ideal LTC concept that uses very early fuel injection timing to obtain a homogeneous mixture of fuel and air before combustion. However, the biggest challenge of HCCI is the combustion phasing control since combustion timing is dominated by chemical kinetics and not controlled by injection timing [80].

This challenge motivates the development of PCCI, which can be considered a mix of CDC and HCCI combustion. In PCCI, control over combustion events can be achieved with direct fuel injection. However, it is found that the combustion control at high loads is difficult due to the high reactivity of diesel fuels [81]. Although using gasoline allows better control at high loads, low load conditions become difficult again [82].

Due to this reason, a type of dual-fuel PCCI, i.e., reactivity-controlled compression ignition (RCCI), is proposed using both gasoline and diesel [83]. Fuel proportion can be adjusted according to load conditions to achieve more stable operations. The potential of RCCI has been confirmed in different engine platforms [84, 85] and with different fuel types [86, 87]. However, it also has limitations, such as that at high loads, the pressure rise rate is excessively high if maintaining both NO_x and soot emissions at ultra-low levels [88].

Based on different fuel types and levels of fuel stratification [89], the existing LTC strategies can be classified as illustrated in Fig. 3.5.

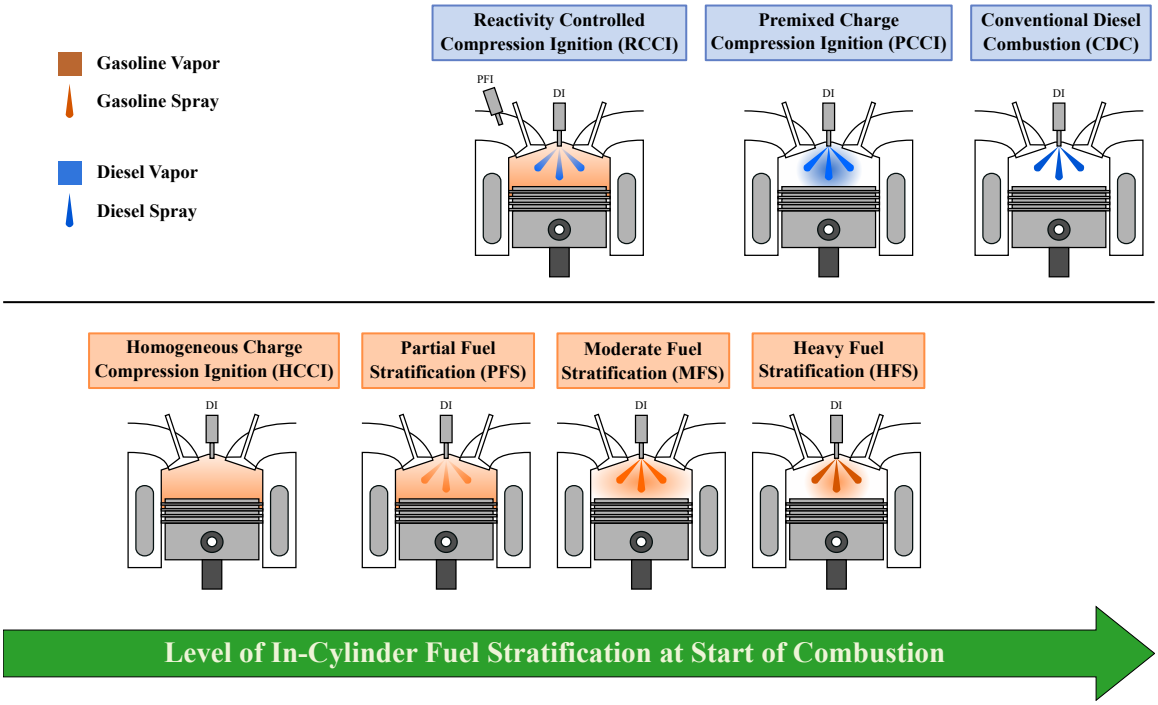

Figure 3.5: The landscape of advanced LTC strategies.

3.2.3 Single-Mode LTC

Powertrain Configuration

Due to the benefits of LTC, researchers have been working on integrating LTC with different hybrid architectures to exploit its fuel-saving and emission reduction potentials. An HCCI engine was examined in eight powertrain configurations with various degrees of hybridization [90], among which the PHEVs were equipped with all-electric range (AER) from 10 to 40 miles. As summarized in Fig. 3.6, results indicate that the fuel-saving benefit of HCCI declines with the increase of vehicle hybridization degree. One reason is that the engine running time is shortened, and therefore fewer opportunities are left for the engine to benefit from HCCI.

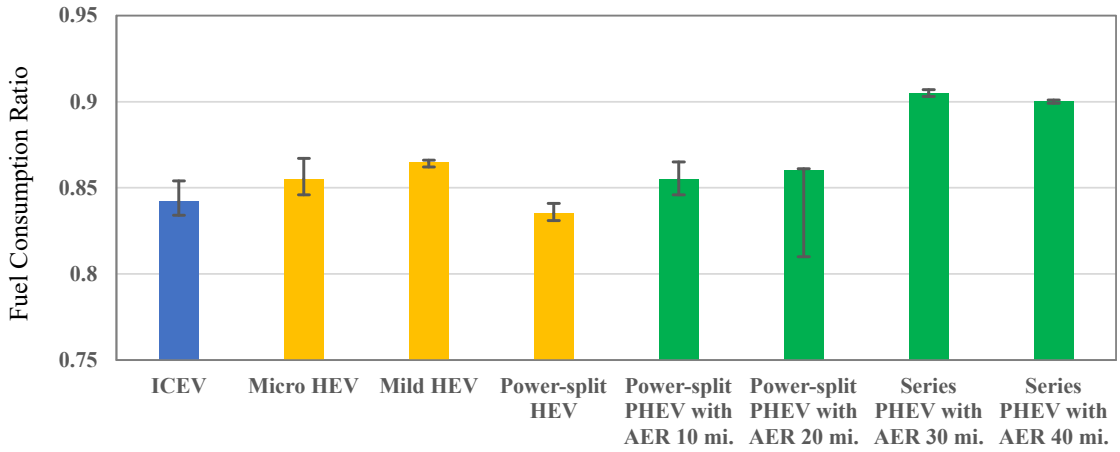

Figure 3.6: Fuel consumption of studied powertrain configurations (data collected from [90]).

However, as stated earlier, the main drawback of LTC is its narrow operating range at low-to-medium engine loads. When LTC is applied in conventional ICEVs, engines have to switch back and forth between LTC mode for low loads and SI/CI mode for high loads, leading to undesired transients. While for HEVs where engines can be decoupled from the drivetrain, it is possible to operate the engine at high-efficiency LTC region only, and combustion control is also less complex due to fewer transients.

As a result, series HEVs and REEVs offer excellent platforms for LTC applications. Solouk A et al. investigated a series HEV with an HCCI engine, and results showed 12.6% fuel reduction compared to the baseline SI engine [91]. In another work of the author [92], both series HEV and REEV were examined with an HCCI engine. Results presented significant fuel reduction of 17.7% and 18%, respectively.

In addition to HCCI, attempts have also been made to integrate RCCI into HEVs. A power-split HEV with an RCCI engine was examined and found with the best performance among all studied hybrid and non-hybrid powertrain configurations [93].

A series HEV equipped with an RCCI engine using dual fuels of EN590 and E85 was evaluated under Real Driving Emissions (RDE) test, and results showed 6.5% energy savings over a conventional diesel vehicle with significant CO_2, NO_x, and soot reductions [94], as illustrated in Table 3.1. In another study of García et al. [95], the RCCI engine was integrated into a parallel HEV that showed ultra-low NO_x and soot emissions. Solouk A et al. also explored a series HEV equipped with an RCCI engine [96]. Results showed 14.2% fuel improvement over an SI-HEV and 3% over a CI-HEV with much lower NO_x emissions.

Table 3.1: Performance of RCCI-HEV vs. ICEV (data collected from [94]).

Parameter	ICEV	RCCI-HEV
Energy consumption [MJ/km]	1.71	1.66
CO_2 [g/km]	1.20	105
NO_x [g/km]	0.49	0.04
Soot [g/km]	0.0089	0.0001
HC [g/km]	0.13	1.72
CO [g/km]	0.69	1.94

One thing to be noted is that LTC-HEVs are likely to enable a simpler and cheaper aftertreatment system (ATS) due to the emission benefit. However, the relatively low exhaust temperature may also deteriorate the conversion efficiency of ATS. This issue should be considered in real applications. Other concerns such as full oxygen storage capacity that may cause additional fuel use should also be accounted for when quantifying its benefit [97].

Control Strategy

As discussed in section 3.2.3, a higher hybridized powertrain may reduce the engine running time, thus impairing the benefit of LTC. On the other hand, it increases the flexibility of decoupling engines from road load, enabling more opportunities for high-efficiency LTC operation. Therefore, tradeoffs must be made to optimize the operation and maximize the overall HEV efficiency.

It is pointed out that the fuel-saving potential will be considerably affected by the vehicle control strategy [90]. Table 3.2 compares two control strategies (original and improved) for a series PHEV with LTC. Significant improvement can be observed in engine efficiency and fuel economy through control strategy optimization. Similarly, different energy management strategies were compared in another work [91], where DP exhibited the best performance, achieving 15.3% higher fuel economy than the rule-based control.

Table 3.2: Comparison of control strategies (data collected from [90]).

Parameter	Original strategy	Improved strategy
Engine efficiency	34.1%	38.4%
Percentage of engine ON	22.5%	27.4%
Percentage of HCCI mode	52.9%	98.7%
Percentage of fuel reduction	1%	8%

It is worthy to note that the combustion mode shift brings out dynamics and thus fuel penalties and torque fluctuations [98]. This cost should be addressed in EMS design to suppress frequent mode shifts.

Driving Condition

Apart from powertrain configurations and vehicle control strategies, LTC-HEV performance also depends on driving conditions [99]. Driving patterns with higher aggressiveness and power demand are advantageous to HCCI-HEVs since engines have to run for a longer time, and thus there are more opportunities to benefit from LTC [92, 96]. Three drive cycles, namely the New European Driving Cycle (NEDC), Urban Dynamometer Driving Schedule (UDDS), and JC08 drive cycle, were compared in Fig. 3.7. Results showed that JC08 presented the greatest fuel improvement in both series HEV and REEV configurations.

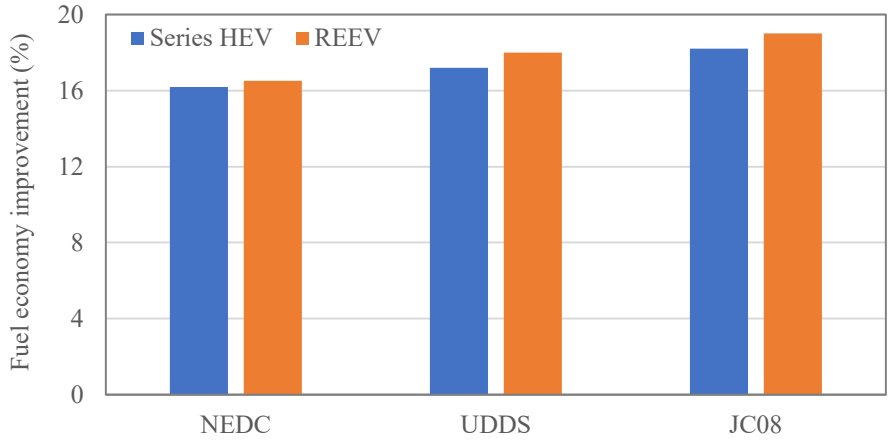

Figure 3.7: Fuel improvement under three drive cycles (data collected from [92]).

However, it should be mentioned that if the driving condition is so acceleration-demanding that the requested torque of the engine is outside its LTC region, the fuel benefit and emission reduction will be deteriorated [90]. Therefore, appropriate engine sizing is essential for a specific application of LTC-HEV.

3.2.4 Multi-Mode LTC

Previously discussed advantages of LTC-HEV are all based on single LTC mode, while multi-mode LTC has been proven more efficient than single-mode LTC [100–102]. A multi-LTC SI-RCCI-HCCI engine was compared with two single-LTC engines, i.e., an RCCI engine and an HCCI engine, in a REEV platform [100]. Results showed a maximum of 1.4% fuel improvement over the single-mode HCCI or RCCI engine under the studied drive cycles, as depicted in Fig. 3.8. Another SI-RCCI-HCCI engine was applied to a series REEV, which offered 2% fuel benefit over the single-mode LTC-HEV [101]. Similarly, an SI-RCCI-HCCI engine was integrated with a parallel HEV, and results presented 8.8% fuel savings over an SI-HEV in UDDS and 1.8% in Highway Fuel Economy Test (HWFET).

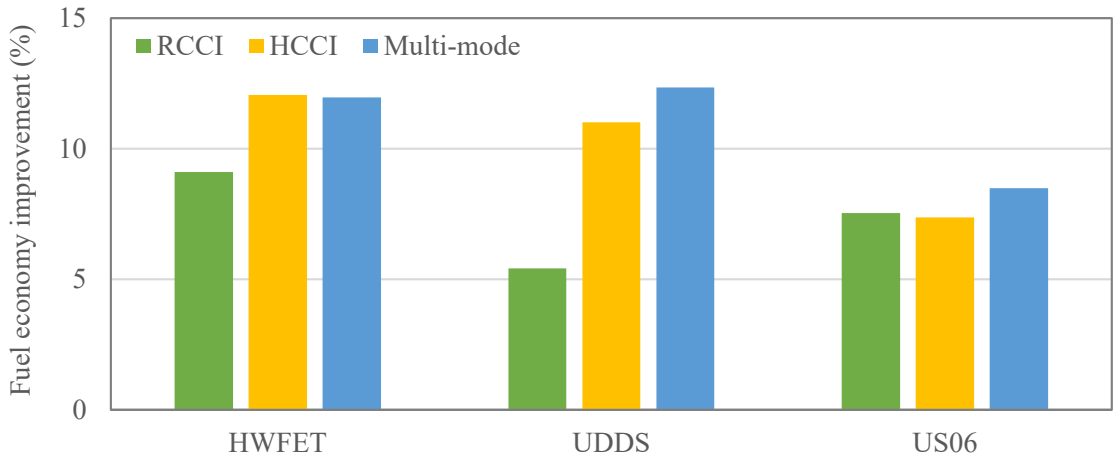

Figure 3.8: Fuel improvement under three drive cycles (data collected from [100]).

These works reveal that multi-mode LTC-HEVs can achieve a few percent of improvement over single-mode LTC-HEVs. However, the complex combustion control and

system design, such as fuel injection system adjustment, might offset these limited benefits. Therefore, it is interesting to see a quantification of such benefits and costs in future research.

3.3 Alternative Fuels

ICEs are popularized in the transportation industry because of their higher power density than other power systems. However, conventional ICEs use petroleum-based fuels and produce harmful emissions and greenhouse gas after combustion, leading to severe environmental challenges. As a result, cleaner alternative fuels are receiving more and more attention. Examples of alternative fuels are hydrogen (H_2), biodiesel, ethanol, compressed natural gas (CNG), liquefied natural gas (LNG), and electricity [103].

Compared to petroleum-based engines, alternative fueled (AF) ICEs are more beneficial to environment and public health due to less CO_2 and hazardous emissions [104]. On the other hand, electrified powertrains can be considered adopting the alternative fuel of electricity. Therefore, combining these two solutions gives the possibility of further improvement in performance, known as alternative-fueled HEV (AF-HEV). AF-HEVs can serve as a bridge to zero-emission alternative vehicles such as fuel cell electric vehicles (FCEVs) and battery electric vehicles (BEVs) [105].

3.3.1 Hydrogen Fueled HEVs

H_2, which can be obtained from natural resources and produce zero emissions when burned with oxygen, is considered the most promising alternative fuel [106]. The basics of H_2 as a sustainable energy source are explained in [107].

H_2 can be used in vehicles via two routes, either as the fuel of fuel cells to generate electricity or as the fuel of ICEs to combust. Since H_2 has a higher heating value and wide range of flammability, H_2-ICEs offer the advantages of a higher power, higher efficiency, and near-zero emission except for NO_x at high loads [108]. Manufacturers such as BMW [109], Mazda [110], and Aston Martin [111] have developed hydrogen-powered ICEVs for commercial and racing purposes.

However, pure H_2-ICEs have drawbacks of lower energy density, poor volumetric efficiency, and high self-ignition temperature [112]. As a result, an alternative way of using H_2 is mixing it into conventional fuels, known as H_2 enriched ICEs. There has been some work on H_2 enriched engines over the years [113–115], which present better fuel economy and lower emissions than ICEs with conventional fuels. However, such engines need an additional injection system and are therefore more complex than pure H_2-ICEs [116].

As HEVs play increasingly crucial roles in the automotive industry, attempts have been made to integrate H_2-ICEs into HEVs [108,112,117–119]. H_2-ICE powered HEVs are much less carbon-intensive and more fuel-efficient compared to petroleum-ICE-based HEVs. Ford Motor Company declared the industry's first hydrogen concept HEV, Ford H^2RV, which integrated a supercharged H_2-ICE [117]. Results showed that

the projected fuel economy could reach 45 miles per gallon (mpg), and emissions were near zero. However, the coexistence of H_2 and high voltage presented safety concerns. Following this, He X et al. designed a hybrid-electric sport utility vehicle (SUV) which was converted from a 2002 Ford Explorer and equipped with an H_2-fueled ICE [118]. Vehicle testing demonstrated the capability of storage and management of H_2 onboard the vehicle. Results indicated a gasoline-equivalent economy of 25 mpg, compared to 15-20 mpg in the original Explorer, with much lower emissions.

Apart from pure H_2-ICE HEVs, H_2 enriched ICE-powered HEVs have also been investigated [108, 119]. Although such vehicles are expected to have less benefit than pure H_2-ICE HEVs, they require fewer costs and easier implementation. Arat HT carried out an experimental study on an SI-HEV with 10% H_2 enrichment [108]. Results showed a 3.56% increase in engine torque and 2.37% in engine power. Fuel consumption and emissions were reduced by 12.6% and 14-33%, respectively, compared to the stock engine. A more striking comparison was conducted in another study [119], where four vehicles, including a diesel ICEV (V1), V1 with 8% H_2 enrichment (V2), hybrid versions of V1 (V3) and V2 (V4), were compared in terms of fuel consumption and emissions. Among all, V4 showed the highest fuel economy with a 14.32% improvement over V1. NO_x and CO_2 emissions were also reduced by 15% and 33%, respectively.

3.3.2 Other Alternative Fueled HEVs

Despite the benefit of hydrogen-powered vehicles, there are also drawbacks and limitations. Lack of appropriate infrastructure for hydrogen supply, high cost, and safety

issues are the biggest challenges [120]. As a result, using or mixing with other alternative fuels presents another promising path to reducing emissions and fuel costs.

Toyota gives an example of such alternative-fueled HEVs. In March 2018, Toyota revealed a prototype of the world's first hybrid electric flexible-fuel vehicle (FFV) in Brazil [121]. The prototype is claimed to combine Toyota's Hybrid Synergy Drive (HSD) with the FFV, which can be fueled by both gasoline and alternative fuels such as ethanol. Initial studies by Toyota indicated that the Hybrid FFV had great potential in CO_2 reductions. In research work [122], an SI-HCCI HEV fueled by methane (CH_4)-H_2 mixture was experimentally examined under different mixing ratios. Results indicated that adding H_2 to CH_4 was beneficial for the combustion process and emission reductions, especially in lean-burn operations. 80% CH_4 with 20% H_2 blend showed the best performance in most operating conditions, as shown in Fig. 3.9. In another study [123], a CNG engine was incorporated in a power-split hybrid powertrain, which declared a 55.9% improvement in fuel economy.

AF-HEVs have demonstrated significant emission reduction benefits with various alternative fuels and their blends. However, such vehicles require new fuel infrastructures, the investment cost of which is usually 4-6 times higher than using petroleum only [124]. At the same time, such vehicles enable simpler and cheaper aftertreatment systems, which may redeem these costs after all. Therefore, it is still recommended to study this subject in-depth in the next decade to exploit its potential thoroughly.

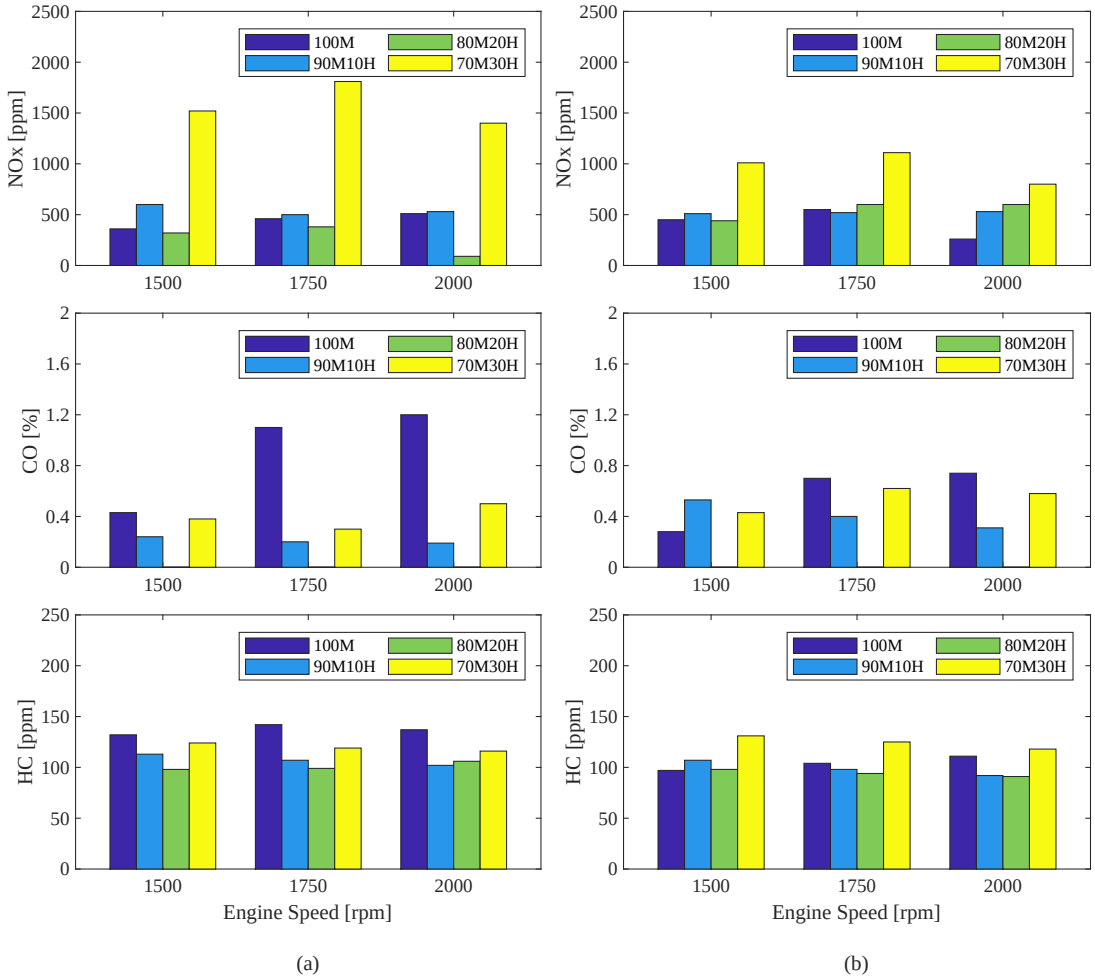

Figure 3.9: Emissions with different fuel blends at (a) 100% WOT; (b) 50% WOT (data collected from [122]).

3.4 Waste Heat Recovery

ICEs are heat engines that convert the chemical energy of fuels into kinetic energy of crankshafts. During the process, more than 60% of the total energy is contained in engine coolant and exhaust gases, later lost as heat [125]. A schematic of power flows in ICEs is shown in Fig. 3.10.

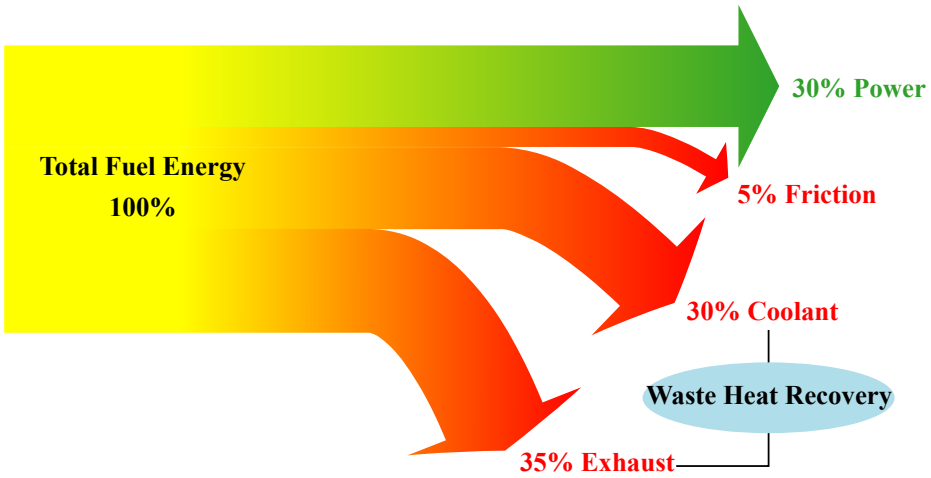

Figure 3.10: Schematic diagram of power flows in ICEs.

The technological solutions discussed previously aim at the in-cylinder process, while WHR aims at the after-combustion process. Instead of optimizing engine combustion, WHR improves fuel efficiency by directly recovering and reusing the wasted energy in engine coolant and exhaust. Although engines are not the only energy source of HEVs, the huge potential in waste heat is still worthy of investigation. Over the years, numerous WHR methods have been proposed and evaluated for automotive applications, among which thermoelectric generators (TEGs) and thermodynamic bottoming cycles have attracted the most attention. A comparison of the two techniques is given in Table 3.3.

Table 3.3: Comparison of TEGs and thermodynamic bottoming cycles.

	Heat source temperature	Advantages	Disadvantages
Thermo-electric generator	Medium/high (Exhaust gas)	Absence of moving parts; Silent operation; Compact system structure; High reliability & scalability; Low maintenance effort	Low efficiency; High cost; Transient control requirement; Engine backpressure increase
Thermo-dynamic bottoming cycle	Low/medium/ high (Coolant/ exhaust gas)	High efficiency; Flexible working fluid	Large scale; High cost; Complex system structure; Engine backpressure increase

3.4.1 Thermoelectric Generators

Among existing approaches, TEG offers the exclusive advantage of direct conversion of heat into electricity without any moving parts, which leads to a noiseless environment [126]. In addition, the compact configuration, high reliability and scalability, and low maintenance make TEGs more suitable for automotive applications [127].

Fundamentals of TEGs

TEG works on the Seebeck effect and converts the waste heat in engine exhaust gas into electrical energy. A general TEG system consists of multiple thermoelectric modules (TEMs) that generate electric current when there is a temperature difference between their ends. Each TEM consists of multiple thermoelectric couples (TCs) connected electrically in series and thermally in parallel. Each TC contains a pair

of p- and n-type semiconductors made with different materials [128]. The working principle of a single TC is depicted in Fig. 3.11.

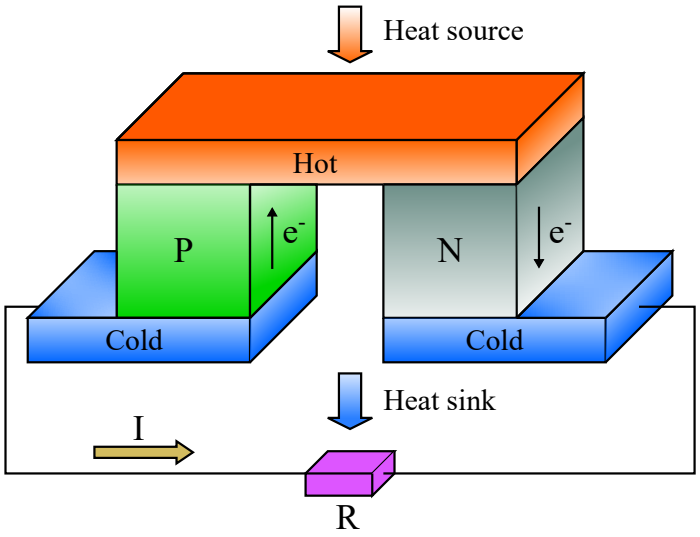

Figure 3.11: Working principle of a single TC.

Generally, there are two locations of TEGs found in the literature for automotive engines, either on the exhaust heat exchanger [129, 130] or on the engine cooling system [131]. Since the former has a simpler layout and higher temperature difference, it is more attractive for vehicle applications. TEMs are usually placed on the surface of an exhaust heat exchanger, and hot exhaust gas flows from inlet to outlet, providing thermal energy to the hot side of TEGs. For the cold side, a coolant heat exchanger is used to maintain the low temperature of the coolant [128]. A typical TEG system configuration is illustrated in Fig. 3.12. Besides the upper and lower sides, TEMs can also be placed on four sides of a flat heat exchanger [132], or all surfaces of a cylindrical heat exchanger [133].

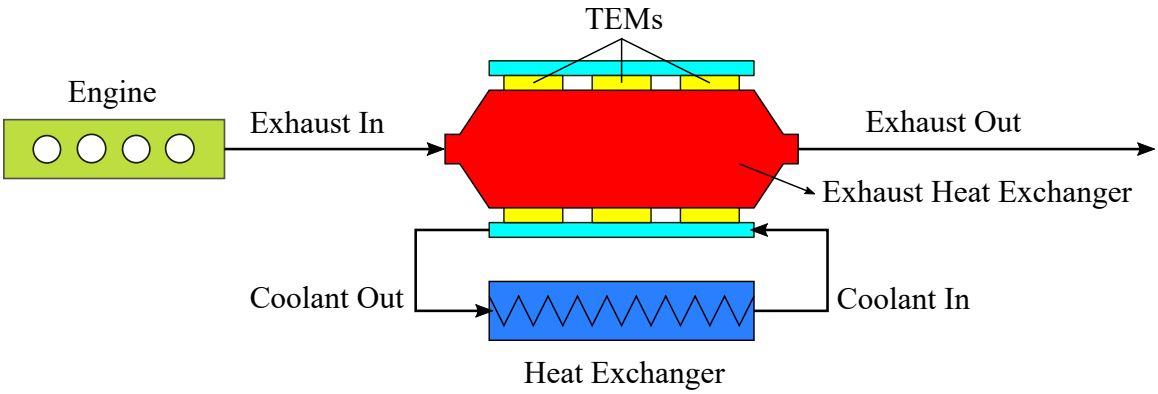

Figure 3.12: A typical TEG system configuration.

TEGs in HEVs

Previous studies on TEGs in conventional ICEVs are notably rich, and their potentials in fuel efficiency improvement have been widely proven [134–136]. In an ICEV, the electricity generated by TEG will be mainly used to power the vehicle's electrical accessories. However, in HEVs, the electrical energy can be fully utilized to either directly propel the vehicle or charge the battery for later use. These additional benefits motivate the expansion of TEGs to HEV applications. Fig. 3.13 presents the structure of a typical HEV integrated with a TEG system.

Over the years, major manufacturers such as BMW [137], Nissan [138], and Hyundai [139] have studied TEGs, and automakers such as Ford [140] and Honda [141] have designed prototypes for HEV applications. For example, the Ford TEG system has an exhaust heat exchanger with multiple parallel channels lined with thermoelectric material. The system claims a peak power of 414 W with 4.6 kg of thermoelectric material. The Honda TEG system includes a flat exhaust heat exchanger with 16 TEMs placed on each upper and lower side. The system is rated to produce a maximum

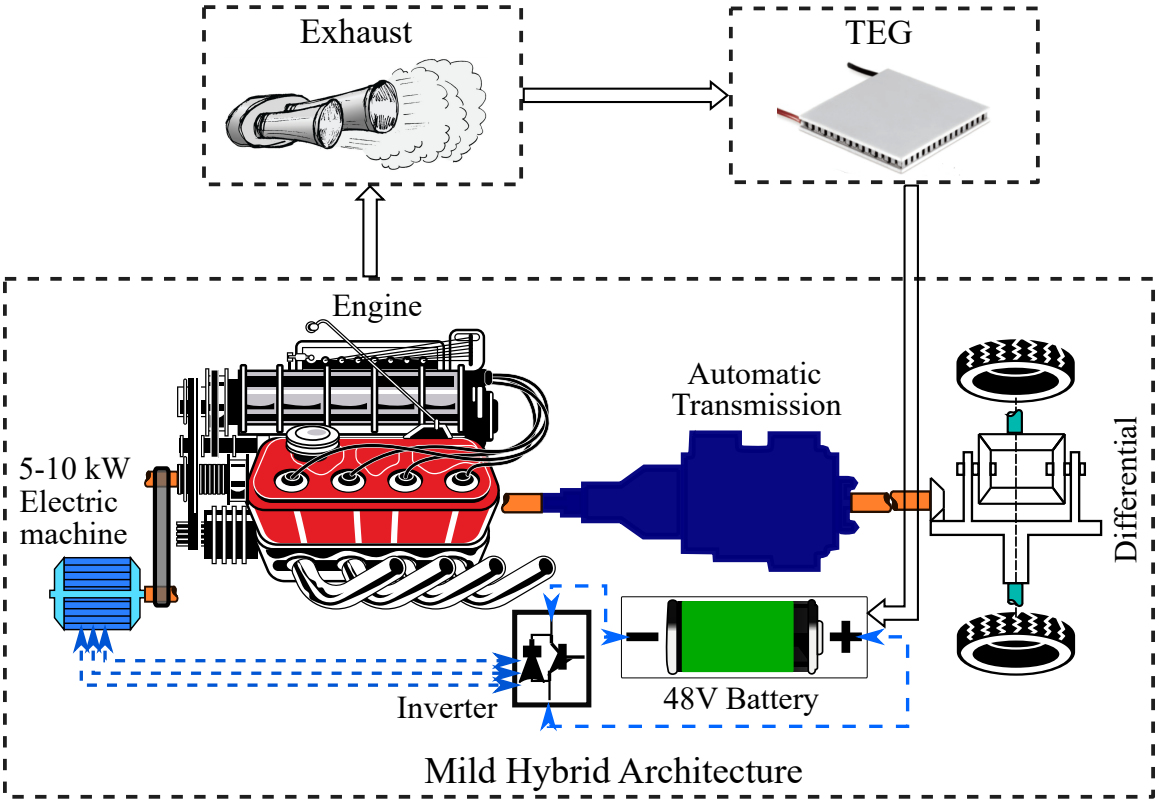

Figure 3.13: Structure of a typical TEG-HEV system.

power of 450 W and achieve 3% fuel improvement in the studied series HEV.

Since engines in HEVs mostly run at higher loads, the exhaust temperature of HEVs is usually higher compared to conventional ICEVs. Therefore, HEVs are considered a more advantageous platform to implement TEGs, which benefit from higher temperatures [142]. However, it is pointed out that not all types of HEVs are suitable for TEGs implementation. Mild HEVs with more engine operating time and higher exhaust energy are likely to be a better platform than full HEVs [143]. Wang R et al. proposed a novel TEG for a mild HEV [144], and results indicated 3.64% and 2.17% fuel savings in UDDS and HWFET, respectively, with slight emission reductions. Apart from mild HEV, TEG-WHR has also been integrated on series [141], parallel [145], power-split [146], and REEV [147] architectures.

The efficiency and power output of TEGs are influenced by engine speed, engine load, and other factors such as fabrication methods of TEMs [148]. Higher engine speeds and loads lead to higher exhaust temperature and mass flow rate, thus higher conversion efficiency and power output due to more significant temperature differences across TEG. It was found that the efficiency of a TEG system for a power-split HEV was around 6% at 2000 rpm, and a maximum power of 1015 W was achieved at 5200 rpm [148]. In another study [149], a compact TEG system targeting a sedan-type HEV showed a maximum power and efficiency of 118 W and 2.1%, respectively, under the highest engine speed-load condition.

The biggest concern about TEG-HEVs is the intermittent engine operations and less energy in the exhaust gas due to higher engine efficiency [145]. However, it is shown that the exergy in the exhaust gas of HEVs might be even higher than conventional

vehicles due to the higher temperature, thus higher potential for TEG-HEV applications [146]. Another concern about TEG systems is the effect of additional weight on vehicle fuel economy, which may increase the burden of vehicle power sources and result in lower mileage or higher fuel use. However, most studies on TEG-HEVs have reported positive benefits when considering the weight of TEG devices [140, 145, 150]. It was claimed that the additional weight of TEG systems had negligible effects on vehicle fuel economy [150].

It is not hard to find from the literature that the efficiency of TEG systems is relatively low, which results from the poor conversion performance of current thermoelectric materials and the slight temperature difference across TEMs. However, as suggested in [151], the TEG system efficiency will be allowed to achieve 15% or higher in the future, along with the progress in material science and nanotechnology.

3.4.2 Thermodynamic Bottoming Cycle

Thermodynamic bottoming cycles are another solution to recover and convert the waste heat of engines into usable work. Organic Rankine cycle (ORC) [152], Kalina cycle [153], and Brayton cycle [154] as ICE-WHR systems have been extensively investigated by scholars and original equipment manufacturers (OEMs). Among them, ORC has the advantages of simple structure, suitable size, high reliability, and capability of recovery from both low- and moderate-grade waste heat sources, i.e., engine coolant and exhaust gas, respectively, thus preferred in ICE-WHR applications [155]. Manufacturers and research groups, such as Cummins [156], Bosch [157], Eaton [158], AVL [159], BMW [160], and Oak Ridge National Laboratory (ORNL) [161], have all

studied ORC-WHR systems for automotive applications.

Organic Rankine Cycle

Generally, an ORC system includes a pump, an evaporator, an expander, and a condenser. The organic working fluid is first pumped to the evaporator and heated by exhaust gas and coolant until evaporated. The high-pressure vapor then arrives at the expander, where the thermal energy is converted into mechanical work and drives the generator. In such a way, the waste heat contained in engine exhaust gas and coolant is recovered. After expansion, the working fluid is cooled by air or water in the condenser, and a new cycle starts afterward. Fig. 3.14 illustrates a typical ORC-WHR system for both engine exhaust gas and coolant.

Over the years, lots of studies have been published on engine ORC-WHR in respect to system configuration [162, 163], component design, e.g., heat exchanger [164, 165], expander [166, 167], and pump [168, 169], as well as working fluid selection [170, 171].

The existing ORC-WHR system configurations can be classified into basic Rankine cycle (B-RC) and B-RC-based modifications, including regeneration-based Rankine cycle (R-RC) and multi-loop Rankine cycle (RC), i.e., cascade-based Rankine cycle (C-RC) and duel-pressure-cycle-based Rankine cycle (D-RC). The modified configurations have a better thermodynamic performance due to the improved thermal matching in both high- and low-temperature cycles [172].

Heat exchangers in ORC-WHR systems include evaporators, condensers, and regenerators in R-RC configurations. Shell-tube [173] and plate [174] heat exchangers

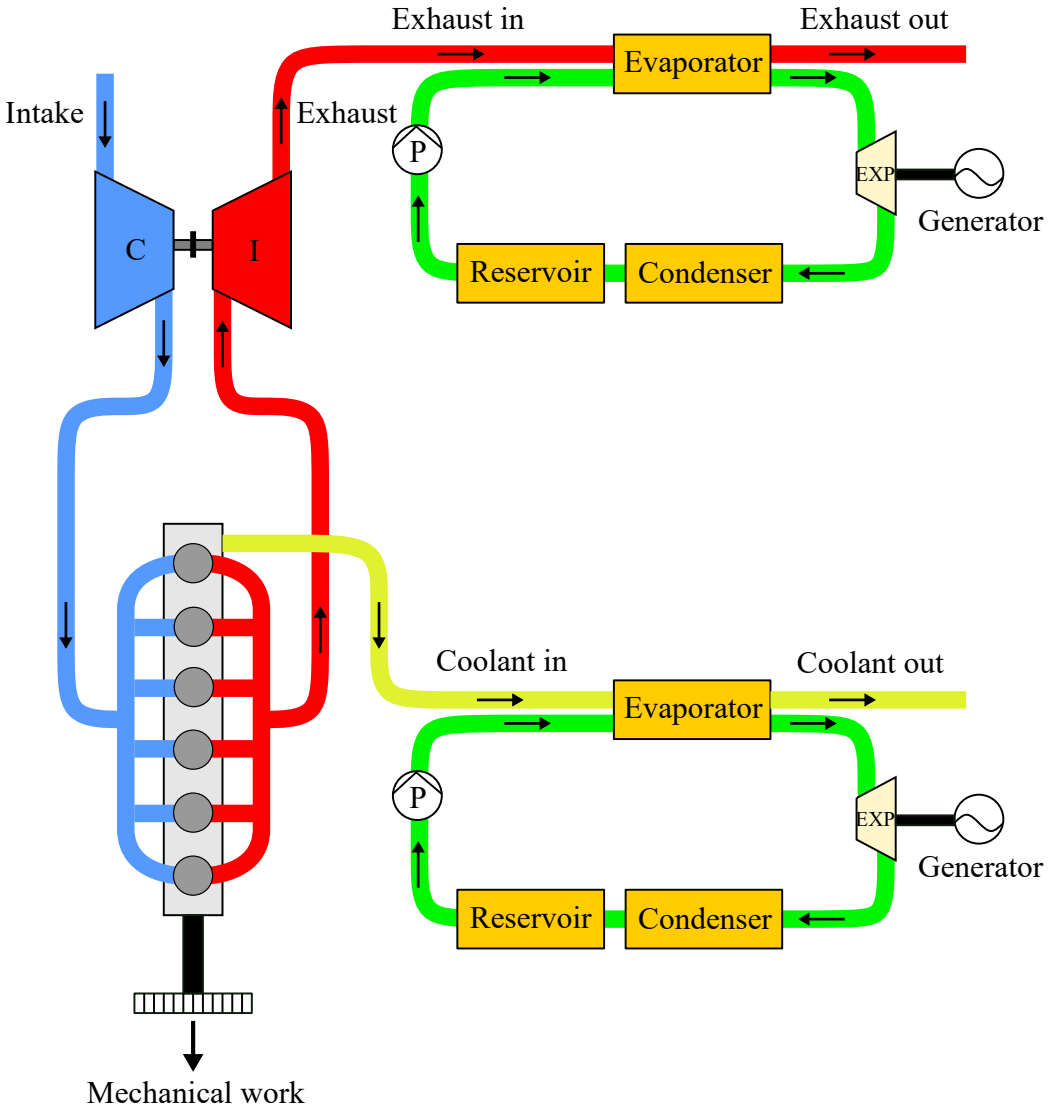

Figure 3.14: Working principle of engine ORC-WHR system.

are the two most common types in ORC-WHR applications. Shell-tube heat exchangers are recommended for evaporators, and plate heat exchangers are preferred in condensers and regenerators [172]. Measures such as inserting fins [173, 174] and metal-foam structures [175,176] are expected to further enhance heat transfer performance. However, trade-offs exist between performance and practical concerns such as increased pressure drop, clogging issues, larger weight, and higher cost.

As the most crucial component of RC systems, expanders significantly influence WHR system efficiency. Generally, expanders in RC systems can be categorized as velocity type (e.g., axial turbine, radial turbine) and volume type (e.g., scroll expander, screw expander) [177]. Among them, turbines are considered the most promising for automotive applications due to the higher efficiency and power output [172]. Pumps in RC systems can be placed in one of these two categories: volumetric pumps [178] or centrifugal pumps [179]. They are usually coupled with expanders to save space and reduce weight [172].

Working fluid selection requires special attention when designing RC systems. Safety issues, environmental impacts, thermo-economic properties, compatibility with vehicles, etc., must be carefully evaluated before applying to vehicles [152]. However, it is a consensus that a single fluid can hardly meet all the requirements [180]. Therefore, trade-offs must be made for a specific case. In ORC systems, organic fluids are adopted as working fluids, most of which are either dry fluids, e.g., R245fa and R245ca, or isentropic fluids, e.g., R123 and R134a [152]. Although traditional refrigerants have been widely researched, there are challenges such as thermal instability and environmental impact. As a result, other working fluids, i.e., CxHyOz, CO_2, and

unconventional working fluids such as nanofluids, have been recently explored, which exhibit promising potentials in the above aspects [172].

ORC in HEVs

Past efforts in ORC-WHR technology have primarily focused on conventional ICEVs, while it is necessary to understand its benefits and limitations in electrified powertrains. Fig. 3.15 presents a typical HEV-ORC-WHR system. Series hybrid [181], parallel hybrid [182–184], and plug-in hybrid [185] architectures have been studied, and aspects of system layout, working fluid selection, and effects of driving conditions and control strategies have been discussed.

System layouts of HEV-ORC-WHR can be different. The recovered mechanical energy after the expander can be converted into electrical energy through a generator, as shown in Fig. 3.15, and then stored in a battery pack to charge the battery, power auxiliaries, or function as a range extender. Alternatively, the mechanical energy can be directly transferred to the engine crankshaft [186]. However, such a method may deteriorate the benefits of ORC-WHR systems for the following reasons. First, with the help of WHR systems, less fuel has to burn to satisfy the power demand for the engine, leading to a lower exhaust temperature and mass flow rate, thus reducing the potential of WHR. In addition, the expander speed is imposed by engine speed due to the mechanical connection, thus not controllable.

In contrast, in the first method, the expander speed can be varied to adjust and optimize working fluid pressure at the expander inlet. Besides, such configurations

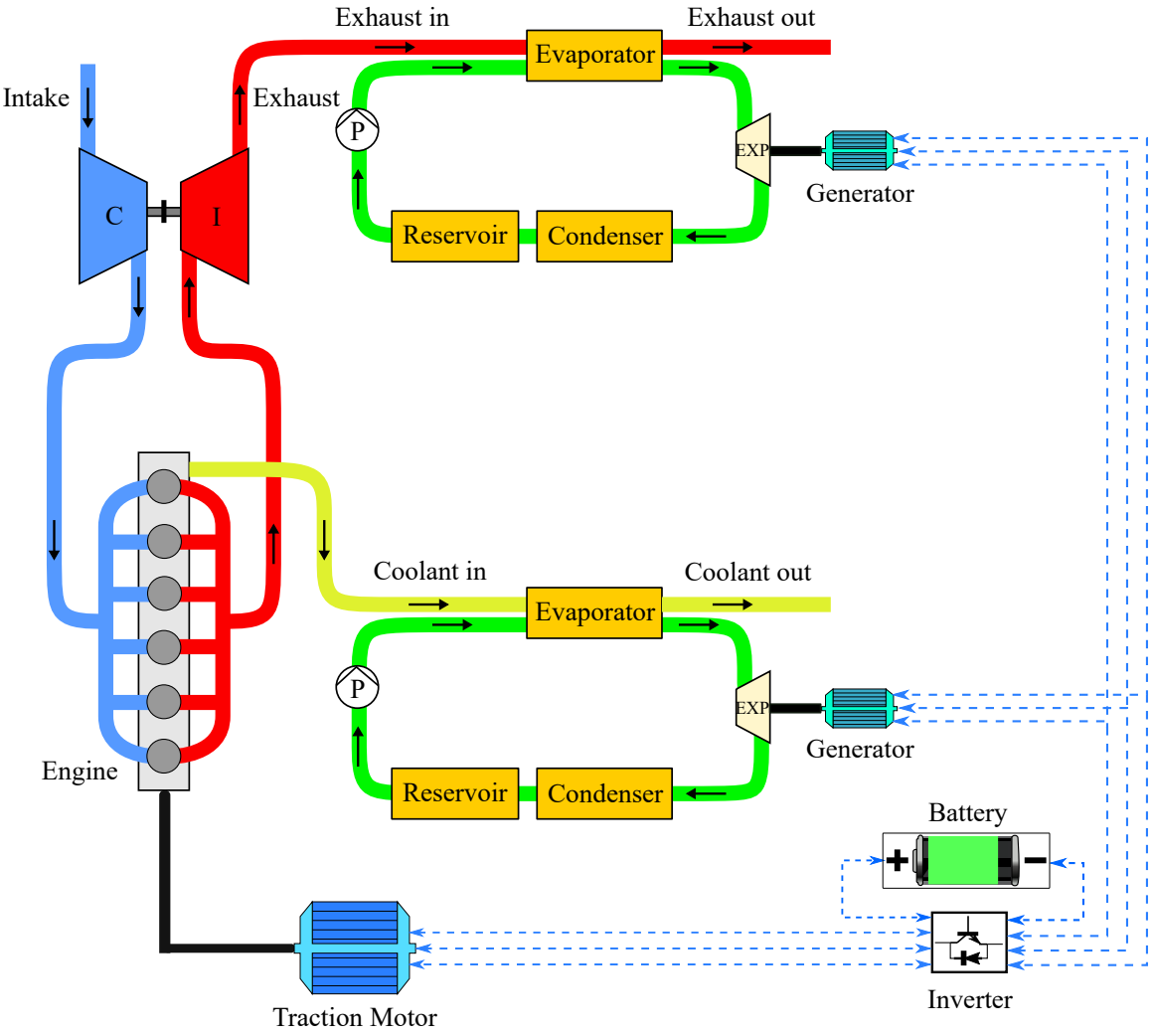

Figure 3.15: System layout of ORC-WHR in HEVs.

can produce and store energy when there is no power demand for the engine, taking advantage of the thermal inertia of evaporators and ATS [187]. Therefore, the first method is more applicable in performance and control feasibility, even though an additional energy conversion from mechanical to electrical will cause extra energy loss.

Based on this configuration, two different layouts regarding the pump are proposed [186]. The pump is directly connected to and powered by the expander through a gearbox in one layout. In the other layout, the pump is powered by an additional EM whose power is provided by the battery. The second layout claims to have higher instantaneous power but lower total stored energy due to the long energy conversion chain.

In order to maximize the HEV-ORC-WHR system efficiency, working fluid must be selected properly. Five working fluids, including dry types, i.e., R134a, R245fa, and R1234yf, and wet types, i.e., water and ethanol, were evaluated for a CNG engine based HEV [181]. Considering system efficiency and practical operating limitations, R245fa was suggested the optimal working fluid with the best overall performance [188]. Apart from R245fa, R1234yf [189], toluene [183, 190], and ethanol [187] have also been found in HEV-ORC-WHR systems.

A major challenge for ORC-WHR in automotive applications is its response to transients since it takes a finite amount of time to reach a certain temperature and pressure for the system to work [191]. Frequent shifting of engine operating points will cause dramatic variations in the exhaust gas, making system control challenging. Electrified powertrains enable engines to be less dependent on road loads, thus more adaptable

to fast-varying driving conditions.

Kruijt K et al. implemented ORC-WHR on a hybrid heavy-duty truck, which declared 2.5% fuel reduction under UDDS [182]. Mansour C et al. examined a mild HEV equipped with ORC-WHR for engine coolant [184]. Results showed a slight improvement in engine and powertrain efficiency, with 2% and 2.4% fuel reduction, respectively, under NEDC and Worldwide Harmonized Light Vehicles Test Procedure (WLTP). Andwari AM et al. studied an ORC-WHR system for a lightweight HEV [188]. Results indicated 10%, 8%, and 7% improvement under FTP-75, NEDC, and US06, respectively. It is revealed from the literature that HEV-ORC-WHR systems are more beneficial for medium- and high-duty trucks, which primarily run on suburban and highway conditions. Therefore, even though HEVs offer the exclusive advantage of independent engine operations, it is still encouraged to apply ORC-WHR systems to HEVs with steadier engine operations such as hybrid trucks.

Brayton Cycle in HEVs

Apart from ORC, Brayton cycle has also been studied to integrate into HEV-WHR. Compared to ORC, the Brayton cycle avoids the need for a condenser since it runs as an open system with air as the working fluid, making it easier to integrate into vehicles. Nader WB et al. conducted a comprehensive assessment on a simple Brayton-WHR system for a series HEV [192]. Considering the added weight by the WHR system, six different Brayton layouts were modeled and compared in terms of fuel consumption. Results indicated that the Brayton cycle with an intercooler offered

the best trade-off between efficiency and complexity, achieving 5.5-7.0% fuel improvement.

3.5 Challenges and Recommendations

As reviewed thus far, advanced hybrid engine technologies present great potential for further fuel economy and emission improvement. Advantages and disadvantages of each reviewed technology are summarized in Table 3.4. Although great progress has been made, significant issues remain to be resolved. This section discusses the major challenges of each reviewed technology, based on which recommendations are provided subsequently.

3.5.1 Over-expansion Cycle

Challenges: The primary challenge for over-expansion engines is the reduced power density due to the charge backflow in Atkinson engines and the reduced valve period in Miller engines. Although electric motors can compensate for the peak power deficiency at high loads in hybrid powertrains, a higher power density is still desired since it enables engine downsizing, which benefits fuel economy.

Recommendations: One recommendation is to use the Otto cycle with the Atkinson cycle in one engine, which operates on the Otto cycle at high loads and the Atkinson cycle at low/medium loads. At higher loads, the Otto cycle intends to increase the power density. Technical measures such as VCR can mitigate the possible knock

Table 3.4: Summary of the reviewed engine technologies.

Technologies	Advantages	Disadvantages
Atkinson cycle	• Higher fuel efficiency • Lower emissions • Compensated power deficiency by electric motors in HEVs	• Reduced peak power & power density • Increased system complexity
LTC	• Higher fuel efficiency • Lower emissions • Simpler & cheaper aftertreatment systems • Fewer transients and easier combustion control due to steadier engine operations in HEVs	• Narrow operating range • Complex combustion control
Alternative fuels	• Significant emission reduction • Better fuel economy • Simpler & cheaper aftertreatment systems	• New fuel infrastructure • Additional fuel injection system • Safety concern • High cost
WHR	• Fuel-saving potentials • Full utilization of generated electric energy for HEV propelling or battery charging • Easier system control due to steadier engine operations enabled by HEVs	• Cost ineffective • Low efficiency • Safety concern • Complex system structure • Complex control design • Increased engine backpressure

issues. At lower loads, the Atkinson cycle is implemented by retarding the valve timing upon the Otto cycle to improve fuel efficiency. Another solution is to use a turbocharged Miller cycle, so the boosted intake pressure can even out the charge loss caused by backflow.

3.5.2 LTC

Challenges: The main obstacles facing LTC engines in hybrid applications are the narrow operating range and complex combustion control.

Recommendations: One recommendation is to increase the in-cylinder fuel stratification to shift from kinetic-driven combustion to injection-driven combustion to improve controllability and operable range. Another suggestion is to investigate suitable fuels. For example, low-octane gasoline is a promising fuel type for LTC engines since its autoignition process is proven sensitive to changes in the equivalence ratio, which can be an indicator for combustion control.

3.5.3 Alternative Fuels

Challenges: The most challenging task of developing alternative-fueled engines for hybrid applications is to find a high-performance, cost-effective fuel solution.

Recommendations: Engineering always involves making trade-offs. The economic performance of alternative-fueled engines is the primary interest of the automotive

industry. Therefore, a comparative analysis of fossil fuels and alternative fuels addressing the economic performance of each fuel type is recommended. Factors including the initial research and development cost, the fueling infrastructure cost, the carbon tax reductions, possible fuel-savings income, etc., should be considered while conducting the research. In the meantime, more research efforts should be put into investigating new alternative fuels and fuel blends such as biodiesel, dimethyl ether (DME), etc.

3.5.4 WHR

TEG

Challenges: The biggest limitation of HEV-TEG applications is the relatively low efficiency. Besides, although hybrid powertrains enable steadier engine operations, the transient nature of the exhaust gas is still a major concern.

Recommendations: The maximum TEG efficiency can be expressed as:

$$\eta_{TEG,max} = \frac{T_h - T_c}{T_h} \frac{\sqrt{1+zT}-1}{\sqrt{1+zT}+\frac{T_c}{T_h}} \tag{3.5.1}$$

where T is the operating temperature, which is the mean value of the hot side temperature T_h and cold side temperature T_c. z and zT are the figure of merit and dimensionless figure of merit of the thermoelectric material. Equation (3.5.1) reveals

that a rise in zT value contributes to an increase in TEG efficiency. Therefore, introducing more efficient thermoelectric materials with higher zT values is beneficial.

To translate the benefits from the material level to the component level and further to the device level, bonding techniques and integrated designs are also highly recommended [11]. On the other hand, previous studies have mainly focused on steady-state behaviors, while transient state analysis should be addressed to bridge the gap [193].

Thermodynamic Bottoming Cycle

Challenges: Although thermodynamic bottoming cycles generally exhibit higher efficiency than TEGs, major challenges must be addressed to advance toward commercialization. Working fluid selection and system control are two critical issues.

Recommendations: Working fluids in bottoming cycles must be safe and efficient with specific thermodynamic properties. However, it is hardly possible and time-consuming to find such a one that meets all the requirements. Therefore, one recommendation is to design new working fluids as per requirement instead of choosing from the existing ones, which can be achieved by adjusting the mixture compositions and ratios [172]. For system control, coordinated control schemes integrating HEV controllers with WHR control modules are required to adapt to the varying engine operations.

3.6 Opportunities for Simplification

Engine designs always involve making trade-offs. Previously discussed engine technologies improve the engine performance but also pose extra challenges such as additional complexity and cost. Therefore, the most efficient and powerful engine might not be the best hybrid engine in real practice. Engine designs for hybrid applications should depend on the mission of an engine in a hybrid platform, which also varies with hybrid architectures.

More specifically, as one of the two/multiple power sources in HEVs, hybrid engines are offered the advantage of being assisted by the battery and electric motors. As a result, hybrid-optimized engines can break the paradigm of pursuing power and efficiency as in traditional ICE-only vehicles and create the opportunity to be simplified and downsized.

For example, in conventional ICEVs, engines should be efficient over the entire speed-load map. However, in HEVs, engines can operate in high-efficiency regions only. Therefore, engine optimization can only aim at high-efficiency regions, and technology elements targeting low-efficiency regions can be removed. Another example is vehicle accessories. All traditionally engine-drive accessories, e.g., alternator, water pump, power steering, air conditioning, can be electrified in HEVs. Therefore, the engine accessory drive can be eliminated.

3.7 Summary

As one of the power sources in electrified powertrains, the engine is a crucial component that significantly impacts the performance of HEVs. Recent years have witnessed tremendous effort toward energy-efficient engine technologies for hybrid applications. Over-expansion cycle, LTC concept, alternative fuels, and WHR techniques provide the most promising technology pathways to clean and efficient hybrid powertrain specific engines. This chapter provides a comprehensive review of each technology, including their working principles, influencing factors, benefit potentials, advantages, and disadvantages. A summary specifying the challenges of each technology pathway is provided, followed by respective recommendations. Finally, opportunities for simplification from a hybrid-optimized engine standpoint are identified.

Chapter 4

Real-time Energy Management for a Power-split Hybrid Electric Vehicle Considering Inertial Dynamics of Powertrain Components

Chapter 3 presents a thorough analysis of technology pathways to energy-efficient hybrid engines, and the rest of the thesis intends to improve HEV system efficiency through the pursuit of improved energy management strategies.

According to the literature review, most disclosed studies on HEV EMS are based on steady-state assumptions where real-world powertrain dynamics are neglected for the sake of simplicity. However, when such strategies are used in real-world driving tasks with dynamic vehicle operations, the lack of consideration of powertrain dynamics for vehicle control strategies will lead to infeasible control solutions and deviations from the predicted fuel economy. Therefore, incorporating powertrain dynamics presents an effective way to improve HEV EMS.

Inertial dynamics of rotational powertrain components such as the engine, electric motors, and the transmission output shaft are important dynamic features of HEVs, especially during mode transition operations. However, they are usually overlooked in previous HEV EMS designs. For example, Chen et al. proposed an intelligent ECMS for a power-split PHEV [194]. It was mentioned that the dynamic characteristics of the hybrid system were neglected in the powertrain modeling to simplify the EMS design. Zhang et al. introduced an ECMS where battery aging was considered, but dynamics of powertrain rotating components were still ignored [39]. Sun et al. designed an adaptive ECMS for a power-split HEV based on a control-oriented vehicle model without inertial dynamics [195]. Atriya et al. investigated the effects of coordinated control on ECMS for a multi-mode hybrid electric powertrain [26]. Although the control strategy was tested on a dynamic powertrain model, the inertial dynamics were not built into the HEV EMS.

To the author's knowledge, the impacts of powertrain inertial dynamics on HEV EMS have not yet been addressed in the literature. In this context, this chapter contributes to filling the research gap by proposing a real-time HEV control strategy considering the inertial dynamics of the powertrain. First, a control-oriented HEV model of a power-split configuration is built in MATLAB® and Simulink®, based on which a real-time ECMS accounting for the rotational inertia of major powertrain components is designed. Then, a comparative study is performed between the proposed dynamic ECMS and a baseline steady-state ECMS without considering inertial dynamics. Simulation results are compared in terms of battery SOC, vehicle mode shifts, powertrain dynamics, engine operation, and fuel consumption.

4.1 Hybrid Powertrain System and Modeling

This section introduces the second-generation Toyota hybrid system (HSD), used in the 2010 third-generation Prius. A schematic of the hybrid powertrain system is illustrated in Fig. 4.1. Details of the vehicle specifications and modeling approaches are explained in the following text.

4.1.1 Hybrid Synergy Drive

The third-generation Prius is equipped with a 1.8-liter Atkinson-cycle gasoline engine and a 1.3-kWh nickel-metal hydride (NiMH) battery, achieving a total power of 100 kW [196]. Detailed parameters of the vehicle are specified in Table 4.1.

Table 4.1: Vehicle specifications of the power-split HEV.

Component	Parameter	Value
Vehicle	Equivalent mass	1531 kg
	Wheel radius	0.3173 m
	Road load coefficient μ_1	82.2921 N
	Road load coefficient μ_2	0.2224 N/(m/s)
	Road load coefficient μ_3	0.4031 N/(m/s)^2
Transmission	PG1 ratio (Ring/Sun)	78/30
	PG2 ratio (Ring/Sun)	58/22
	Final drive ratio	3.268
	Mass moment of inertia	0.1 kg $\cdot$ m^2
Engine	Displacement	1.8 L
	Idle speed	600 rpm
	Maximum power	73 kW
	Maximum torque	142 Nm
	Maximum speed	5500 rpm
	Mass moment of inertia	0.128 kg $\cdot$ m^2
MG2	Maximum power	60 kW
	Maximum torque	200 Nm
	Maximum speed	13000 rpm
	Mass moment of inertia	0.0226 kg $\cdot$ m^2
MG1	Maximum power	42 kW
	Maximum torque	40.8 Nm
	Maximum speed	13500 rpm
	Mass moment of inertia	0.01 kg $\cdot$ m^2
Battery	Capacity	6.5 Ah
	Nominal voltage	201.6 V
	Maximum voltage	252 V
	Minimum voltage	168 V
	Maximum power	27 kW

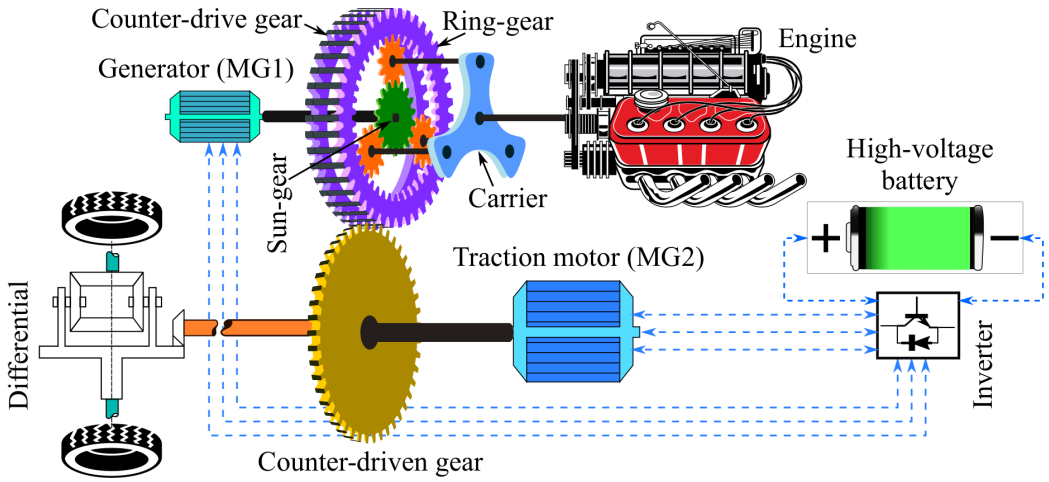

Figure 4.1: Schematic diagram of powertrain configuration in 2010 Toyota Prius.

The hybrid electric powertrain is integrated with two planetary gear (PG) systems, a power-split PG and a motor speed reduction PG. They coordinate powertrain components during driving and allow various power flow schemes from the engine and battery to the driving wheels. The primary electric motor (MG2), coupled to the output shaft through a gear reduction ratio, can provide traction power to assist propulsion or work as a generator during regenerative braking to recharge the battery. A secondary electric motor (MG1) and the ICE are connected to the sun (S1) and carrier gear (C1), respectively, of the power-split PG, which splits the engine power into two paths.

On one path, engine power directly flows from the carrier gear through the ring gear to the driving wheels. On the other path, MG1 performs as a generator to transfer engine power to the battery, where the charged electrical energy supplies MG2 to propel the vehicle eventually. The transmission system, referred to as an electronically controlled continuously variable transmission (ECVT), relies on the electric motors to continuously vary the gear ratios between the engine and the wheels

so that engine speed and torque can be optimized to maximize the entire hybrid system efficiency [197].

The hybrid system enables two driving modes, i.e., all-electric and hybrid-electric. In all-electric mode, the engine is shut down, the propelling torque is provided by MG2 only, and MG1 spins without delivering any torque. In hybrid electric mode, the vehicle is propelled by the engine and MG2, and MG1 applies reaction torque on the PG.

4.1.2 Control-Oriented Vehicle Model

Engine

Since the energy management problem in this chapter aims at fuel economy optimization, only fuel consumption is concerned in engine modeling. The BSFC map, as shown in Fig. 4.2, is employed to calculate the fuel mass flow rate of the engine. Furthermore, the actual outputs of engine speed and torque are constrained by physical limits, as expressed in Eq. (4.1.1), where ω_{ICE} and T_{ICE} are engine rotational speed and torque, respectively.

$$\begin{cases} \omega_{ICE,min} \leq \omega_{ICE} \leq \omega_{ICE,max} \\ T_{ICE,min} \leq T_{ICE} \leq T_{ICE,max} \end{cases} \tag{4.1.1}$$

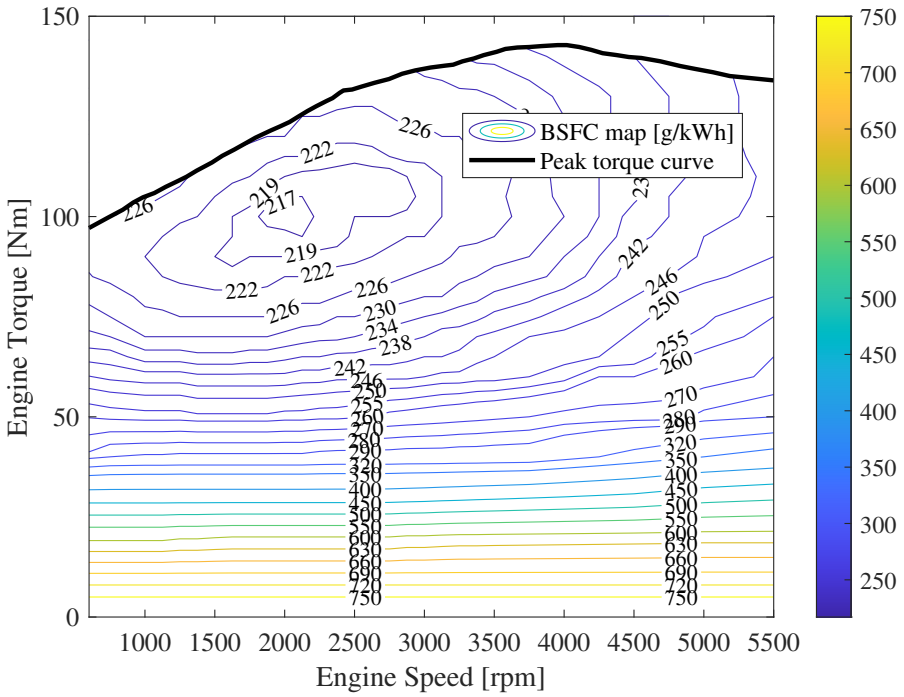

Figure 4.2: Engine BSFC map.

Motor

The two electric motors are modeled based on combined efficiency maps that specify the conversion between mechanical power and electrical power. The motor torque output is bounded by its upper and lower limits, as shown in Eq. (4.1.2) and (4.1.3):

$$P_{elec,m} = \begin{cases} T_m \omega_m / \eta_m(T_m, \omega_m), & T_m \geq 0 \\ T_m \omega_m \eta_m(T_m, \omega_m), & T_m < 0 \end{cases} \tag{4.1.2}$$

$$T_{m,min}(\omega_m) \leq T_m \leq T_{m,max}(\omega_m) \tag{4.1.3}$$

where $P_{elec,m}$, T_m, and ω_m are motor power, torque, and speed, respectively. η_m is the motor efficiency, which is a function of motor torque and speed. Fig. 4.3 and 4.4 present the efficiency maps of MG1 and MG2, respectively.

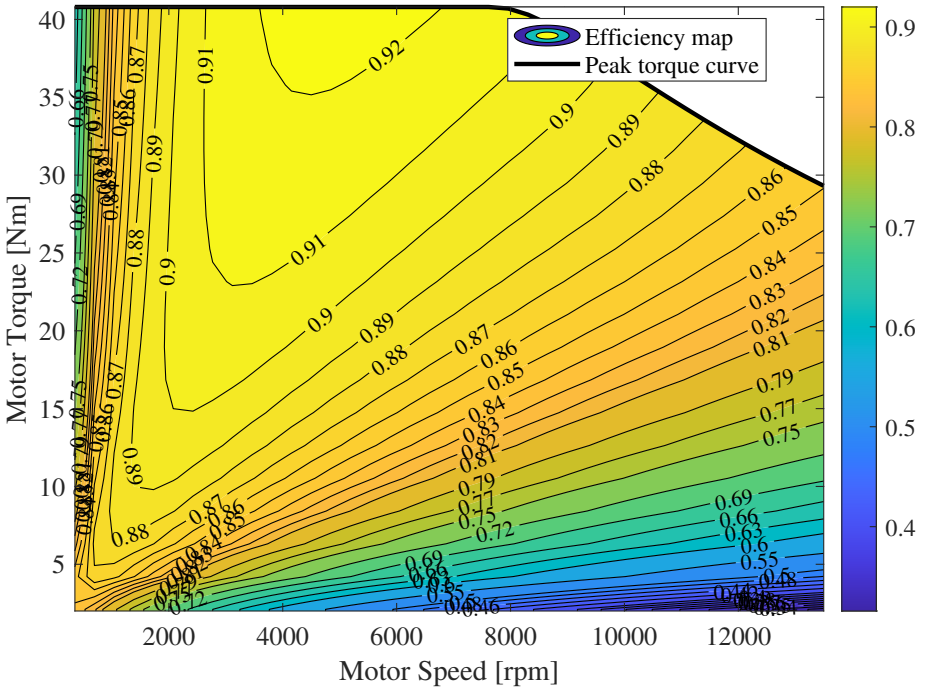

Figure 4.3: MG1 efficiency map.

Battery

The battery pack is modeled by the equivalent circuit approach. The battery current can be calculated from Ohm's law, as given in Eq. (4.1.4):

$$I_{batt}(t) = \frac{V_{oc}(SOC) - \sqrt{V_{oc}(SOC)^2 - 4R(SOC)P_{batt}}}{2R(SOC)} \tag{4.1.4}$$

where V_{oc} and R are battery open circuit voltage and internal resistance, which both

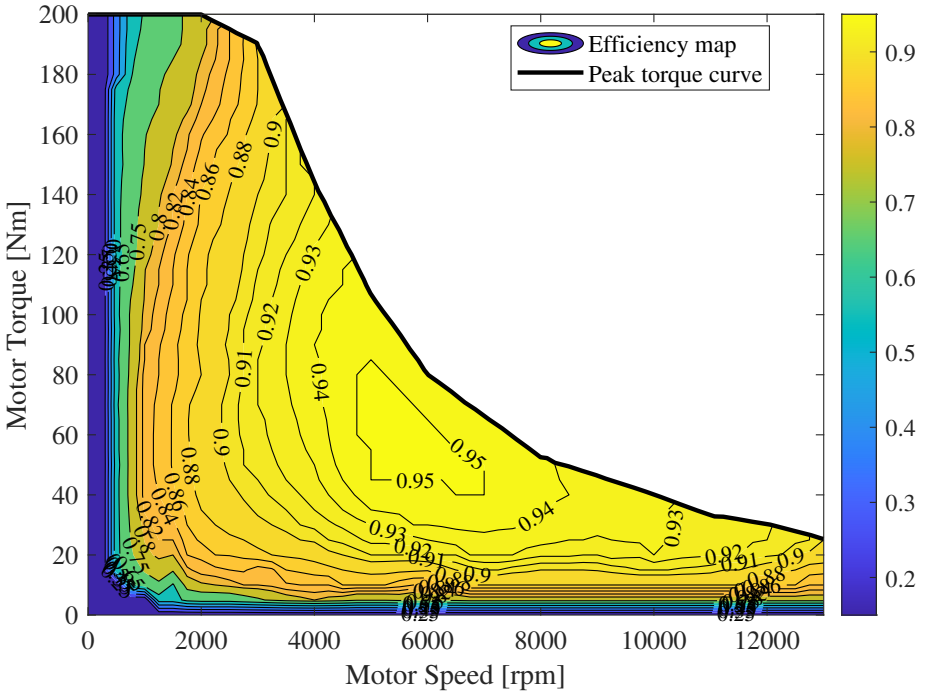

Figure 4.4: MG2 efficiency map.

depend on battery SOC. P_{batt} denotes the battery power. The battery terminal voltage and SOC can be then obtained from current, as shown in Eq. (4.1.5) and (4.1.6), where $SOC(t_0)$, η, and Q_{batt} are the initial SOC, coulombic efficiency, and battery capacity, respectively.

$$V_t = V_{oc}(SOC) - R(SOC)I_{batt}(t) \tag{4.1.5}$$

$$SOC(t) = SOC(t_0) - \frac{\eta}{Q_{batt}} \int_{t_0}^{t} I_{batt}(t)dt \tag{4.1.6}$$

Planetary Gear System

For HEV control strategies considering powertrain inertial dynamics, the PG dynamics are a matter of concern. Considering the rotational inertia of MG1, MG2, engine, and the transmission output shaft while neglecting the inertia of gears in PG sets, the dynamics of the power-split system can be illustrated by the lever diagram shown in Fig. 4.5. The rotational acceleration and torque relations of the powertrain components are described by Eq. (4.1.7):

$$\begin{bmatrix} 1 & 0 & \dfrac{1}{1+\beta_1} & 0 \\ 0 & \beta_2 & \dfrac{\beta_1}{1+\beta_1} & 1 \\ 0 & 0 & 0 & 0 \\ 0 & 0 & 0 & 0 \end{bmatrix} \begin{bmatrix} T_{MG1} \\ T_{MG2} \\ T_{ICE} \\ T_{OUT} \end{bmatrix} = \begin{bmatrix} J_{MG1} & 0 & \dfrac{1}{1+\beta_1}J_{ICE} & 0 \\ 0 & \beta_2 J_{MG2} & \dfrac{\beta_1}{1+\beta_1}J_{ICE} & J_{OUT} \\ 1 & 0 & -(1+\beta_1) & \beta_1 \\ 0 & -1 & 0 & \beta_2 \end{bmatrix} \begin{bmatrix} \ddot{\theta}_{MG1} \\ \ddot{\theta}_{MG2} \\ \ddot{\theta}_{ICE} \\ \ddot{\theta}_{OUT} \end{bmatrix} \tag{4.1.7}$$

where T_{MG1}, T_{MG2}, T_{ICE}, and T_{OUT} represent the torque of MG1, MG2, engine, and the transmission output shaft, respectively. J_{MG1}, J_{MG2}, J_{ICE}, and J_{OUT} represent the mass moment of inertia of MG1, MG2, engine, and transmission output shaft, respectively. $\ddot{\theta}_{MG1}$, $\ddot{\theta}_{MG2}$, $\ddot{\theta}_{ICE}$, and $\ddot{\theta}_{OUT}$ represent the rotational acceleration of MG1, MG2, engine, and transmission output shaft, respectively. β_1 and β_2 are gear ratios of PG1 and PG2, respectively. Rearranging Eq. (4.1.7) derives the rotational acceleration and torque relations of the powertrain components as given in Eq. (4.1.8)

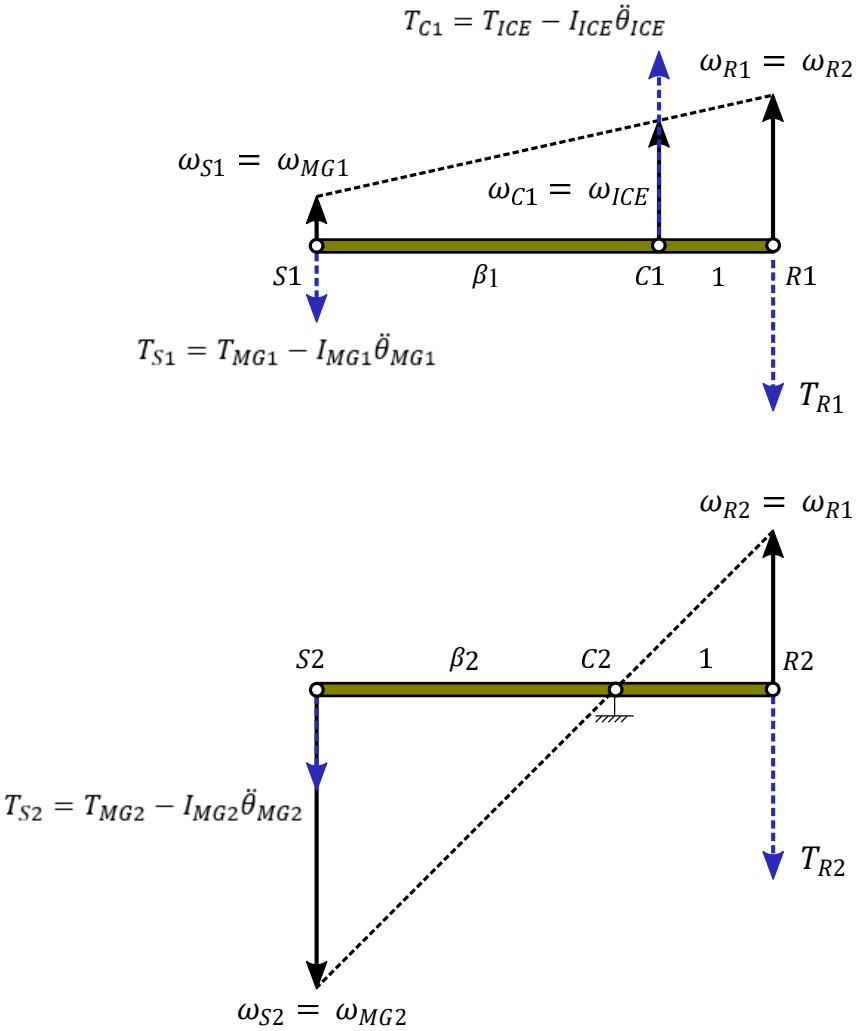

Figure 4.5: Lever diagram of the PG system.

and (4.1.9):

$$\begin{cases} \ddot{\theta}_{MG1} = (1+\beta_1)\ddot{\theta}_{ICE} - \beta_1\ddot{\theta}_{OUT} \\ \ddot{\theta}_{MG2} = \beta_2\ddot{\theta}_{OUT} \end{cases} \tag{4.1.8}$$

$$\begin{cases} (T_{OUT} - J_{OUT}\ddot{\theta}_{OUT}) = \beta_1(T_{MG1} - J_{MG1}\ddot{\theta}_{MG1}) - \beta_2(T_{MG2} - J_{MG2}\ddot{\theta}_{MG2}) \\ (T_{ICE} - J_{ICE}\ddot{\theta}_{ICE}) = -(1+\beta_1)(T_{MG1} - J_{MG1}\ddot{\theta}_{MG1}) \end{cases} \tag{4.1.9}$$

Since $\ddot{\theta}_{OUT}$ can be known from the vehicle acceleration profile, there is one DOF when $\ddot{\theta}_{ICE}$ is non-zero in the hybrid electric mode and zero DOF when $\ddot{\theta}_{ICE}$ is zero in the all-electric mode. In terms of torque equations, T_{OUT} can be known from the vehicle power demand. If the rotational acceleration of each powertrain component is solved first, there is one DOF when T_{ICE} is non-zero in the hybrid electric mode and zero DOF when T_{ICE} is zero in the all-electric mode. Combining Eq. (4.1.8) and (4.1.9), there are totally two DOF in the hybrid electric mode and zero DOF in the all-electric mode.

Vehicle Longitudinal Dynamics

Vehicle speed can be calculated from longitudinal dynamics, which consist of rolling resistance, aerodynamic resistance, and road grade resistance, as illustrated in Eq.

(4.1.10):

$$v_{veh} = \frac{1}{m_{equiv}} \int \left(\frac{T_{wh}}{R_{wh}} - \mu_1 - \mu_2 v_{veh} - \mu_3 v_{veh}^2 \right) dt \tag{4.1.10}$$

where m_{equiv} is the equivalent mass of the vehicle with inertia, T_{wh} is the torque at the wheels, R_{wh} is the wheel radius, and μ_1, μ_2, and μ_3 are the road load coefficients.

4.1.3 Model Validation

Before introducing the vehicle control strategy, the HEV model is validated on both UDDS and HWFET drive cycles. Firstly, the simulated vehicle speed is compared with the drive cycle speed. As shown in Fig. 4.6, the simulated speed follows the reference speed perfectly under both cycles, indicating the vehicle power demand is fully fulfilled. Secondly, the simulated vehicle tractive effort is compared with the test data disclosed by Argonne National Laboratory (ANL) [198]. As depicted in Fig. 4.7, the simulated profile follows closely with the test data under both drive cycles, which proves the model validity.

Finally, an energy balance analysis is conducted as further validation of the simulation model. Energy balance analysis is based on energy conservation, requiring the total energy losses of each powertrain component equal the total energy supplied by the engine and battery [26]. The total energy losses in the built model are composed of MG1 loss, MG2 loss, auxiliary loss, friction brake loss, road load loss, primary transmission loss, battery loss, and inertial loss. Table 4.2 summarizes the simulation

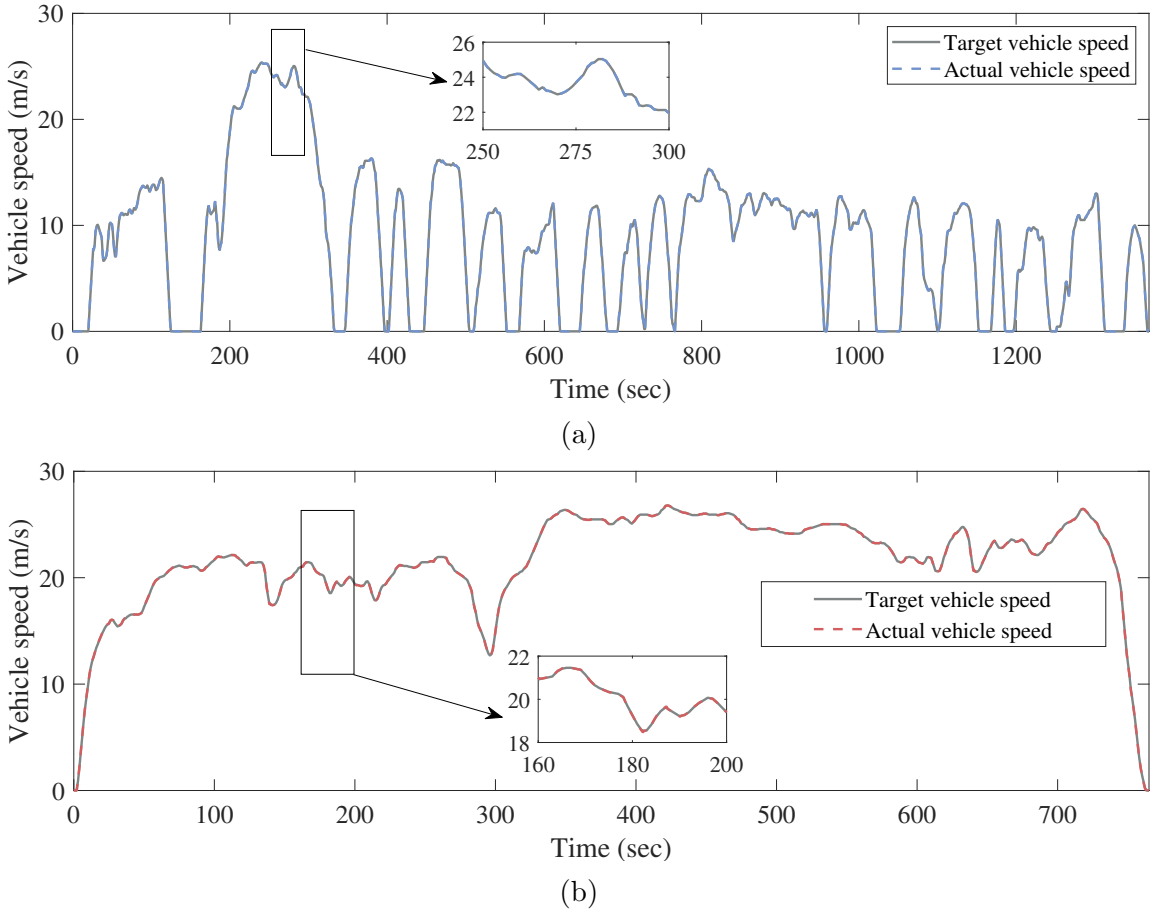

Figure 4.6: Comparison of vehicle speed under (a) UDDS and (b) HWFET.

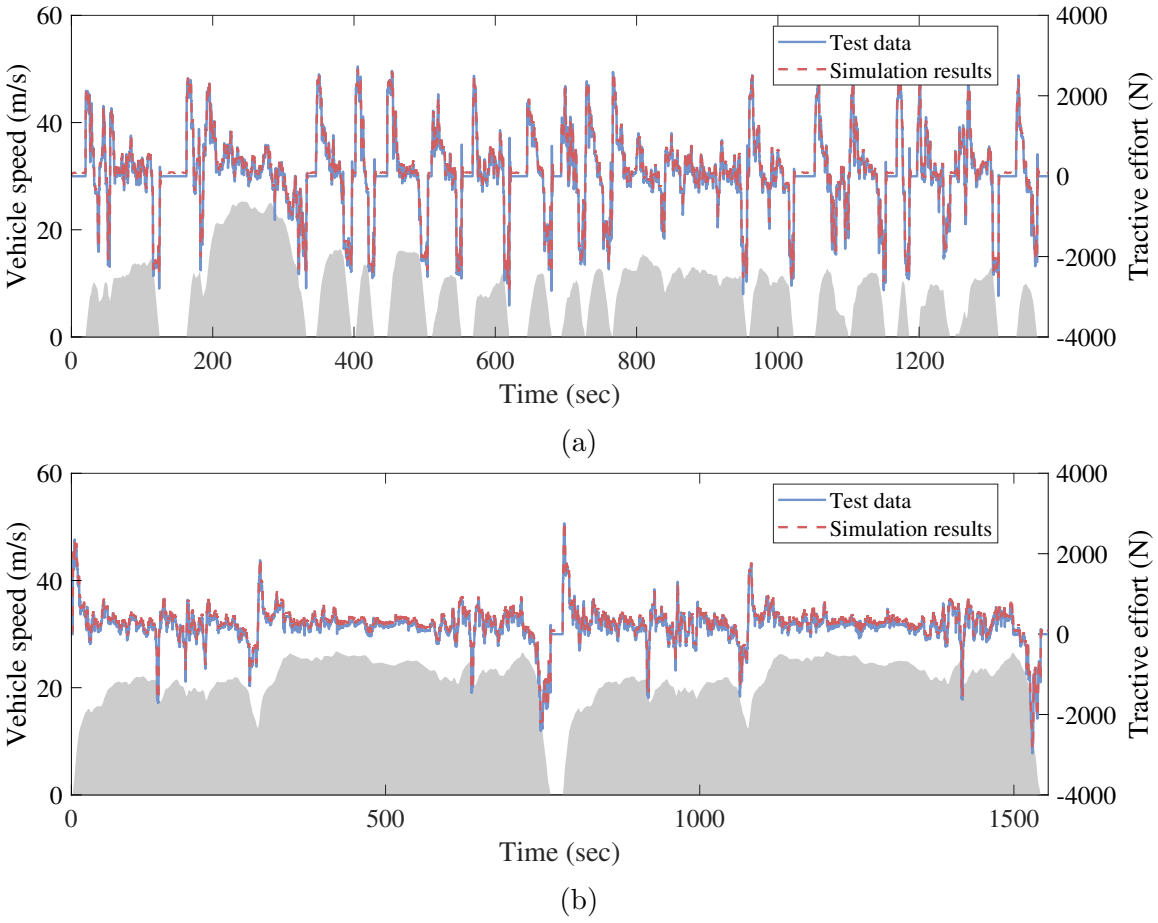

Figure 4.7: Comparison of vehicle tractive effort under (a) UDDS and (b) HWFET.

statistics with a time step of 0.1 seconds. Since the energy is perfectly balanced under both drive cycles, the simulation model is deemed credible.

Table 4.2: Energy balance analysis under (a) UDDS and (b) HWFET.

Energy Balance		**UDDS**	**HWFET**
Energy loss	MG1 loss (kJ)	344.01	438.54
	MG2 loss (kJ)	1276.41	632.84
	Auxiliary loss (kJ)	616.10	344.30
	Friction brake loss (kJ)	0.00	0.00
	Road load loss (kJ)	2041.12	4878.13
	Primary transmission loss (kJ)	0.00	0.00
	Battery loss (kJ)	813.26	283.42
	Inertial loss (kJ)	12.35	4.41
	Total energy loss (kJ)	5103.24	6581.65
Engine statistics	Total fuel consumption (g)	348.55	410.26
	Total mechanical energy (kJ)	5103.09	6583.59
Battery statistics	SOC at the start (%)	40.00	40.00
	SOC at the end (%)	40.00	40.04
	Total electrical energy (kJ)	0.15	-1.94
Unbalanced energy		**0.00**	**0.00**

4.2 Optimal Control Problem

The objectives of the vehicle control strategy in this chapter are identified as follows:

(1) *Providing driver's power demand.*

(2) *Maintaining battery SOC at desired level.*

(3) *Minimizing total fuel consumption and thus CO_2 emissions.*

Based on the drive cycle information, the total driver's power demand can be calculated backward to trace the power sources. Since there are two power sources, i.e., engine and battery, optimally distributing the power between the two with minimal fuel consumption is the key problem of the energy management strategy. Therefore, the optimal control problem is defined to minimize the total fuel consumption over a certain drive cycle from starting time t_0 to ending time t_f, which can be formulated as:

$$u^* = \arg\min_u \left\{ \int_{t_0}^{t_f} \dot{m}_{fuel}(x,u)dt \right\} \tag{4.2.1}$$

where $\dot{m}_{fuel}$ denotes the fuel mass flow rate. In this problem, battery SOC is chosen as the state variable x. Since there are two DOF in the hybrid electric mode, engine torque and rotational speed are chosen as the two control variables u_1 and u_2, as shown in Eq. (4.2.2).

$$\begin{cases} x(t) = SOC(t) \\ u_1(t) = T_{ICE}(t) \\ u_2(t) = \omega_{ICE}(t) \end{cases} \tag{4.2.2}$$

HEVs require a charge sustaining (CS) operation where battery SOC at the end of a drive cycle is approximately the same as it is at the beginning. Besides, the powertrain components should also be restrained within their physical limits. Thus,

the optimal control problem is subject to the following constraints, where the *max* and *min* indexes denote the upper and lower limits.

$$\begin{cases} SOC_{min} \leq SOC(t) \leq SOC_{max} \\ SOC(t_f) \approx SOC(t_0) \\ P_{batt,min} \leq P_{batt}(t) \leq P_{batt,max} \\ I_{batt,min} \leq I_{batt}(t) \leq I_{batt,max} \\ T_{ICE,min} \leq T_{ICE}(t) \leq T_{ICE,max} \\ \omega_{ICE,min} \leq \omega_{ICE}(t) \leq \omega_{ICE,max} \\ T_{MG1,min} \leq T_{MG1}(t) \leq T_{MG1,max} \\ \omega_{MG1,min} \leq \omega_{MG1}(t) \leq \omega_{MG1,max} \\ T_{MG2,min} \leq T_{MG2}(t) \leq T_{MG2,max} \\ \omega_{MG2,min} \leq \omega_{MG2}(t) \leq \omega_{MG2,max} \end{cases} \tag{4.2.3}$$

4.3 Implementation of Equivalent Consumption Minimization Strategy

4.3.1 Baseline ECMS

In HEVs with CS operation, all the consumed energy essentially comes from the engine through fuel combustion. However, during the trip, the battery is either discharged to alleviate engine loads with fuel savings or charged by the engine causing extra fuel

use. To quantify these additional fuel savings or consumption, an equivalence factor (EF) reflects the battery electrical energy as an equivalent amount of fuel. In such a way, the instantaneous equivalent fuel consumption can be minimized at each instant, thus enabling the real-time optimization [199].

EF serves as a critical tuning parameter that supervises the CS condition and the optimal solution in ECMS. For each drive cycle, an optimal EF exists and is usually found through a trial-and-error approach [200]. The EF tuning process is illustrated in Fig. 4.8.

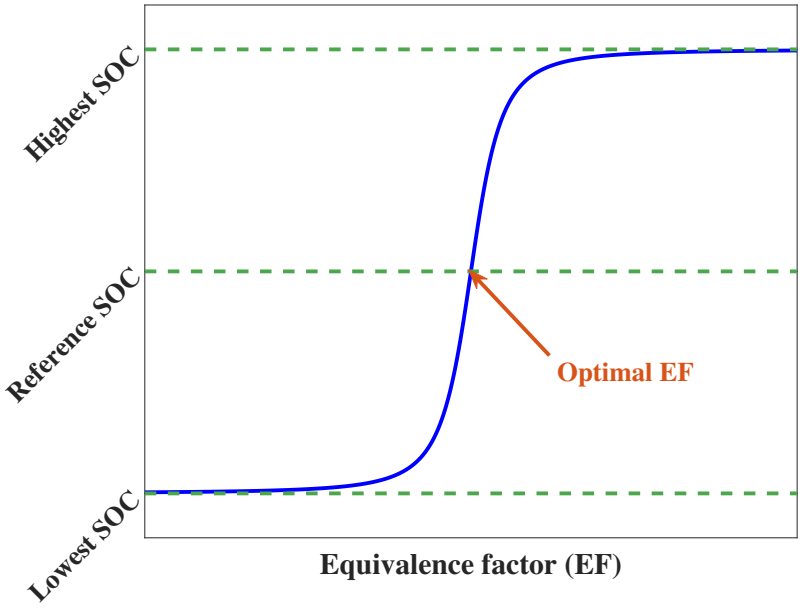

Figure 4.8: Illustration of EF tuning.

The upper and lower limits of the SOC variation are fixed for a certain vehicle model and drive cycle. If the battery SOC is higher than the reference value, it indicates a larger penalty has been attributed to the electrical energy consumption. Therefore, a smaller EF would make battery discharging more likely. Contrarily, a lower SOC indicates the overuse of the battery energy, and a larger EF would suppress too

much battery discharging. Moreover, as can be seen from Fig. 4.8, SOC variation is extremely sensitive when approaching the optimal EF.

With the objectives of fuel minimization, the cost function of ECMS can be formulated as:

$$J = \dot{m}_{fuel}(x(t), u(t)) \cdot \text{LHV}_{fuel} + \lambda \cdot P_{batt}(x(t), u(t)) \tag{4.3.1}$$

where LHV_{fuel} denotes the lower heating value of the fuel, and λ denotes the EF. However, such a cost function has no sufficient controls over powertrain mode shifts or engine activation/deactivation events, which may cause infeasible solutions for powertrain operation when such events are excessively frequent. Accordingly, a penalty term is added in the cost function to ensure the vehicle drivability, as shown in Eq. (4.3.2). Γ denotes a large weighting factor, and the infeasible mode shifts are defined as engine activation/deactivation events that last less than 10 seconds.

$$J = \dot{m}_{fuel}(x(t), u(t)) \cdot \text{LHV}_{fuel} + \lambda \cdot P_{batt}(x(t), u(t)) + \Gamma \cdot \{\text{infeasible mode shifts}\} \tag{4.3.2}$$

4.3.2 Dynamic ECMS Considering Powertrain Inertial Dynamics

In the baseline ECMS without considering rotational inertial dynamics of powertrain components, the desired torque for MG1 and MG2 can be expressed as:

$$T_{MG1,des} = -\frac{1}{1+\beta_1} T_{ICE} \tag{4.3.3}$$

$$T_{MG2,des} = -\frac{1}{\beta_2}\frac{\beta_1}{1+\beta_1} T_{ICE} - \frac{1}{\beta_2} T_{OUT} \tag{4.3.4}$$

While in dynamic ECMS considering the rotational inertia, the desired torque for MG1 and MG2 can be derived from Eq. (4.1.7) as:

$$T_{MG1,des} = -\frac{1}{1+\beta_1} T_{ICE} + \left[\frac{1}{1+\beta_1} J_{ICE} + (1+\beta_1) J_{MG1}\right] \ddot{\theta}_{ICE} - J_{MG1}\beta_1 \ddot{\theta}_{OUT} \tag{4.3.5}$$

$$T_{MG2,des} = -\frac{1}{\beta_2}\frac{\beta_1}{1+\beta_1} T_{ICE} - \frac{1}{\beta_2} T_{OUT} + \frac{1}{\beta_2}\frac{\beta_1}{1+\beta_1} J_{ICE} \ddot{\theta}_{ICE} + \left(\frac{1}{\beta_2} J_{OUT} + \beta_2 J_{MG2}\right) \ddot{\theta}_{OUT} \tag{4.3.6}$$

The additional battery power demand due to the inertial dynamics can be obtained from Eq. (4.3.3)-(4.3.6) as follows:

$$\Delta P_{MG1,mech} = \left[\left(\frac{1}{1+\beta_1} J_{ICE} + (1+\beta_1) J_{MG1} \right) \ddot{\theta}_{ICE} - J_{MG1} \beta_1 \ddot{\theta}_{OUT} \right] \dot{\theta}_{MG1} \quad (4.3.7)$$

$$\Delta P_{MG2,mech} = \left[\frac{1}{\beta_2} \frac{\beta_1}{1+\beta_1} J_{ICE} \ddot{\theta}_{ICE} + \left(\frac{1}{\beta_2} J_{OUT} + \beta_2 J_{MG2} \right) \ddot{\theta}_{OUT} \right] \dot{\theta}_{MG2} \quad (4.3.8)$$

$$\Delta P_{MG1,elec} = \begin{cases} \Delta P_{MG1,mech} / \eta_{MG1}, & P_{MG1,mech} \geq 0 \\ \Delta P_{MG1,mech} \eta_{MG1}, & P_{MG1,mech} < 0 \end{cases} \quad (4.3.9)$$

$$\Delta P_{MG2,elec} = \begin{cases} \Delta P_{MG2,mech} / \eta_{MG2}, & P_{MG2,mech} \geq 0 \\ \Delta P_{MG2,mech} \eta_{MG2}, & P_{MG2,mech} < 0 \end{cases} \quad (4.3.10)$$

$$\Delta P_{batt} = \Delta P_{MG1,elec} + \Delta P_{MG2,elec} \quad (4.3.11)$$

Comparing Eq. (4.3.2) and (4.3.11), it is obvious that the cost function under evaluation at each time step would be different if taking the rotational inertia into account. From the energy conservation perspective, the inertial loss will result in an increase

in fuel consumption, thus affecting the control strategy performance.

Compared to the baseline ECMS without inertial impacts, the dynamic ECMS considering rotational inertia will provide a more accurate prediction of fuel economy and thus yield a more convincing and effective optimal solution for real-world driving tasks.

4.4 Results and Discussions

In this section, a simulation model integrating the vehicle plant model explained in Section 4.1 and the dynamic ECMS introduced in Section 4.3.2 is constructed in MATLAB® and Simulink® to test the performance of the proposed control strategy. The entire HEV model is built based on a forward-looking approach. To better evaluate the performance, a comparative study is performed between the proposed dynamic ECMS and the baseline ECMS. Simulation is conducted on both UDDS and HWFET with a time step of 0.1 seconds.

4.4.1 Battery SOC and Mode Shifts

Fig. 4.9 compares the battery SOC and mode shift profiles of the two strategies. An initial battery SOC of 40% is defined based on several considerations including the battery safety limits, the vehicle characteristics, and the drive cycles under evaluation. The vehicle is controlled to comply with a CS criterion where only ±0.1% deviation is allowed for the terminal SOC.

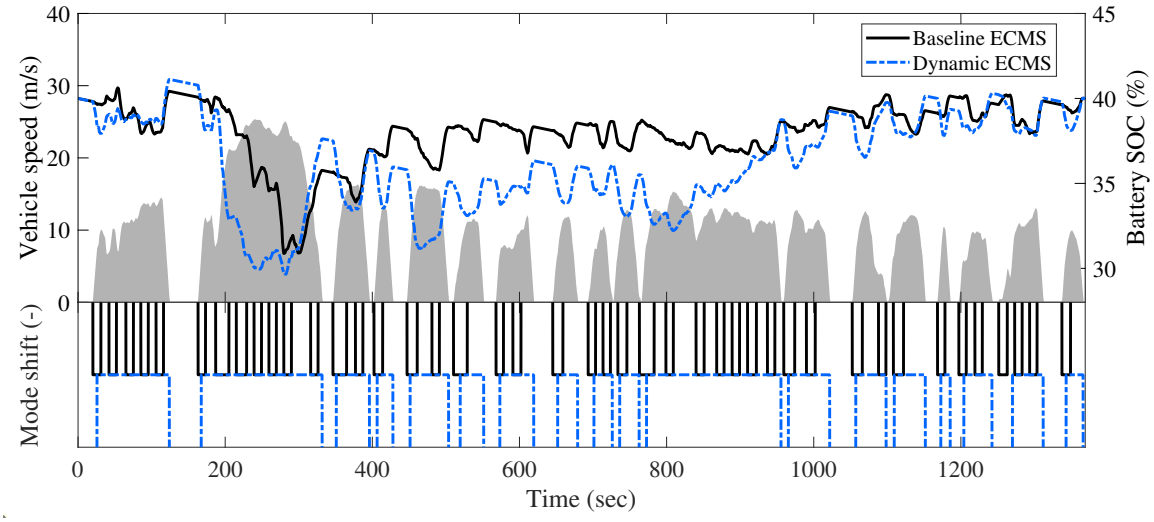

(a)

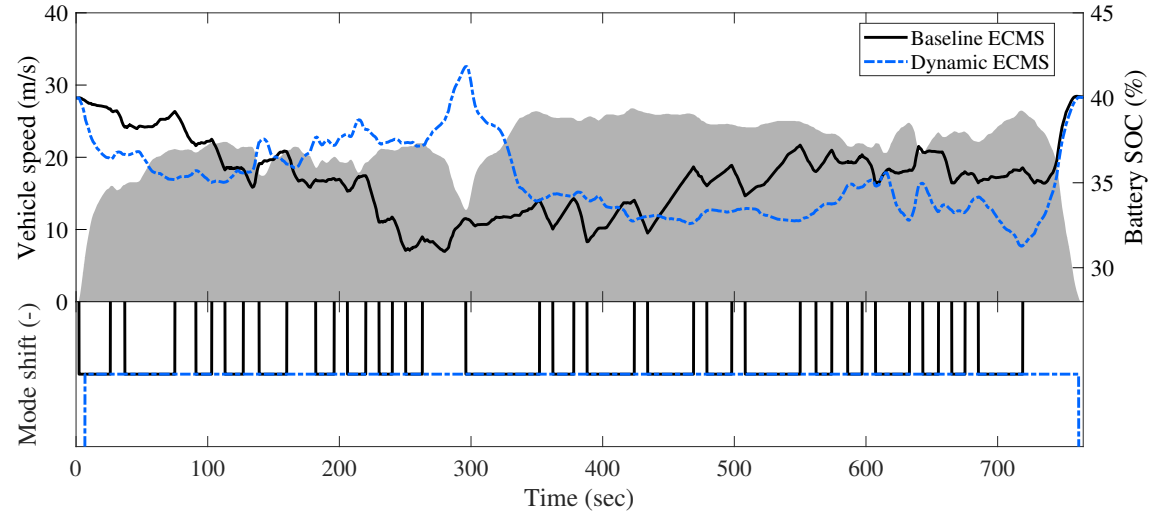

(b)

Figure 4.9: Comparison of battery SOC and mode shift profiles under (a) UDDS and (b) HWFET.

Simulation results present a largest SOC deviation of 0.048%, so the CS operation is considered satisfied. Although the two strategies present different SOC trajectories, they are both capable of maintaining SOC within the battery operating range. As reflected in the figures, the SOC trajectory of the dynamic ECMS is more dramatic than the baseline ECMS due to the additional instantaneous inertial power. This behavior indicates the complexity of battery SOC scheduling in practical vehicle control, where powertrain inertial dynamics cannot be neglected, and the upper and lower SOC limits must be carefully defined to protect the battery.

Owing to the penalty imposed for mode transitions, there are no excessive mode shifts in both ECMS. Comparing the two strategies, mode shifts are more significantly reduced by the dynamic ECMS on both drive cycles. This is because, when the engine tends to make a mode shift, the resulting inertial dynamics will cause a higher instantaneous cost, as given in Eq. (4.3.2), which makes the vehicle reluctant to change modes and thus suppressing the mode shifts. Such effects are equivalent to adding a mode shift penalty term in the cost function, which benefits the vehicle drivability and riding comfort. Compared to UDDS, HWFET is more power-demanding, so the vehicle mostly runs in hybrid electric mode with the engine on to deliver the power continuously.

4.4.2 Powertrain Dynamics

Engine, MG2, and MG1 operating profiles reflect the vehicle dynamic response to a certain driving task. To better emulate real-world engine operations and ensure vehicle drivability, a constraint of a maximum rotational acceleration of 120 rad/s^2

and deceleration of 600 rad/s^2 is imposed on the engine in the dynamic ECMS.

Fig. 4.10 compares the engine speed profiles between the two ECMS. Since the baseline ECMS is constructed on a steady-state HEV model, the engine will immediately reach the target speed without delay. In the dynamic ECMS, however, engine activation/deactivation events are followed by speed climbing/dropping with constrained acceleration/deceleration. It can be observed that engine speed in the dynamic ECMS is much steadier than the baseline ECMS. At some moments, the engine prefers to idle rather than shut down to zero speed and then rev up again when required. This is because, with the underlying penalty for inertial dynamics, the engine is unlikely to frequently and dramatically vary its speed.

Fig. 4.11 and 4.12 illustrate the torque profiles of the engine, MG2, and MG1 under both drive cycles. Comparing Eq. (4.3.3)-(4.3.4) with Eq. (4.3.5)-(4.3.6), additional torque is required from MG2 and MG1 in the dynamic ECMS to coordinate the powertrain when there is a change in engine and vehicle speed. For instance, when engine is activated, MG1 directly exhibits negative torque reversely proportional to the engine torque output in the baseline ECMS, given by Eq. (4.3.3). However, in the dynamic ECMS, MG1 will first deliver positive torque to assist in engine accelerating then apply negative reaction torque when engine reaches steady state, as implied in Eq. (4.3.5).

It can also be observed that the engine torque varies in a steadier manner with fewer fluctuations in the dynamic ECMS, while MG2 presents a wider torque swing due to the additional torque caused by inertial dynamics.

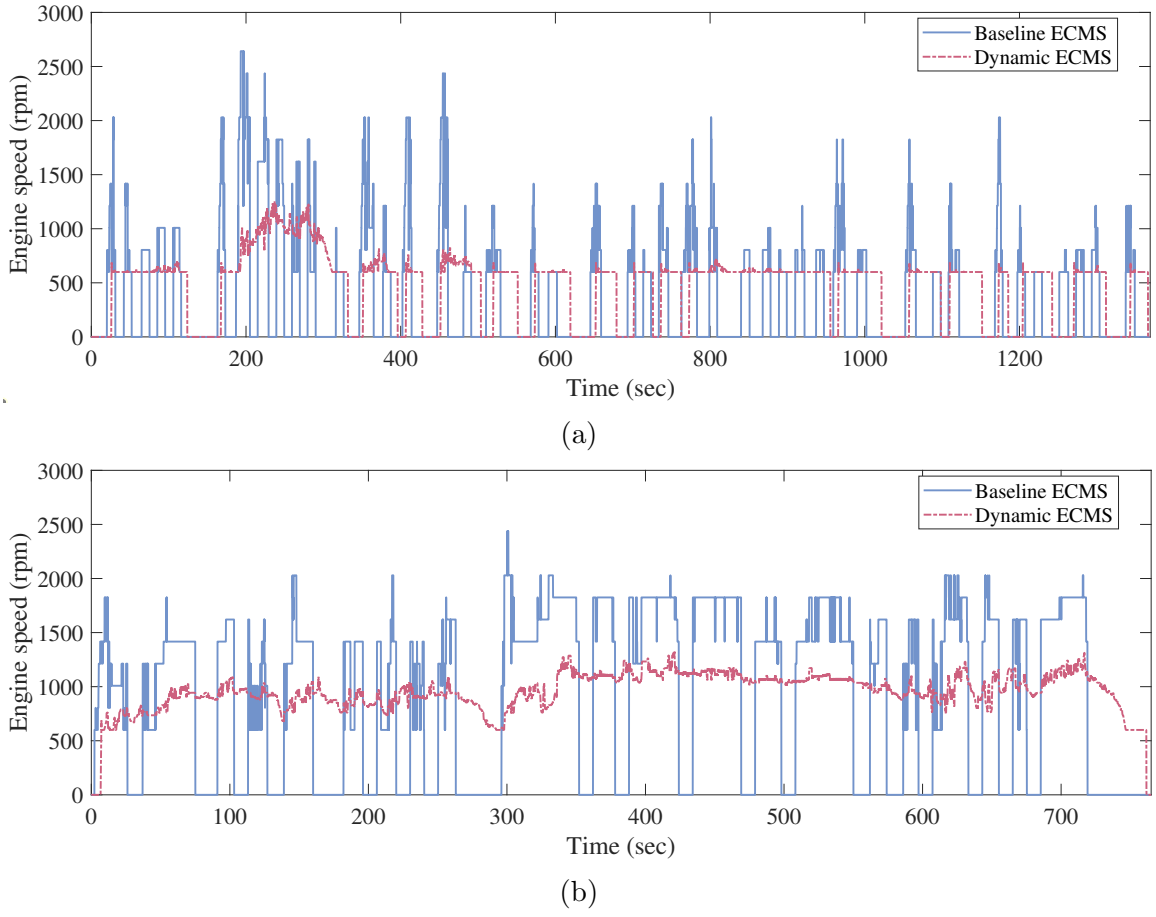

Figure 4.10: Comparison of engine speed in (a) UDDS and (b) HWFET.

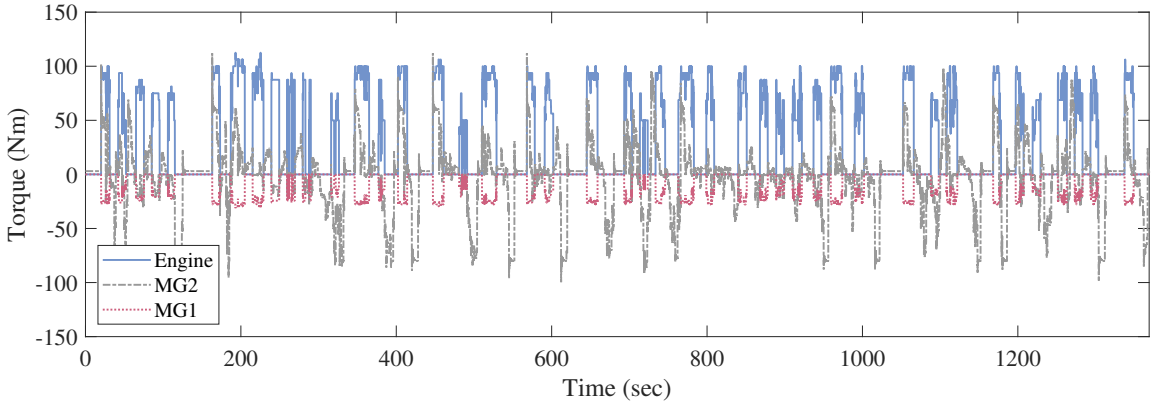

(a)

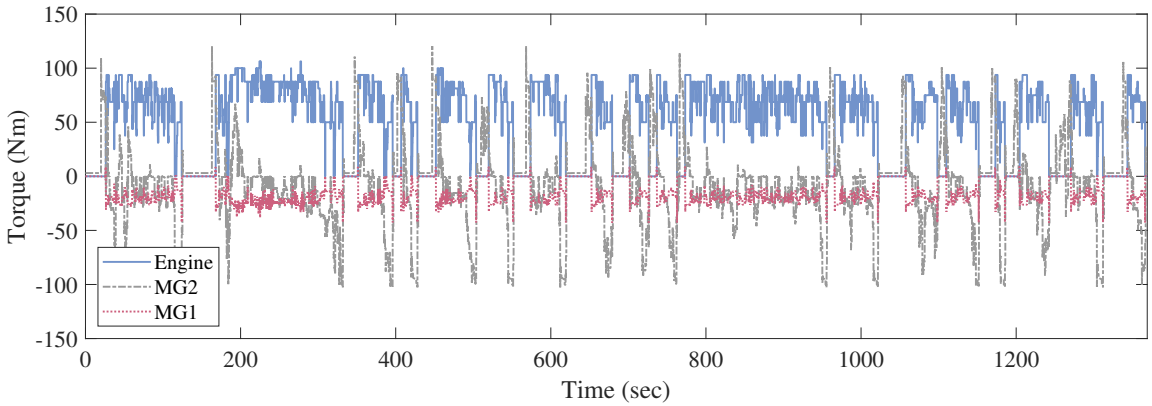

(b)

Figure 4.11: Torque profiles of engine, MG2, and MG1 in (a) baseline ECMS and (b) dynamic ECMS under UDDS.

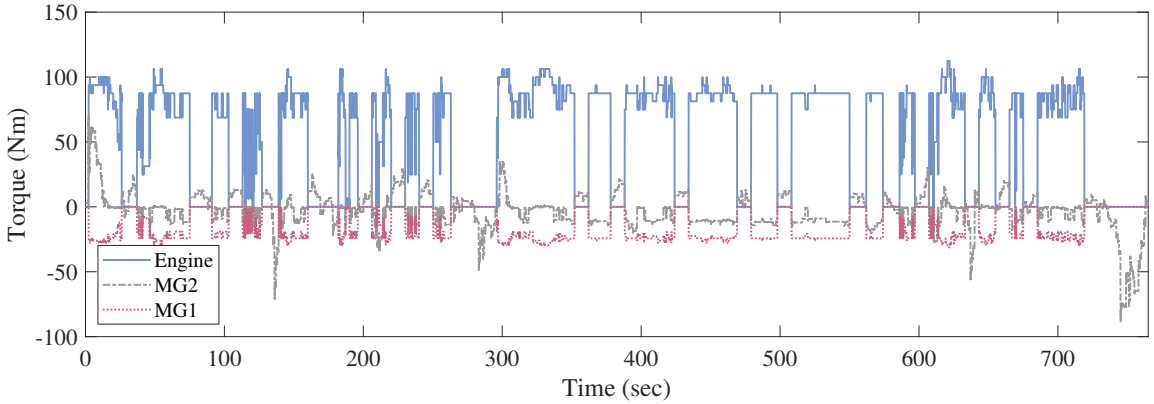

(a)

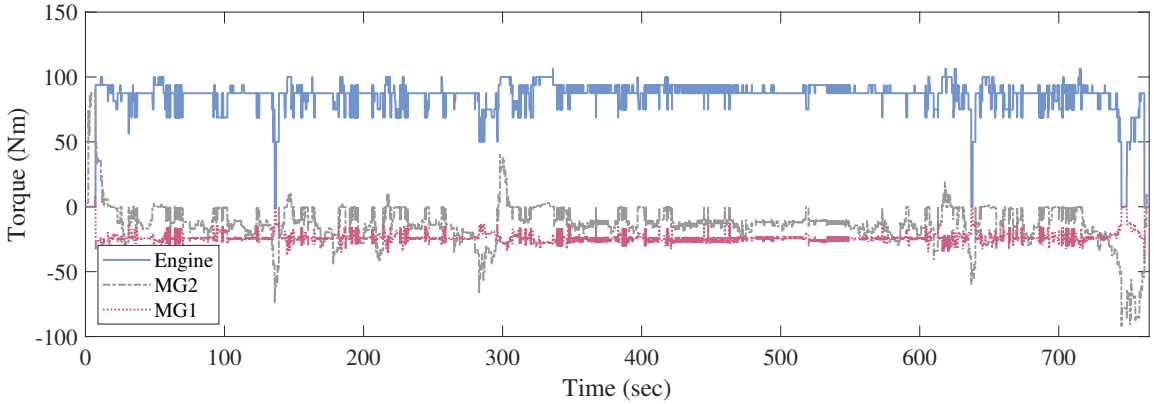

(b)

Figure 4.12: Torque profiles of engine, MG2, and MG1 in (a) baseline ECMS and (b) dynamic ECMS under HWFET.

4.4.3 Engine Operation

Fig. 4.13 and 4.14 present the engine operation performance of the two control strategies. For both ECMS, engine operating points are constrained by the peak torque curve and appear to stay within feasible limits all the time.

Generally, each engine has a peak efficiency line, also known as the optimal operation line (OOL), that depicts a series of torque values corresponding to each speed where the engine efficiency presents a maximum. Mostly, the engine is designed to operate along this line whenever possible. However, as reflected in the figures, the actual operating points may deviate from this line since engine operation in HEVs is also restrained by other powertrain components.

Comparing the two ECMS, the dynamic ECMS exhibits a narrower engine operating range, which can also be observed in Fig. 4.10. This is favorable in engine control since it causes fewer transients and losses. However, a drawback is that the engine operating points locate further from the most efficient region, which will inevitably deteriorate the overall fuel economy. Besides, the engine tends to operate at lower speed points since climbing to higher speeds will lead to undesired dynamics.

Table 4.3 demonstrates the engine operation statistics of the two ECMS. It can be observed that engine activations are effectively mitigated in the dynamic ECMS due to the effects of additional inertial penalty. However, the engine tends to stay on for longer since the additional inertial dynamics require the engine to provide more power. Compared to the baseline ECMS, the dynamic ECMS reduces the number of engine activations by 58.14% in UDDS and 95.24% in HWFET while extends the

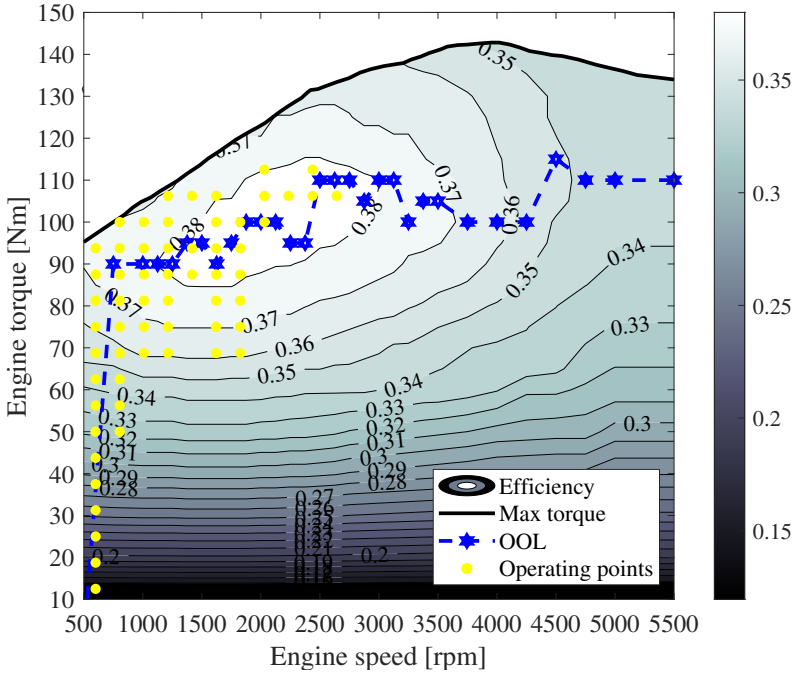

(a)

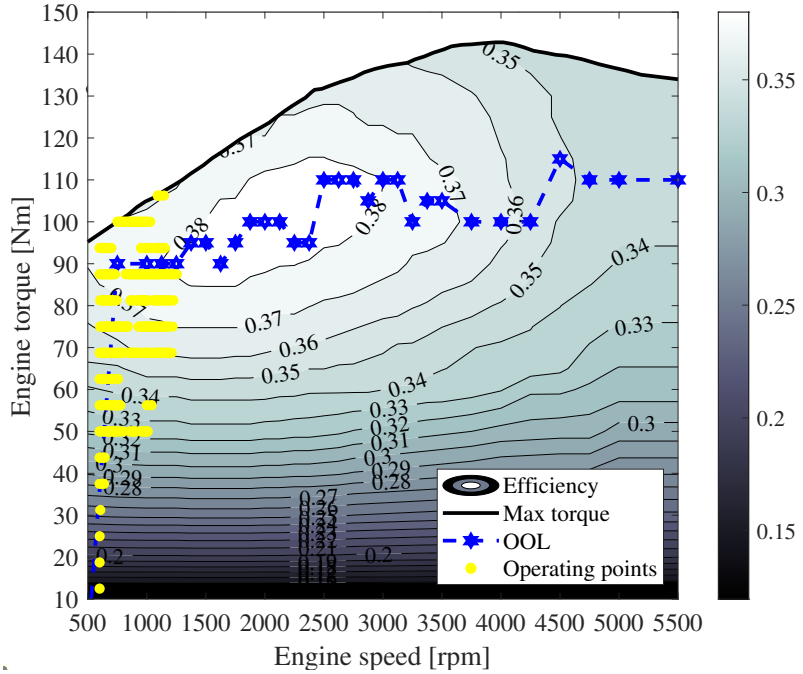

(b)

Figure 4.13: Engine operation in (a) baseline ECMS and (b) dynamic ECMS under UDDS.

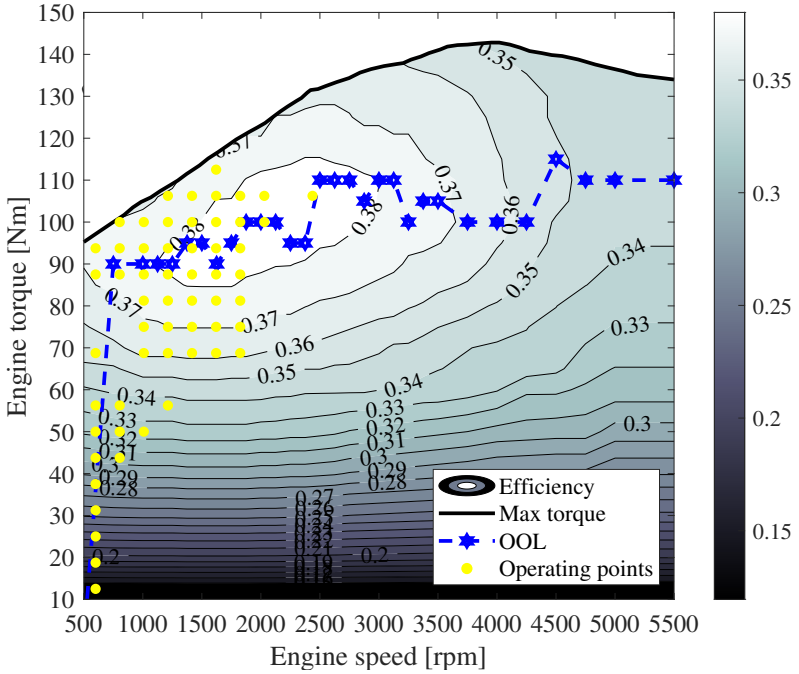

(a)

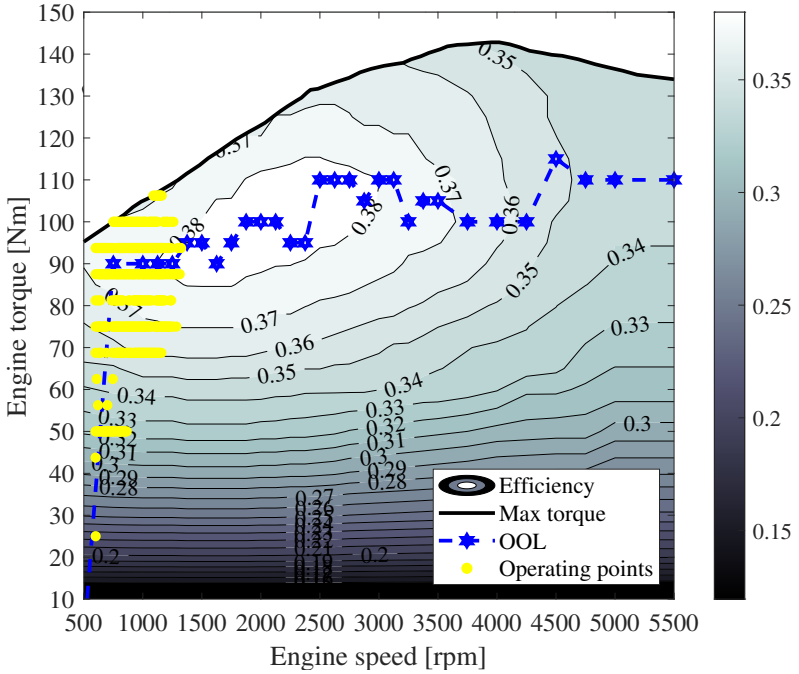

(b)

Figure 4.14: Engine operation in (a) baseline ECMS and (b) dynamic ECMS under HWFET.

engine operation time by 92.57% in UDDS and 61.51% in HWFET.

Table 4.3: Engine operation statistics of the dynamic ECMS vs. baseline ECMS.

Drive cycle	ECMS	Engine on/offs	Engine-on time
UDDS	Dynamic	18	71.25%
	Baseline	43	37.00%
HWFET	Dynamic	1	98.65%
	Baseline	21	61.08%

4.4.4 Fuel Consumption

For a fairer comparison of fuel consumption between the two ECMS, powertrain inertial dynamics are penalized in the plant model for the baseline ECMS. The resulting extra battery electrical power is added as an equivalent amount of fuel to the base fuel consumption. Fig. 4.15 illustrates the total fuel consumption given by the baseline ECMS under both drive cycles, where the area colored blue denotes the penalized fuel consumption.

Fig. 4.16 demonstrates the fuel consumption statistics of both the baseline and dynamic ECMS. As shown in the figure, the dynamic ECMS presents higher fuel consumption than the baseline ECMS, around 13.34% and 4.50% increase on UDDS and HWFET, respectively. According to previous analyses, one reason is that the inertial loss and other losses caused by inertia dynamics, such as the battery losses, essentially require more fuel. Another reason is that engine operating points are shifted to less-efficient regions. Due to the additional inertial dynamics, powertrain operations are affected. Powertrain components, which are constrained by their physical limits,

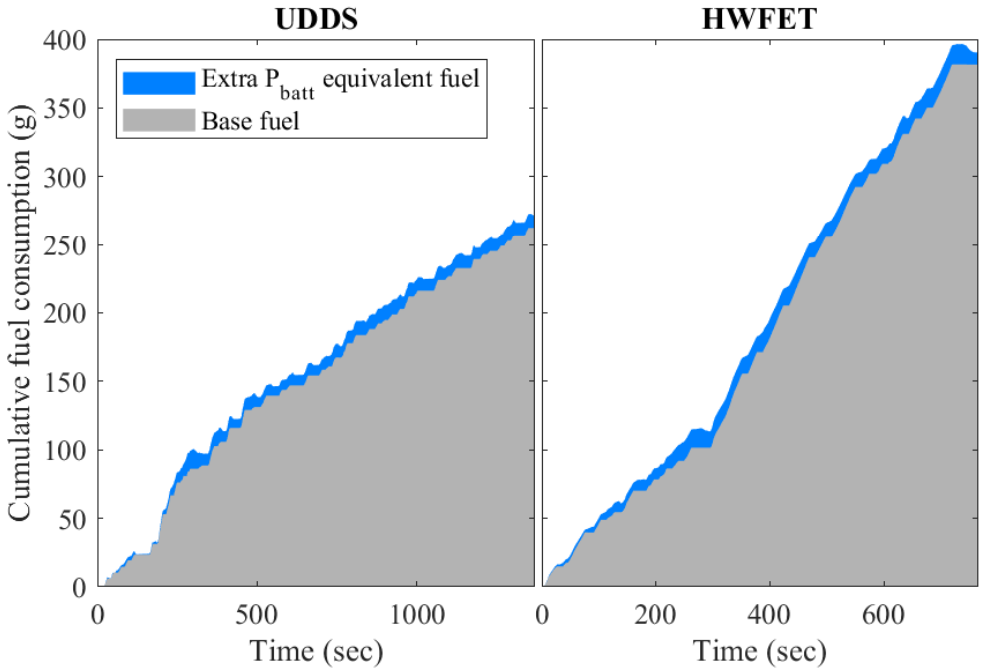

Figure 4.15: Cumulative fuel consumption in baseline ECMS under UDDS and HWFET.

have to compromise some fuel efficiency for feasible operating solutions.

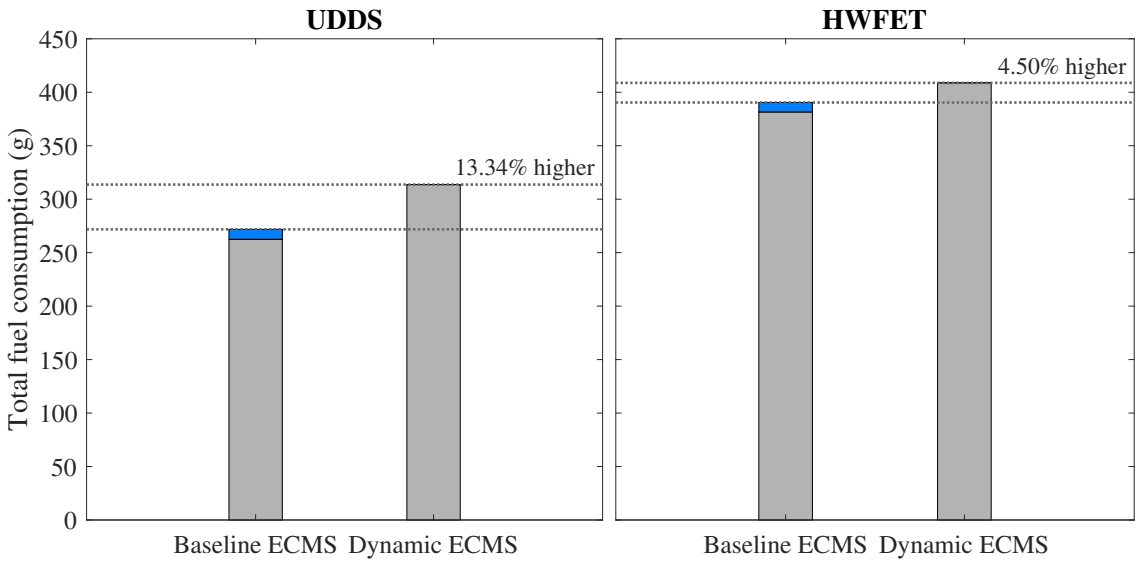

Figure 4.16: Comparison of fuel consumption between dynamic and baseline ECMS under UDDS and HWFET.

Actually, the higher fuel consumption is fully expected and only because the control-oriented model for developing the dynamic ECMS is closer to reality by incorporating powertrain inertial dynamics. Therefore, if the dynamic ECMS is considered the benchmark, the baseline ECMS is actually overestimating the fuel economy. When adopting the baseline ECMS as the tool to evaluate new hybrid powertrain architecture, the prediction of fuel economy would be inaccurate. On the contrary, the dynamic ECMS considering powertrain inertial dynamics will provide a more accurate prediction of fuel economy and thus yield a more convincing and effective optimal solution for real-world driving tasks.

Another advantage of the dynamic ECMS is that the vehicle drivability can be improved. In real-world driving tasks, vehicles are always running with dynamics. Applying baseline ECMS which is built based on steady-state HEV models will cause a mismatch between the desired and actual vehicle speed and thus damage the vehicle drivability. Fig. 4.17 illustrates the vehicle speed trajectory of using the baseline ECMS on an inertia-based dynamic vehicle model. It can be observed that the vehicle failed to follow the desired speed at several locations. On the contrary, since vehicle drivability participates in the decision-making of the control solutions in the dynamic ECMS, a better vehicle control which ensures the vehicle drivability can be achieved. Therefore, even though some fuel economy is compromised in the dynamic ECMS, it improves the vehicle drivability and provides more accurate predictions on fuel economy, presenting improvement in practicality for real-world driving tasks and fuel economy assessment.

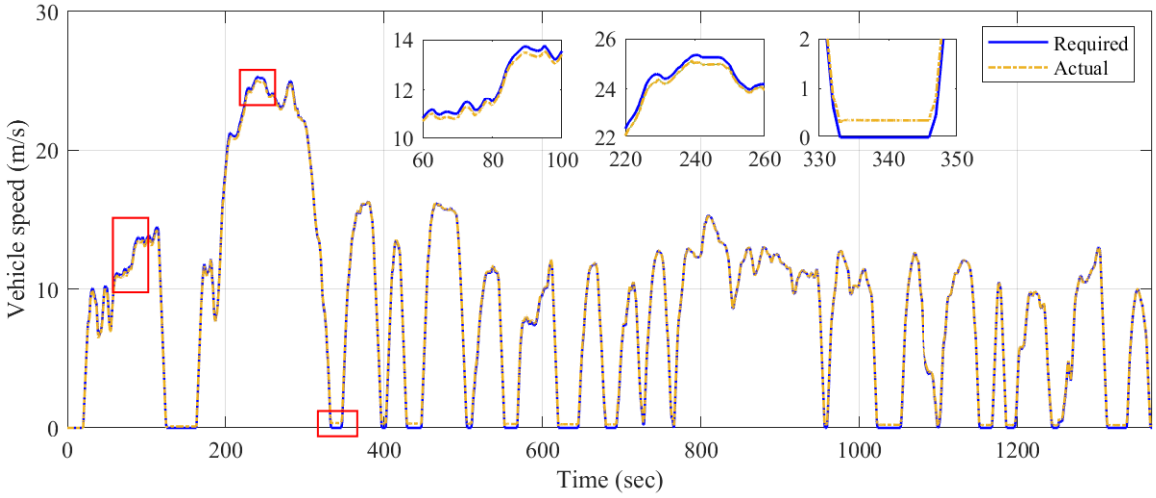

Figure 4.17: Vehicle speed trajectory of using baseline ECMS on an inertia-based dynamic HEV model.

4.5 Summary

This chapter aims to improve the practicality of HEV EMS by incorporating powertrain inertial dynamics. First, an inertial-based dynamic vehicle model of a power-split HEV is built systematically. The HEV model is numerically verified through an energy balance analysis and experimentally validated through comparison with disclosed testing results. Results indicate sufficient accuracy for the current research purpose. Then, a real-time ECMS incorporating powertrain inertial dynamics is formulated and compared with a baseline steady-state ECMS.

Simulation results indicate that the dynamic ECMS leads to a more dramatic variation in battery SOC but contributes to drivability improvement by reducing driving mode shifts. Additionally, the dynamic ECMS is more beneficial for engine control by enabling a steadier engine operating pattern and a narrower operating range. Compared to the baseline ECMS, the dynamic ECMS improves the vehicle drivability and provides a more accurate prediction of fuel economy. Therefore, as an improvement of the baseline ECMS, the dynamic ECMS offers a more practical optimal solution for HEV control.

With the proposed dynamic ECMS, novel hybrid powertrain configurations can be evaluated more realistically and critically. Another contribution of this work lies in the extension capability of the proposed methodology to other optimal control strategies, such as DP, and the developed tool to other electrified powertrain configurations, such as PHEVs.

Chapter 5

Adaptive Real-time Energy Management for a Multi-mode Hybrid Electric Powertrain

As emphasized in Chapter 4, EF is an important parameter that has substantial impacts on vehicle CS performance and fuel economy since it directly controls the power distribution between the engine and battery in ECMS based control strategies [201]. In basic non-adaptive ECMS, the EF is constant throughout each drive cycle but varies from one drive cycle to another. As can be seen in Fig. 5.1, a certain EF that achieves CS in WLTP cannot maintain battery SOC in either UDDS or HWFET. Therefore, for different driving tasks, the EF must be designed specifically. Moreover, a fine tuning of the EF to achieve CS requires a prior knowledge of the entire drive cycle and is usually done off-line through trial and error, making it difficult to use basic non-adaptive ECMS in real-time [202]. As a result, ECMS with the capability of adaptation and real-time EF tuning is introduced, referred to as A-ECMS.

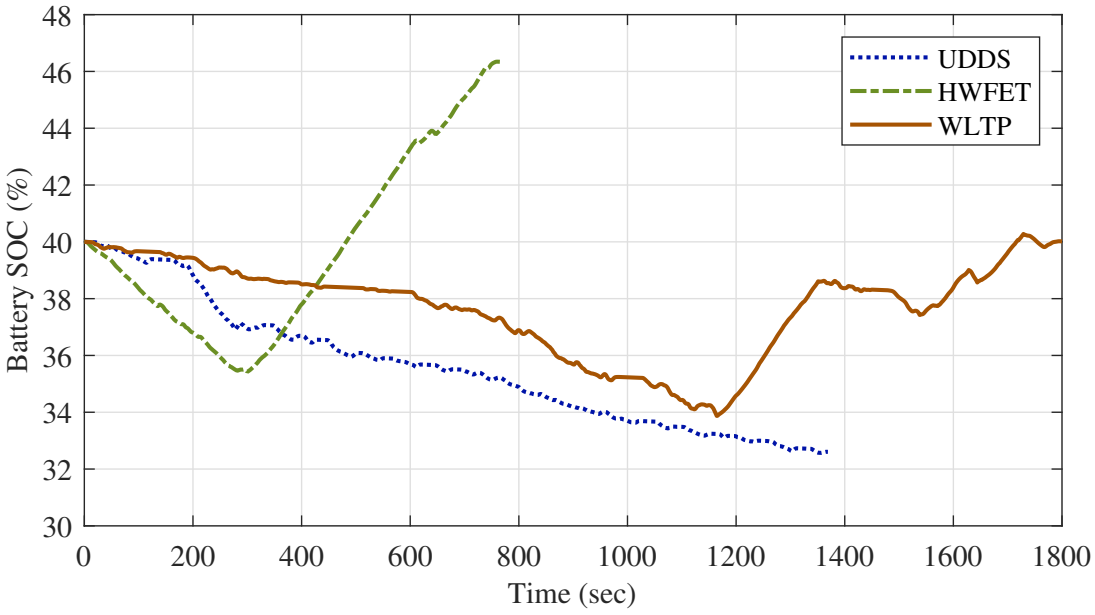

Figure 5.1: Responses of three different drive cycles to a certain EF.

Based on different adaptation methods, the existing A-ECMS can be categorized into rule-based A-ECMS [203], PID-based A-ECMS [204], and predictive A-ECMS [200].

Rule-based A-ECMS determines the EF through searching maps that are constructed off-line for certain drive cycles. Therefore, it is suitable for HEVs with daily routine, such as city buses. PID-based A-ECMS uses PID control to regulate battery SOC but it theoretically guarantees no optimality. Predictive A-ECMS is A-ECMS with prediction capabilities. It updates the EF periodically through predicting the future driving conditions and has become one of the most promising control strategies in real-time HEV energy management [205].

In this context, this chapter proposes a predictive A-ECMS for a multi-mode hybrid powertrain architecture. First, a control-oriented HEV model is constructed with primary powertrain component modeling. Second, the optimal control problem of HEV energy management is described, and the formulation of the proposed A-ECMS is explained thoroughly. Then, a basic non-adaptive ECMS is also implemented, and simulation results of the two ECMS are compared and discussed in detail.

5.1 Hybrid Powertrain System and Modeling

This section introduces a multi-mode HEV. A schematic of the powertrain architecture and main components is shown in Fig. 5.2. Details regarding the vehicle specifications, operation modes, and modeling approaches are described below.

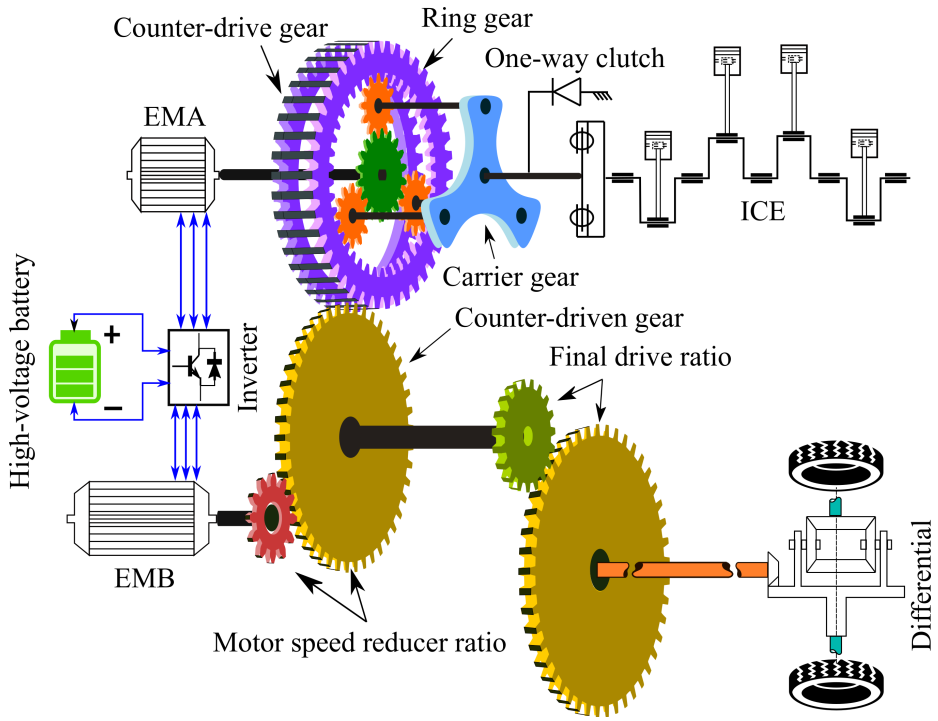

Figure 5.2: Schematic of a multi-mode hybrid powertrain architecture and main components.

5.1.1 Hybrid Powertrain Architecture

The studied hybrid powertrain system incorporates an engine, two electric motors, and a high-voltage battery. Both electric motors (EMA and EMB) can provide traction power and work as generators thanks to the presence of a one-way clutch (OWC). A planetary gear is equipped to coordinate powertrain components so that engine torque and speed can be varied for fuel-efficiency optimization. Specifications of the studied HEV are given in Table 5.1.

The hybrid powertrain system has three operation modes, including one hybrid electric mode and two all-electric modes: single-motor EV mode and dual-motor EV mode. In the hybrid electric mode, both the engine and EMB deliver traction torque to wheels, while EMA reacts on the transaxle without any torque output. Since there are two DOF in the transmission kinematics, engine torque and speed can be controlled to optimize fuel efficiency. In all-electric modes, EMB is the primary traction motor, and EMA can share part of the power demand through the ring gear of the PG if the OWC is engaged. When the OWC is disengaged, only EMB delivers tractive power. In addition, both EMB and EMA can work as generators, specifically, when EMB charges the battery during regenerative braking, and the engine charges the battery through EMA.

Table 5.1: Vehicle specifications of the multi-mode HEV.

Component	Parameter	Value
Vehicle	Equivalent mass	2260 kg
	Wheel radius	0.345 m
	Road coefficient μ_1	145.2261 N
	Road coefficient μ_2	3.3872 N/(m/s)
	Road coefficient μ_3	0.4831 N/(m/s)^2
Transmission	PG ratio β_1 (Ring/Sun)	68/22
	EMB speed reducer ratio β_2	78/30
	Final drive ratio	3.52
Engine	Displacement	3.0 L
	Maximum power	154 kW
	Maximum torque	302 Nm
	Maximum speed	6500 rpm
EMB	Maximum power	80 kW
	Maximum torque	300 Nm
	Maximum speed	13000 rpm
EMA	Maximum power	60 kW
	Maximum torque	120 Nm
	Maximum speed	13000 rpm
Battery	Capacity	48 Ah
	Nominal voltage	388 V

5.1.2 Control-Oriented Vehicle Model

Engine

Since the control strategy in this chapter aims at fuel optimization, only fuel consumption is concerned in engine modeling. Therefore, the engine is modeled by a 2-D quasi-static fuel flow rate map. The actual outputs of engine speed and torque are constrained by its upper and lower physical limits, as given in Eq. (5.1.1), where ω_{ICE} and T_{ICE} are engine rotational speed and torque, respectively.

$$\begin{cases} \omega_{ICE,min} \leq \omega_{ICE} \leq \omega_{ICE,max} \\ T_{ICE,min} \leq T_{ICE} \leq T_{ICE,max} \end{cases} \tag{5.1.1}$$

Motor

Both electric motors are modeled by combined efficiency maps, with the torque output bounded by their upper and lower limits, as expressed in Eq. (5.1.2) and (5.1.3), where $P_{elec,m}$, T_m, ω_m, and η_m denote motor power, torque, rotational speed, and efficiency, respectively.

$$P_{elec,m} = \begin{cases} T_m \omega_m / \eta_m(T_m, \omega_m), & T_m \geq 0 \\ T_m \omega_m \eta_m(T_m, \omega_m), & T_m < 0 \end{cases} \tag{5.1.2}$$

$$T_{m,min}(\omega_m) \leq T_m \leq T_{m,max}(\omega_m) \tag{5.1.3}$$

Battery

The battery is modeled as a pack using the equivalent circuit model approach, where the current is obtained from Ohm's law, as shown in Eq. (5.1.4):

$$I_{batt}(t) = \frac{V_{oc}(SOC) - \sqrt{V_{oc}(SOC)^2 - 4R(SOC)P_{batt}}}{2R(SOC)} \tag{5.1.4}$$

where V_{oc} and R are battery open circuit voltage and internal resistance, respectively, which are both dependent on battery SOC. P_{batt} is the battery power. Battery SOC can be then calculated using current, as given in Eq. (5.1.5), where Q_{batt} and η are battery capacity and coulombic efficiency, respectively.

$$SOC(t) = SOC(t_0) - \frac{\eta}{Q_{batt}} \int_{t_0}^{t} I_{batt}(t)dt \tag{5.1.5}$$

Planetary Gear System

The gear ratio between the counter-drive gear and the counter-driven gear is assumed to be 1:1. Based on the kinematic relations of the planetary gear system, the rotational speed of the engine and motors can be represented as follows:

$$\begin{aligned} \omega_{EMA} &= (1 + \beta_1) \cdot \omega_{ICE} - \beta_1 \cdot \omega_{out} \\ \omega_{EMB} &= \beta_2 \cdot \omega_{out} \end{aligned} \tag{5.1.6}$$

where ω_{EMA}, ω_{EMB}, ω_{ICE}, and ω_{out} are the rotational speed of EMA, EMB, engine, and transmission output shaft, respectively. Since ω_{out} can be known from the vehicle speed, there is one DOF in Eq. (5.1.6) when ω_{ICE} is non-zero in hybrid electric mode and zero DOF when ω_{ICE} is zero in all-electric modes.

The torque relations of the powertrain components in dual-motor EV mode are given in Eq. (5.1.7), where T_{EMA}, T_{EMB}, and T_{out} are the torque of EMA, EMB, and transmission output shaft, respectively. Since T_{out} can be known from the vehicle speed and driver's power demand, there is one DOF.

$$-\beta_1 \cdot T_{EMA} + \beta_1 \cdot T_{EMB} = T_{out} \tag{5.1.7}$$

For HEV mode and the single-motor EV mode, there is another constraint given by Eq. (5.1.8). In HEV mode where the engine torque T_{ICE} is non-zero, combining Eq. (5.1.7) and (5.1.8) gives a total of one DOF. However, since engine torque T_{ICE} is zero in EV operation, there is zero DOF in the single-motor EV mode.

$$-(1 + \beta_1) \cdot T_{EMA} = T_{ICE} \tag{5.1.8}$$

Combining Eq. (5.1.6)-(5.1.8), in total there are two DOF in HEV mode, one DOF in dual-motor EV mode, and zero DOF in single-motor EV mode.

Vehicle Longitudinal Dynamics

Instantaneous vehicle speed can be derived from longitudinal vehicle dynamics, as given in Eq. (5.1.9):

$$v_{veh} = \frac{1}{m_{equiv}} \int \left(\frac{T_{wh}}{R_{wh}} - \mu_1 - \mu_2 v_{veh} - \mu_3 v_{veh}^2 \right) dt \tag{5.1.9}$$

where m_{equiv} is the equivalent mass of the vehicle with inertia, T_{wh} is the torque at the wheels, R_{wh} is the wheel radius, and μ_1, μ_2, and μ_3 are the road load coefficients.

5.2 Optimal Control Problem

Section 5.1 describes the control-oriented HEV model, and the formulation of the HEV optimal control problem is given in this section. Since fuel consumption is taken as the only optimization target, the optimal control problem is formulated as:

$$u^* = \arg\min_u \left\{ \int_{t_0}^{t_f} \dot{m}_{fuel}(x, u) dt \right\} \tag{5.2.1}$$

where $\dot{m}_{fuel}$ denotes the fuel mass flow rate. Battery SOC is chosen as the state variable x. Since there are two DOF in HEV operation, engine torque T_{ICE} and speed ω_{ICE} are chosen as the two control variables u_1 and u_2. Since there is one DOF in dual-motor EV operation, EMB torque T_{EMB} is chosen as the only control

variable. The state and control variables are listed in Eq. (5.2.2).

$$\begin{aligned} & x(t) = SOC(t) \\ & \begin{cases} u_1(t) = T_{ICE}(t) \\ u_2(t) = \omega_{ICE}(t) \end{cases}, \quad for \text{ HEV } mode \\ & u(t) = T_{EMB}(t), \quad for \text{ dual} - \text{motor EV } mode \end{aligned} \tag{5.2.2}$$

The optimal control problem is subject to the following constraints to ensure the main powertrain components remain within their operating limits:

$$\begin{cases} SOC_{min} \leq SOC(t) \leq SOC_{max} \\ SOC(t_f) \approx SOC(t_0) \\ P_{batt,min} \leq P_{batt}(t) \leq P_{batt,max} \\ I_{batt,min} \leq I_{batt}(t) \leq I_{batt,max} \\ T_{ICE,min} \leq T_{ICE}(t) \leq T_{ICE,max} \\ \omega_{ICE,min} \leq \omega_{ICE}(t) \leq \omega_{ICE,max} \\ T_{EMA,min} \leq T_{EMA}(t) \leq T_{EMA,max} \\ \omega_{EMA,min} \leq \omega_{EMA}(t) \leq \omega_{EMA,max} \\ T_{EMB,min} \leq T_{EMB}(t) \leq T_{EMB,max} \\ \omega_{EMB,min} \leq \omega_{EMB}(t) \leq \omega_{EMB,max} \end{cases} \tag{5.2.3}$$

To suppress frequent mode shifts, mode shift penalties are implemented in the cost function to improve drivability and riding comfort. The overall cost function is given

as follows:

$$J = \dot{m}_{fuel}(x(t), u(t)) \cdot \mathrm{LHV}_{fuel} + \lambda \cdot P_{batt}(x(t), u(t)) + \alpha_{\mathrm{EV\_HEV}} + \alpha_{\mathrm{HEV\_EV}} \quad (5.2.4)$$

where $\alpha_{\mathrm{EV\_HEV}}$ and $\alpha_{\mathrm{HEV\_EV}}$ represent the penalty cost from EV to HEV mode and HEV to EV mode, respectively. LHV_{fuel} denotes the lower heating value of the fuel.

5.3 Adaptive Equivalent Consumption Minimization Strategy

In the proposed A-ECMS, the EF is calculated in real-time. Instead of requiring the entire drive cycle information, only a short period ahead in the future time domain is required. Therefore, a particular drive cycle can be considered a series of consecutive shorter drive cycles segmented based on the availability of future driving conditions. Then, an optimal EF is predicted at the beginning of each drive cycle segment and updated with the drive cycle segment until the end of the trip. To sum up, the proposed A-ECMS takes advantage of a prior knowledge of the future driving conditions and uses a series of "local" optimal/suboptimal EF to approach the "global" optimality.

5.3.1 Searching Bounds of the EF

In HEVs, the engine is controlled on and off along the drive cycle. The vehicle power demand is provided by the engine and battery together following the optimal power split strategy, which is reflected as the EF in ECMS, as shown in Eq. (5.3.1). A higher EF will lead to a higher battery SOC since it indicates battery power is more expensive than fuel use, and therefore more engine operation is encouraged.

However, an upper bound of the EF exists beyond which battery SOC will no longer increase. When the EF reaches this threshold, the vehicle will run with the engine on all the time as long as the required engine operation, which is constrained by powertrain coordination, is within its physical limits. The engine will be asked to provide the vehicle power demand alone as much as possible since battery power is too expensive. In such a driving scenario, the cost of battery power is higher than the cost of engine power, giving Eq. (5.3.2). For a given vehicle power demand P_{demand}, Eq. (5.3.2) can be rewritten as Eq. (5.3.3) by incorporating powertrain component efficiency. The upper bound of the EF can be therefore obtained, as given in Eq. (5.3.4), where η_{batt}, η_{mot}, and η_{ICE} are battery, motor, and engine efficiency, respectively.

$$P_{ICE} + \lambda \cdot P_{batt} = P_{demand} \tag{5.3.1}$$

$$\lambda \cdot P_{batt} > P_{ICE} \tag{5.3.2}$$

$$\lambda \cdot \frac{P_{demand}}{\eta_{batt} \cdot \eta_{mot}} > \frac{P_{demand}}{\eta_{ICE}} \tag{5.3.3}$$

$$\lambda > \frac{\eta_{batt} \cdot \eta_{mot}}{\eta_{ICE}} \tag{5.3.4}$$

The situation is different when defining the lower bound of the EF. In conventional ECMS, the EF is designed on a full drive cycle mixed with acceleration, deceleration, cruising, start/stop, etc., where the net vehicle power demand is positive. For such drive cycles, it is possible to find an EF to achieve CS by strategically splitting the vehicle power demand between the engine and the battery.

However, in A-ECMS, SOC balancing is enforced on each short drive cycle segment. There might be some driving segments where the vehicle is mostly braking or decelerating, presenting negative net power demand. For these driving segments, it is impossible to achieve strict CS since the terminal SOC will inevitably increase even if the engine is always off during. Nonetheless, engine activation should be highly discouraged to avoid redundant battery charging. On this account, an infinitesimal number is adopted as the lower bound of the EF to discourage engine activation as much as possible for these occasions.

5.3.2 Biesection Method for EF Searching

In the proposed A-ECMS, the optimal EF for each drive cycle segment is determined by enforcing battery SOC back to its reference value as much as possible, as given in

Eq. (5.3.5), where ϵ represents a small tolerance.

$$|SOC_{end\_of\_cycle\_segment} - SOC_{reference}| \leq \epsilon \tag{5.3.5}$$

To find the optimal EF that meets Eq. (5.3.5), the bisection method [206], which is a common root-finding method based on Bolzano's theorem, is adopted. Fig. 5.3 illustrates the workflow of the bisection algorithm.

Step 1. The input of the algorithm $f(x)$ is defined as the deviation of the battery SOC at the end of each drive cycle segment $SOC_{end\_of\_cycle\_segment}$ from the reference value $SOC_{reference}$, i.e., $f(x) = SOC_{end\_of\_cycle\_segment} - SOC_{reference}$. The endpoints a and b stand for the lower and upper bound of the EF, which are 4 and 1e-7, respectively. The tolerance tol, also denoted as the ϵ in Eq. (5.3.5), is set to 1e-3. A maximum number of iterations i_{max} is imposed on the algorithm to save computing resources, which is set as 20.

Step 2. In the first iteration, calculate the midpoint c, its value $f(c)$, as well as the values of the endpoints $f(a)$ and $f(b)$. If $|f(c)| > tol$, check the sign of $f(c)$. If $f(c)$ presents the same sign as $f(a)$, replace a with c and keep b unchanged. Otherwise, replace b with c and keep a unchanged. If $|f(c)| \leq tol$, c is the root that satisfies Eq. (5.3.5).

Step 3. Repeat ***Step 2*** until the root c is found or the maximum number of iterations is exceeded.

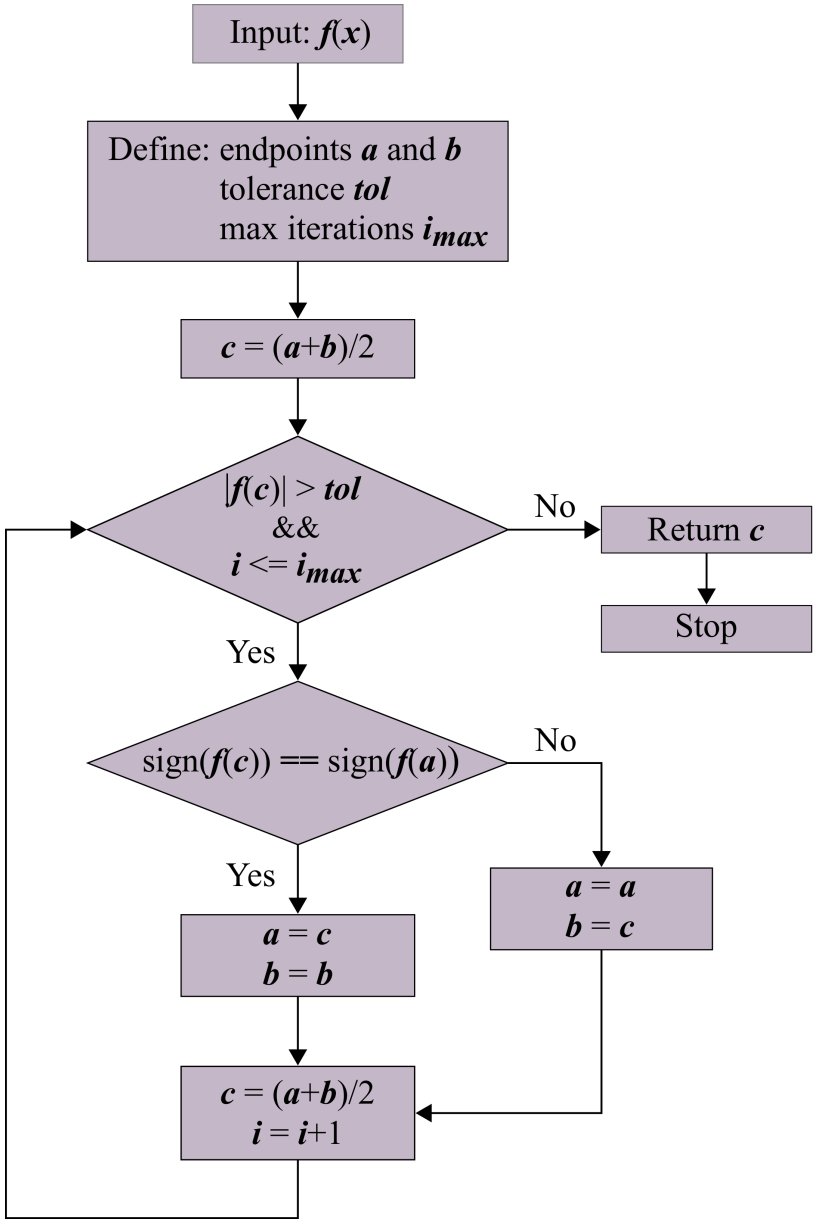

Figure 5.3: Flowchart of the bisection method.

5.3.3 A-ECMS

As discussed at the beginning of this section, A-ECMS requires the current and upcoming driving conditions to define the instantaneous power requirement so that the optimal EF prediction for the upcoming drive cycle segment can be found. This information can be obtained from modern road recognition techniques such as the Global Positioning System (GPS) [200], geographic information system (GIS) [207], support vector machine (SVM) [208], etc.

With the knowledge of the upcoming driving conditions, the optimal EF is searched at the beginning of each drive cycle segment using the bisection method and then implemented for real-time power distributing as a basic ECMS. The EF updating repeats periodically until the end of the entire drive cycle. Since battery operation is constrained by SOC safety range and charge sustainability, instantaneous battery SOC feedback is also required to determine the EF in real-time. The overall system diagram of the A-ECMS is depicted in Fig. 5.4.

5.4 Results and Discussions

To test the control performance of the proposed A-ECMS, simulation is conducted in MATLAB® and Simulink® under three drive cycles, i.e., UDDS, HWFET, and WLTP, with a time step of 0.1 seconds. The initial battery SOC is assumed to be 40%, and the prediction horizon of future driving conditions is set to 60 seconds. Simulation statistics are reported in Fig. 5.5. To better prove the effectiveness of

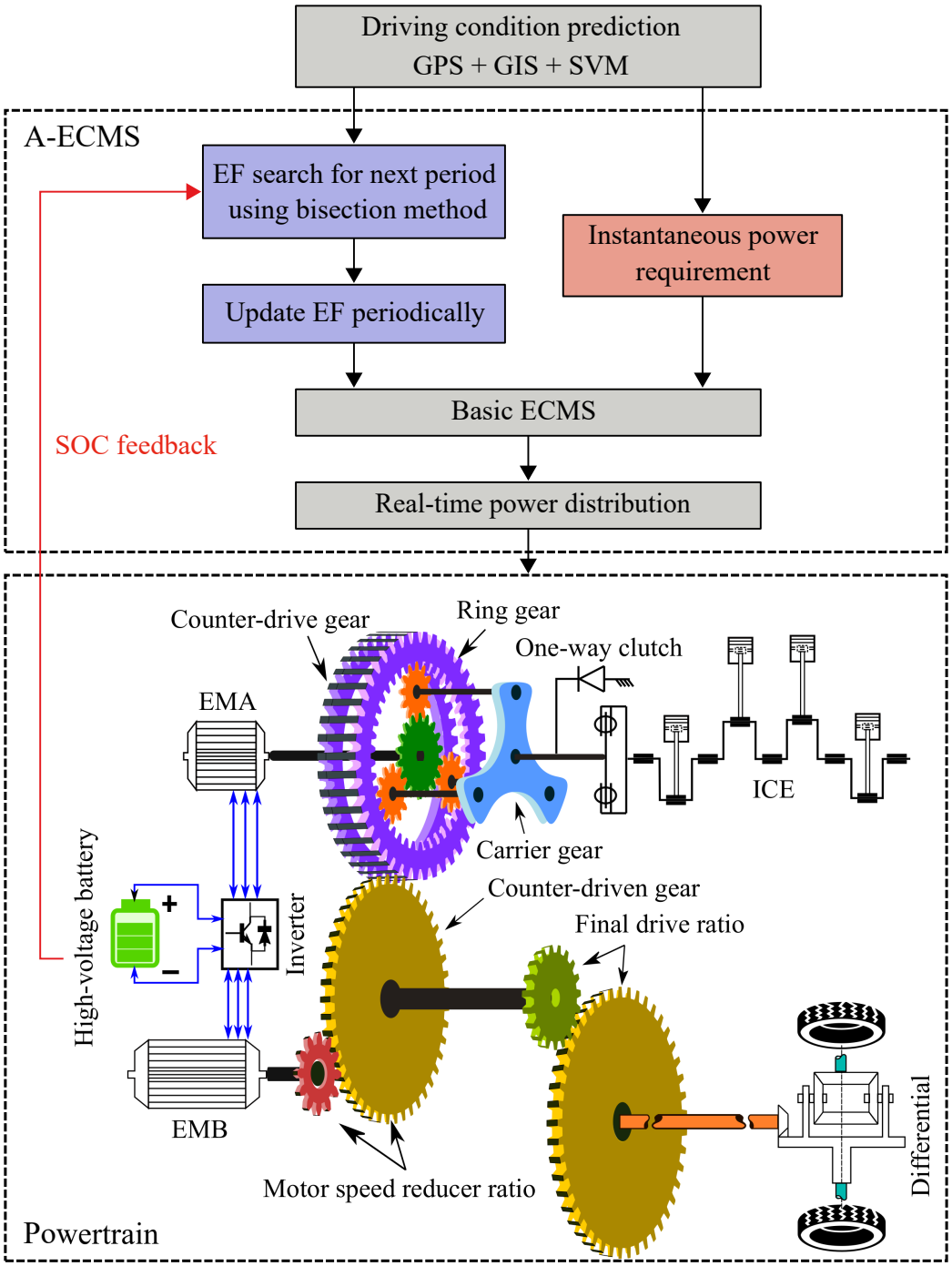

Figure 5.4: System diagram of A-ECMS for the multi-mode HEV.

the proposed A-ECMS, a basic non-adaptive ECMS is implemented on the same simulation platform under the same drive cycles for a fair comparison. Simulation results are discussed in detail as follows.

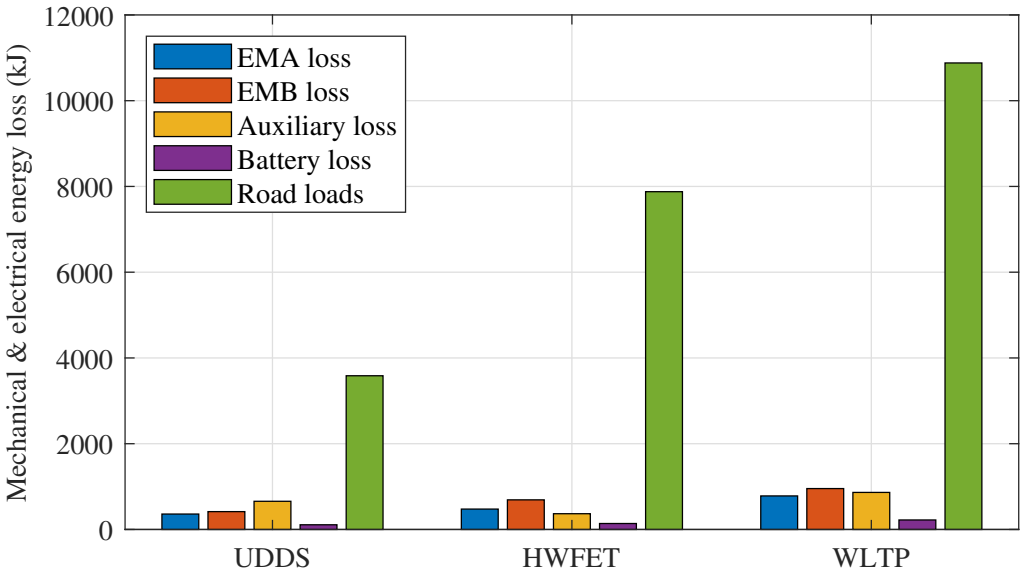

Figure 5.5: Simulation statistics of the hybrid electric powertrain with A-ECMS.

5.4.1 Battery SOC

Fig. 5.6 compares the battery SOC trajectories of the two ECMS. It can be observed that, for the proposed A-ECMS, battery SOC starts from 40% and ends up at approximately 40% with 0.289%, 0.9918%, and 0.1158% deviation under UDDS, HWFET, and WLTP, respectively. Therefore, it is reasonable to consider the proposed A-ECMS is capable of maintaining battery SOC and achieving CS operation.

The small deviation is due to the shorter prediction horizon of the A-ECMS compared to the basic non-adaptive ECMS. Although the A-ECMS aims to enforce the ending

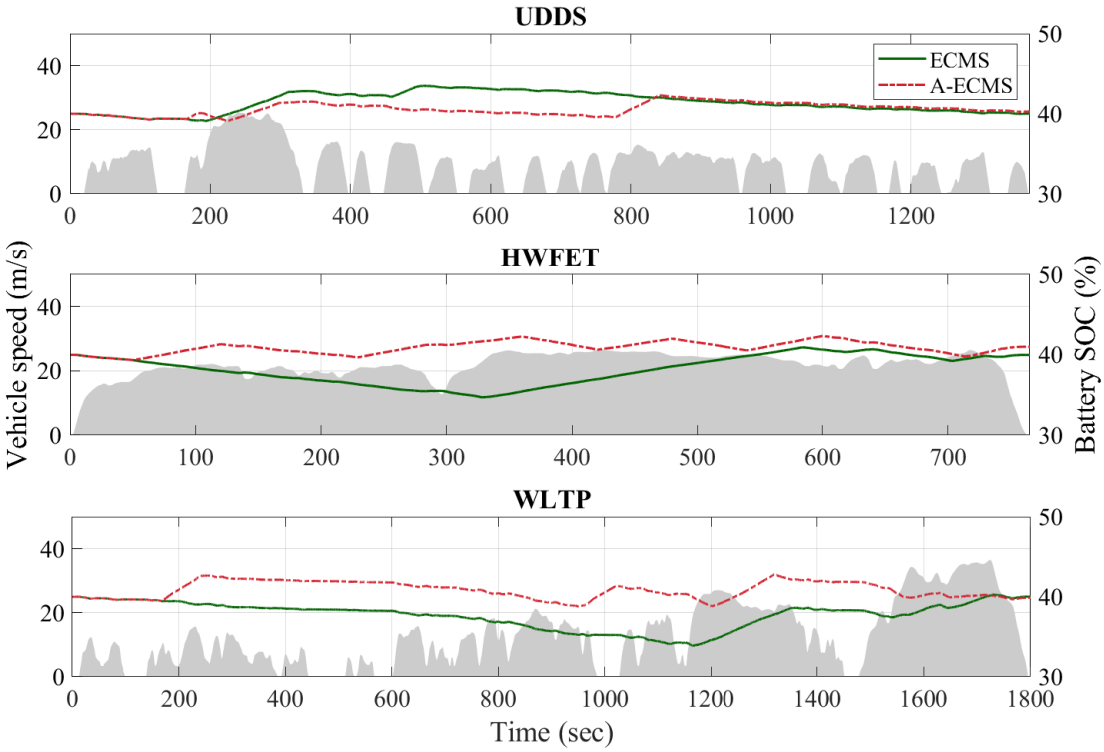

Figure 5.6: Comparison of battery SOC trajectories under three drive cycles.

SOC of each updating period back to its initial or reference value, it is impossible for some updating periods where the vehicle decelerates or stops most of the time. Since regenerative braking events dominate in these periods, the net vehicle power demand is negative, and thus the battery will be charged to a higher SOC inevitably. This is especially true for the last updating period of the drive cycle, where the vehicle mainly decelerates. However, as the updating period extends, the deviation can be mitigated.

In addition, compared to the basic non-adaptive ECMS, the A-ECMS shows a narrower SOC window since the SOC constraints are imposed on a shorter period, allowing fewer opportunities for deep charging or discharging. Although this might slightly sacrifice the global optimality, it is beneficial for battery longevity since excess depletion is prevented.

Different from the basic non-adaptive ECMS with a constant EF throughout the drive cycle, the proposed A-ECMS maintains battery SOC through the real-time update of the EF. Fig. 5.7 depicts the EF updating profiles of the A-ECMS. It can be seen that the EF stays within the defined searching bounds (1e-7 to 4) all the time and is updated every 60 seconds. Results indicate that the EF will increase/decrease accordingly to prevent battery SOC from constant drop/rise. When SOC tends to drop, it enables a larger EF to discourage battery using, and a smaller EF will be enabled to encourage battery using when SOC tends to rise.

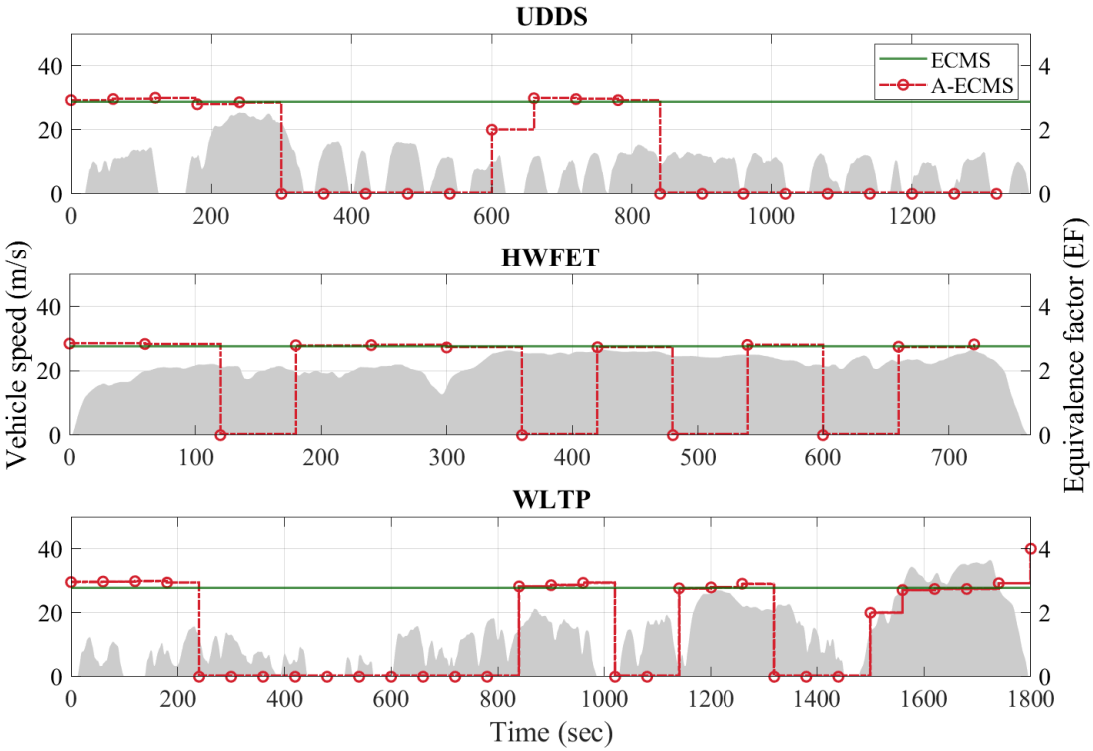

Figure 5.7: Comparison of EF trajectories under three drive cycles.

5.4.2 Engine Operation

Fig. 5.8 illustrates the power split between the battery and engine enabled by the A-ECMS. It can be observed that the battery provides the propelling power most of the time. When activated, the engine will operate at the most efficient point selected by the A-ECMS.

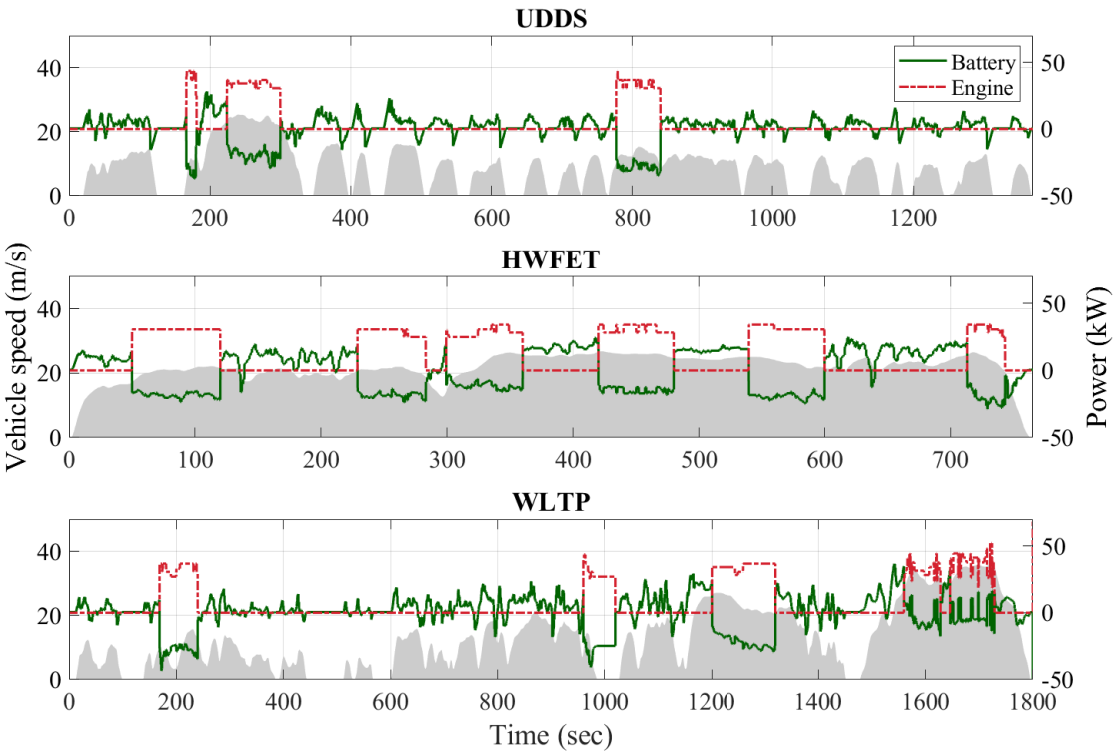

Figure 5.8: Power split between battery and engine in A-ECMS.

Fig. 5.9 and 5.10 compares the engine speed and torque profiles between the two ECMS. Thanks to the mode shift penalty imposed on the control strategies, there are no excessive mode shifts along the drive cycles for both ECMS. However, the mode shifts in A-ECMS are a few more than the basic ECMS since SOC balancing

is enforced on each short updating period rather than the entire long drive cycle. In addition, the A-ECMS also enables a slight longer engine-on time under HWFET and WLTP, as summarized in Table 5.2.

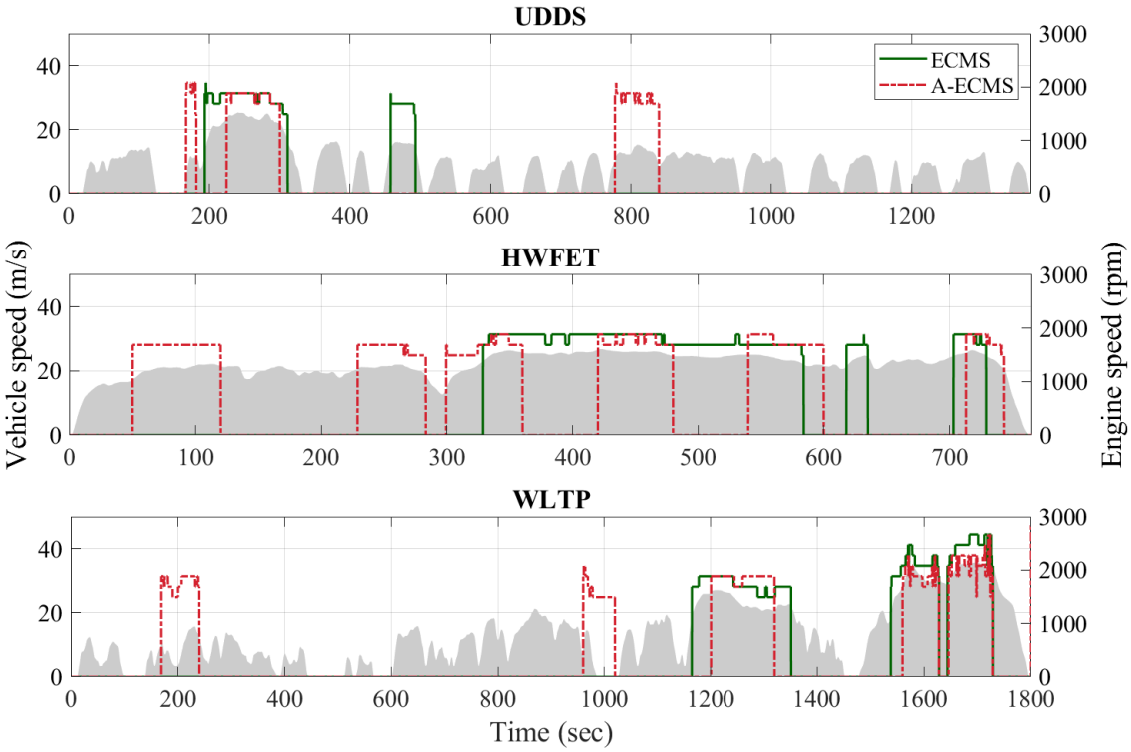

Figure 5.9: Comparison of engine speed under three drive cycles.

5.4.3 Fuel Consumption

As shown in Fig. 5.6, the terminal SOC is not exactly the same as the initial SOC in both ECMS, albeit the differences are small. To make a fair comparison, the change of electrical energy stored in the battery due to SOC difference should still be accounted for to correct the total fuel consumption. Fig. 5.11 presents the total fuel

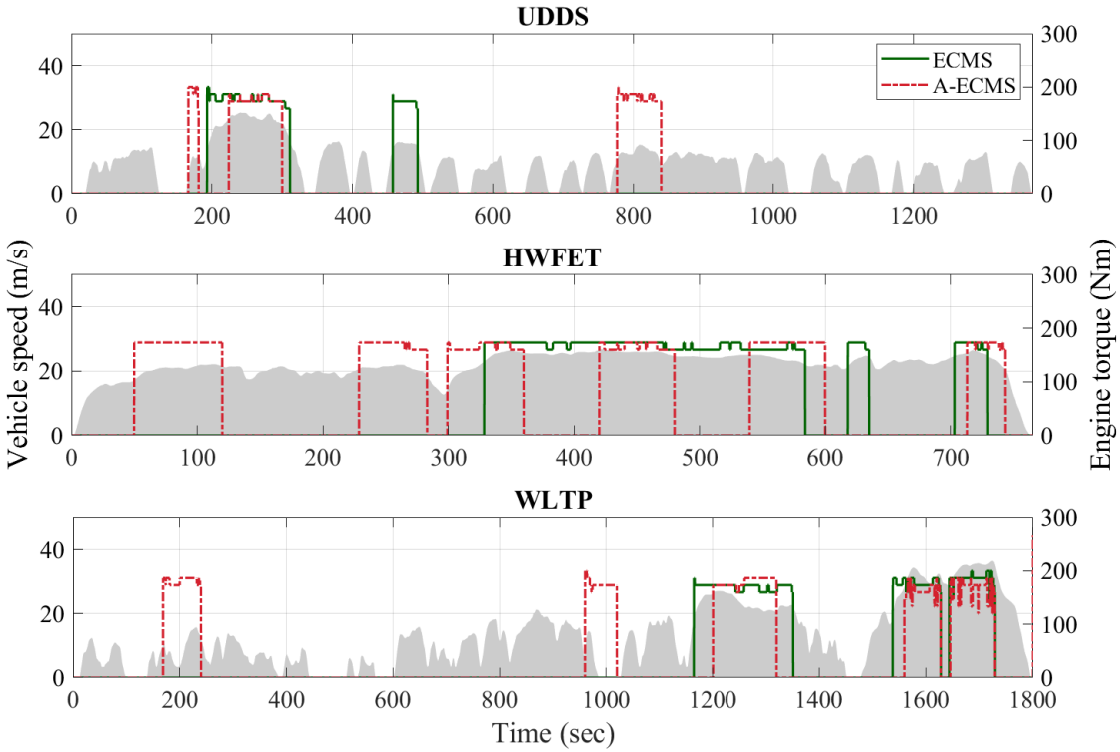

Figure 5.10: Comparison of engine torque under three drive cycles.

Table 5.2: Engine operation statistics of the A-ECMS.

Drive cycle	Control strategies	Engine on/offs	Engine-on time
UDDS	A-ECMS	3	11.21%
	Basic ECMS	2	11.21%
HWFET	A-ECMS	6	43.78%
	Basic ECMS	3	39.02%
WLTP	A-ECMS	5	22.28%
	Basic ECMS	3	20.11%

consumption of the two ECMS after SOC correction. As can be seen from the figure, the proposed A-ECMS shows slightly higher fuel consumption of 2.36%, 4.13%, and 1.09% on UDDS, HWFET, and WLTP, respectively.

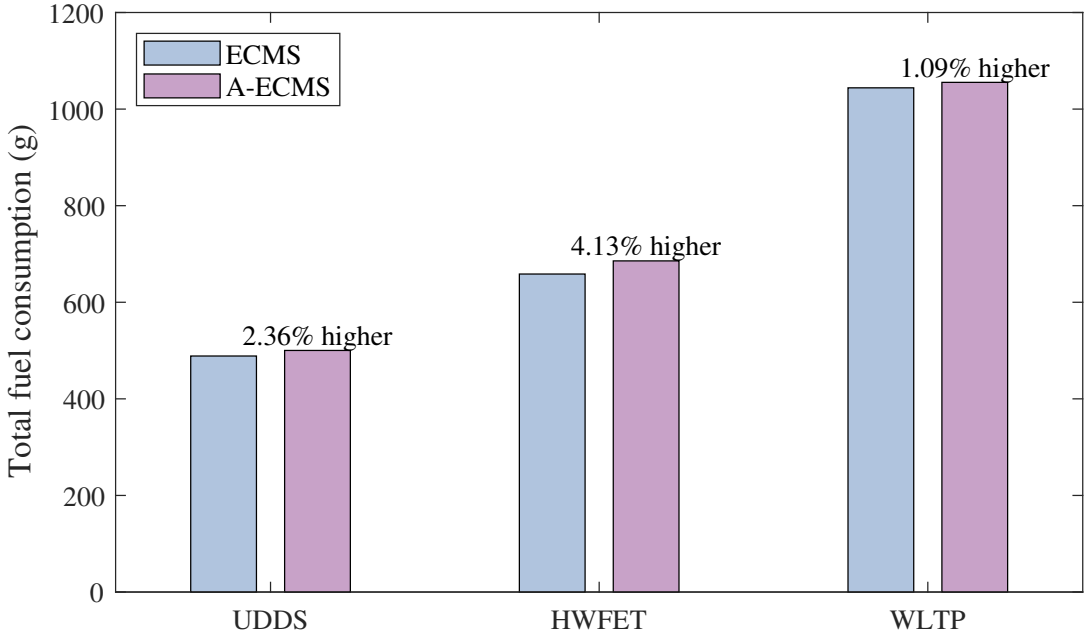

Figure 5.11: Comparison of fuel consumption under three drive cycles.

As mentioned earlier, the A-ECMS uses a series of "local" optimal/suboptimal EF to approach the "global" optimality. However, the exact "global" optimality can hardly be reached unless the prediction horizon is as long as the entire drive cycle. Consequently, the A-ECMS with a shorter prediction horizon will inevitably increase the overall fuel consumption as the control solutions are globally suboptimal.

Even though, the proposed A-ECMS reduces the dependency on the prior knowledge of the drive cycle, eliminates the need for manual tuning of the EF, and presents an online self-updating control scheme. With the help of road recognition techniques, the "real" real-time application can be realized.

5.5 Summary

This chapter aims to improve the real-time applicability of HEV EMS by proposing an A-ECMS with online EF calculation and real-time power splitting. First, a control-oriented model of a multi-mode HEV is presented, based on which the A-ECMS is proposed. Formulation of the proposed A-ECMS is described in detail. Simulation is then conducted on three drive cycles, and results are compared with a basic non-adaptive ECMS.

The proposed A-ECMS proves its real-time performance by exhibiting great CS capabilities on all studied drive cycles, with only slight increases in fuel consumption compared to the basic non-adaptive ECMS. Besides, the proposed A-ECMS enables a narrower SOC window which benefits the battery longevity. Moreover, with a real-time self-updating EF profile, dependency on the drive cycle information and manual tuning of the EF is also reduced. Therefore, the proposed A-ECMS achieves great improvement over the basic non-adaptive ECMS in real-time applicability.

The proposed A-ECMS can also be implemented on other powertrain architectures. Future work can be done on exploring other improved methods for EF searching, such as Brent's method and the Aberth method, to improve the computational efficiency of the A-ECMS.

Chapter 6

Deep Reinforcement Learning-based Energy Management for a Series Hybrid Electric Vehicle

The predictive A-ECMS proposed in Chapter 5 presents the capability of online EF tuning and real-time implementation. However, the success of EF tuning to achieve CS for a driving task still more or less relies on the knowledge of future driving conditions. Even though the proposed A-ECMS achieves improvements in real-time performance compared to the basic non-adaptive ECMS, there is still room for further improvements.

The past few decades have witnessed the great rise of artificial intelligence and machine learning (ML) technologies, which have played indispensable roles in many fields including transportation [209]. Among them, reinforcement learning (RL) is a popular ML paradigm to solve sequential decision-making problems and has thus attracted significant research interest in real-time optimization tasks [56]. Deep reinforcement learning (DRL), by combining the power of RL and DL, has shown promising potentials in HEV energy management problems [210]. With the recent progress in computer science, more and more research activities can be expected.

On this account, this chapter aims to investigate the DRL-based HEV energy management on a series HEV platform. First, the fundamentals of RL are reviewed, including key concepts and algorithms. Then, a control-oriented HEV model is described, based on which the optimal control problem is identified. Following that, a DRL-based energy management strategy featuring the state-of-the-art A3C algorithm is formulated and explained comprehensively. The training process and results are provided in the following section.

6.1 Fundamentals of Reinforcement Learning

6.1.1 Reinforcement Learning

RL is one of the three broad categories of ML techniques, together with supervised learning and unsupervised learning. RL learns its experience from repeated interactions with the **environment** where the **agent** observes the **state** and sends the **action**. The environment, which can be described as a Markov Decision Process (MDP), receives the action, changes to the next state, and tells the goodness of that action in the form of a **reward**. Based on that reward, the agent updates its control scheme and sends the action for the next state. This observation-action-reward cycle continues until the end of learning. Therefore, RL learns the optimal control scheme on a trial-and-error basis [211]. Fig. 6.1 depicts the agent-environment interactions in RL.

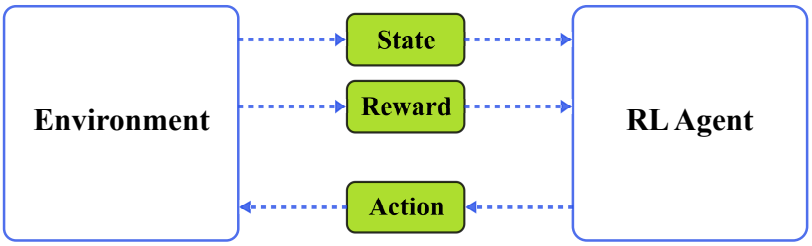

Figure 6.1: Illustration of agent-environment interactions in RL.

In many real-world decision-making tasks, the state space of the MDP is large. Solving such problems with traditional RL algorithms is challenging. As a result, the DL algorithm is incorporated, using neural networks to represent the policy, which is a mapping from state to action [212]. Such a combination of RL and DL is called DRL. DRL can solve various complex decision-making problems and has become the most

trending machine learning technique [213].

6.1.2 Key Concepts in Reinforcement Learning

Return

In RL, there are generally two kinds of tasks, i.e., **episodic tasks** and **continuing tasks**. In episodic tasks, the agent-environment interactions can be broken into subsequences, known as episodes. Each episode ends in a terminal state, after which a new episode starts independently of the previous episode by resetting to the initial state. In contrast, continuing tasks run continually with neither terminal states nor identifiable episodes.

Return is defined as the cumulative future rewards. However, the return would be infinity in continuing tasks since the time goes to infinity. To this end, it is beneficial to introduce a **discount factor**, $\gamma \in [0, 1]$, which determines the present value of future rewards. For instance, a reward received k steps ahead in the future r_{t+k} is equivalent to a discounted value of $\gamma^{k-1} r_{t+k}$ at present. $\gamma = 0$ leads to a short-sighted agent which only focuses on the immediate reward. $\gamma = 1$ encourages the agent to look infinitely far into the future, indicating that future rewards are equally important as the immediate reward. Return R can be expressed as Eq. (6.1.1), where r denotes the immediate reward, and t denotes the current time step.

$$R_t = r_{t+1} + \gamma r_{t+2} + \cdots = \sum_{k=t+1}^{\infty} \gamma^{k-t-1} r_k \tag{6.1.1}$$

Policy

Policy and **value function** are two important elements in RL algorithms. There are mainly two types of policies, i.e., **target policy** and **behavior policy**. Target policy or update policy is the policy that the agent tries to learn and improve, while behavior policy is the policy that the agent uses to choose actions. Generally, behavior policy is a mapping from states to actions, and more specifically, a probability distribution over actions in a certain state, as shown in Eq. (6.1.2).

$$\pi(a|s) = \mathbb{P}_\pi \{a_t = a | s_t = s\} \tag{6.1.2}$$

Depending on whether the target policy and the behavior policy are the same one, RL algorithms can be divided into **on-policy RL** and **off-policy RL**. In on-policy RL, the target policy and behavior policy are the same, so the agent attempts to improve the same policy that is used for selecting actions [214]. Examples of on-policy algorithms are Proximal Policy Optimization (PPO), Trust Region Policy Optimization (TRPO), and asynchronous advantage actor-critic (A3C). In off-policy RL, by contrast, the target policy is different from the behavior policy. The agent uses the target policy to learn and the behavior policy to behave [215]. The most famous representatives of off-policy RL include Q-learning and Deep Q-Network (DQN). Compared to off-policy algorithms, on-policy algorithms are more beneficial for tasks where the agent explores significantly.

Value Function

As the RL agent aims to find the optimal policy that maximizes the expected return, **value functions** are employed to evaluate the policy by a prediction of the return. **State value function** $V^{\pi}(s)$ specifies the expected return in state s following policy π, as shown in Eq. (6.1.3). It quantifies how advantageous it is to be in a particular state.

$$V^{\pi}(s) = \mathbb{E}_{\pi}\left\{R_t | s_t = s\right\} = \mathbb{E}_{\pi}\left\{\sum_{k=t+1}^{\infty} \gamma^{k-t-1} r_k | s_t = s\right\} \tag{6.1.3}$$

Action value function $Q^{\pi}(s, a)$ specifies the expected return for taking action a in state s according to policy π, as given in Eq. (6.1.4). The action value, also called Q value, quantifies how rewarding an action is for a certain state. Therefore, the state-value function $V^{\pi}(s)$ and the action value function $Q^{\pi}(s, a)$ are correlated through the policy $\pi(a|s)$, as given in Eq. (6.1.5).

$$Q^{\pi}(s, a) = \mathbb{E}_{\pi}\left\{R_t | s_t = s, a_t = a\right\} = \mathbb{E}_{\pi}\left\{\sum_{k=t+1}^{\infty} \gamma^{k-t-1} r_k | s_t = s, a_t = a\right\} \tag{6.1.4}$$

$$V^{\pi}(s) = \sum Q^{\pi}(s, a)\pi(a|s) \tag{6.1.5}$$

6.1.3 Asynchronous Advantage Actor-Critic Algorithm

Actor-Critic Algorithm

The policy structure and algorithm are closely intertwined in RL. Based on different policy structures, there are three main types of RL algorithms, i.e., policy function-based algorithms, value function-based algorithms, and actor-critic algorithms [211]. Policy structures of these three algorithms are illustrated in Fig. 6.2.

In **policy function-based algorithms**, a neural network receives the state observations and gives the learning agent's best actions for that state. The neural network, called the actor, directly represents the optimal policy.

In **value function-based algorithms**, a neural network receives the state observations and one possible action in that state. The neural network, called the critic, calculates the value of taking that action. The optimal policy is then defined by checking all possible actions and choosing the one with the highest value.

However, both algorithms have downsides. Policy function-based algorithms may converge slowly or on local optima rather than global optima. Value function-based algorithms cannot deal with continuous action spaces since an exhaustive search in infinite or large action spaces is impossible or computationally expensive. As a result, combining the two algorithms by keeping the benefits and eliminating the drawbacks gives the **actor-critic (AC)** method [216].

AC algorithms take advantage of two complementing models, i.e., an actor and a critic. The actor chooses an action for the environment as in policy function-based

(a)

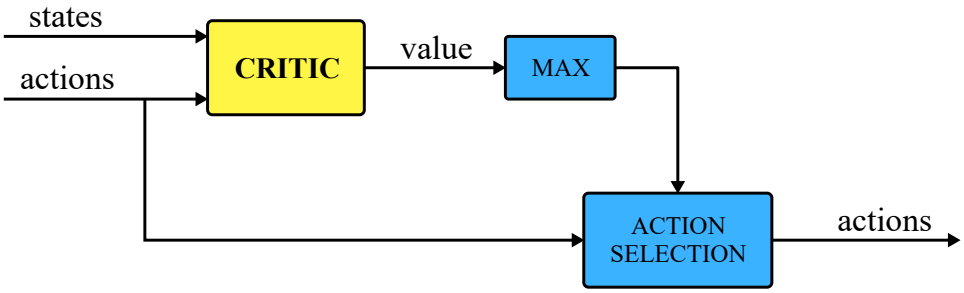

(b)

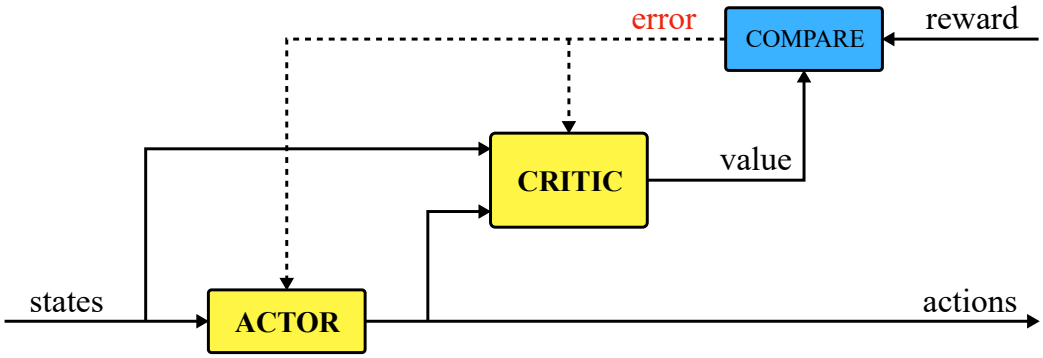

(c)

Figure 6.2: Policy structures in (a) policy function-based algorithms; (b) value function-based algorithms; (c) actor-critic algorithms.

algorithms. The critic predicts the value of that action and calculates the error with the reward received from the environment. The error is then used to update the critic and actor so that the policy ascends toward the direction the critic suggests.

Advantage Actor-Critic Algorithm

Advantage function $A^{\pi}(s,a)$ specifies the difference between the action value function and the state value function, as shown in Eq. (6.1.6). The advantage value, also called A value, describes how much better the reward is than its expectation.

$$A^{\pi}(s,a) = Q^{\pi}(s,a) - V^{\pi}(s) \tag{6.1.6}$$

In advantage actor-critic (A2C) algorithm, the critic learns the advantage function (A function) instead of the action value function (Q function). In such a way, the action is evaluated based on not only how good the action is but also how better the action is. As indicated in Eq. (6.1.6), advantage function $A(s,a)$ can be calculated from Q value function $Q(s,a)$ and state value function $V(s)$. However, the Q value function is difficult to be directly calculated, and therefore an n-step estimate is formulated, as shown in Eq. (6.1.7). The advantage function can be then estimated by Eq. (6.1.8).

$$Q(s,a) = \sum_{i=0}^{n-1} \gamma^{i} r_{t+i} + \gamma^{n} V(s_{t+n}) \tag{6.1.7}$$

$$A(s,a) = \sum_{i=0}^{n-1} \gamma^i r_{t+i} + \gamma^n V(s_{t+n}) - V(s_t) \tag{6.1.8}$$

Unlike most algorithms with only one learning agent, the A2C algorithm can employ multiple learning agents, called workers, each of which has its own set of network parameters and a copy of the environment. These workers are trained in parallel and synced with the global network periodically and synchronously. The global network merges the gradients from each worker, updates the global parameters, and then sends the new global parameters to each worker again [217].

However, a problem is that the workers likely complete their tasks at different times. Due to the synchronization requirement, some workers have to wait until all of them are done, resulting in a waste of computational resources.

Asynchronous Advantage Actor-Critic Algorithm

The asynchronous advantage actor-critic (A3C) algorithm is introduced to address this drawback [218]. As an extension of A2C, A3C breaks the synchronization barrier and allows for an asynchronous updating of the global network. The workers interact with their respective environments independently and update the global network asynchronously. This enables the agent to explore a larger part of the state-action space within a shorter time, improving the learning speed. Fig. 6.3 provides an illustration of the A3C algorithm.

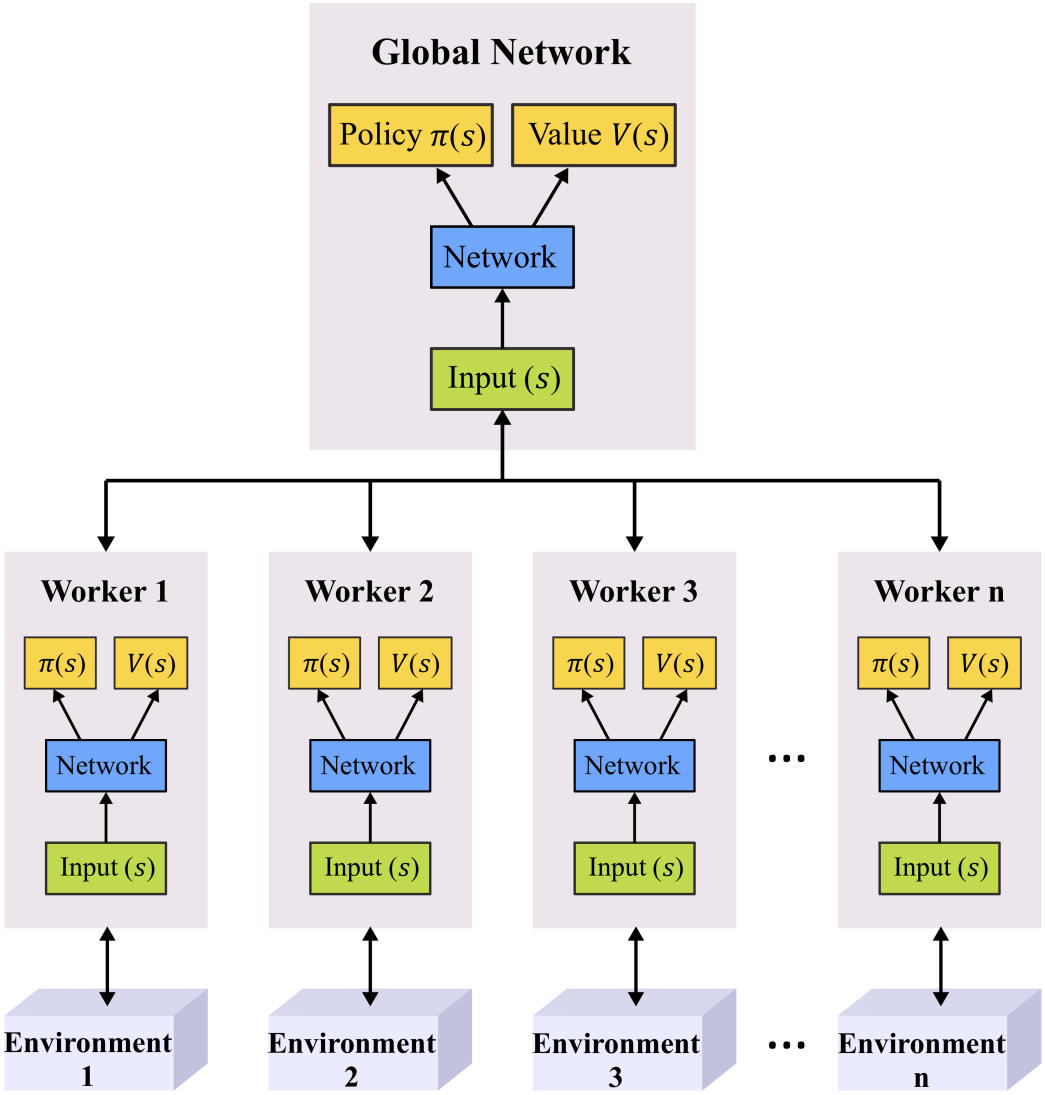

Figure 6.3: Illustration of A3C algorithm.

6.2 Powertrain Modeling and Problem Formulation

The hybrid powertrain investigated in this chapter is a series configuration. A schematic diagram of the powertrain system is depicted in Fig. 6.4. Details of the vehicle specifications and modeling approaches are presented as follows.

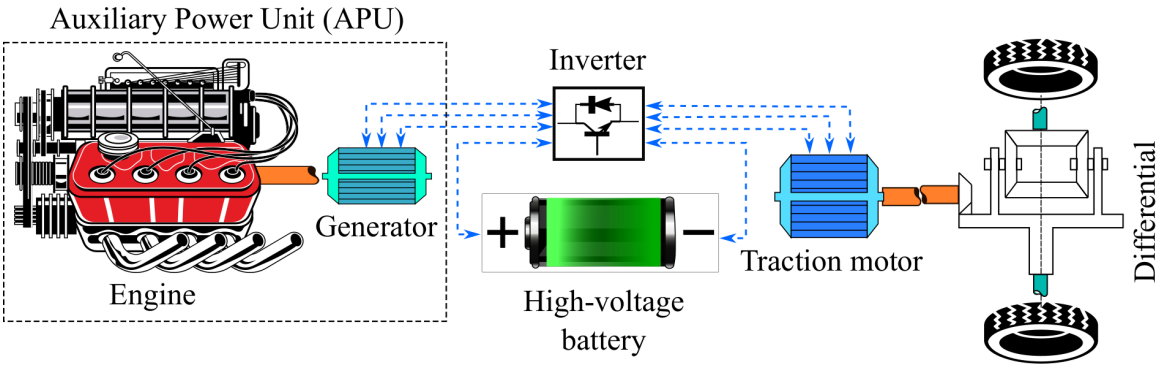

Figure 6.4: Schematic diagram of the series HEV configuration.

6.2.1 Hybrid Powertrain Architecture

The studied hybrid powertrain system incorporates an ICE, a generator, a traction motor, and a battery. The battery constantly supplies electrical power to drive the traction motor for vehicle propulsion, while the engine-generator set, i.e., the auxiliary power unit (APU), charges the battery when necessary. Therefore, the hybrid system enables two operating modes, i.e., EV mode if the engine is off and HEV mode if the engine is on. The traction motor is directly coupled to the transmission output shaft through a final drive ratio. Vehicle specifications are listed in Table 6.1.

Table 6.1: Vehicle specifications of the series HEV.

Component	Parameter	Value
Vehicle	Equivalent mass	3500 kg
	Wheel radius	0.375 m
	Road coefficient μ_1	208.9664 N
	Road coefficient μ_2	6.9720 N/(m/s)
	Road coefficient μ_3	0.5841 N/(m/s)^2
	Final drive ratio	9.8
Engine	Displacement	3.0 L
	Maximum power	200 kW
	Maximum torque	330 Nm
	Maximum speed	6000 rpm
Motor	Maximum power	388 kW
	Maximum torque	780 Nm
	Maximum speed	15000 rpm
Generator	Maximum power	196 kW
	Maximum torque	320 Nm
	Maximum speed	6400 rpm
Battery	Capacity	302.6 Ah
	Nominal voltage	320.8 V

6.2.2 Control-Oriented Vehicle Model

Auxiliary Power Unit

In the series HEV, the engine and generator are coaxially coupled together as an APU, and thus share the same speed and torque, as expressed in Eq. (6.2.1). The operation of the APU should be simultaneously constrained by the physical limits of the engine and generator, as illustrated in Eq. (6.2.2).

$$\begin{aligned} \omega_{APU} &= \omega_{ICE} = \omega_{gen} \\ T_{APU} &= T_{ICE} = T_{gen} \end{aligned} \tag{6.2.1}$$

$$\begin{aligned} max\left(\omega_{ICE,min}, \omega_{gen,min}\right) \leq \omega_{APU} \leq min\left(\omega_{ICE,max}, \omega_{gen,max}\right) \\ max\left(T_{ICE,min}, T_{gen,min}\right) \leq T_{APU} \leq min\left(T_{ICE,max}, T_{gen,max}\right) \end{aligned} \tag{6.2.2}$$

The power output of the APU is the engine power multiplied by a factor of generator efficiency, which is a function of generator torque and speed, as shown in Eq. (6.2.3). The fuel flow rate of the engine $\dot{m}_{fuel}$ can be calculated from engine efficiency η_{ICE}, as given in Eq. (6.2.4), where LHV_{fuel} denotes the lower heating value of the fuel. With Eq. (6.2.4), Eq. (6.2.3) can be then reformulated as Eq. (6.2.5), which indicates that for a given power demand, fuel consumption can be optimized by maximizing the combined efficiency of the engine and generator.

$$P_{APU} = P_{ICE} \cdot \eta_{gen}(T_{gen}, \omega_{gen}) = T_{ICE} \cdot \omega_{ICE} \cdot \eta_{gen}(T_{gen}, \omega_{gen}) \tag{6.2.3}$$

$$\dot{m}_{fuel} = \frac{P_{ICE}}{\eta_{ICE}(T_{ICE}, \omega_{ICE}) \cdot \text{LHV}_{fuel}} = \frac{T_{ICE} \cdot \omega_{ICE}}{\eta_{ICE}(T_{ICE}, \omega_{ICE}) \cdot \text{LHV}_{fuel}} \tag{6.2.4}$$

$$P_{APU} = \dot{m}_{fuel} \cdot \text{LHV}_{fuel} \cdot \eta_{ICE}(T_{ICE}, \omega_{ICE}) \cdot \eta_{gen}(T_{gen}, \omega_{gen}) \tag{6.2.5}$$

Motor

The electric motor is modeled by a 3-D combined efficiency map which is dependent on motor torque, speed, and voltage. The motor power is given by Eq. (6.2.6), where $P_{mot,elec}$, T_{mot}, ω_{mot}, η_{mot}, and V_{mot} denote motor electrical power, torque, rotational speed, efficiency, and voltage, respectively. Since the electric motor is directly connected to the transmission shaft, its torque and speed can be derived from vehicle longitudinal dynamics, as given in Eq. (6.2.7) and (6.2.8), where fd denotes the final drive ratio. T_{wh} and ω_{wh} denote the torque and rotational speed at wheels, respectively.

$$P_{mot,elec} = \begin{cases} T_{mot} \cdot \omega_{mot} / \eta_{mot}(T_{mot}, \omega_{mot}, V_{mot}), & T_{mot} \geq 0 \\ T_{mot} \cdot \omega_{mot} \cdot \eta_{mot}(T_{mot}, \omega_{mot}, V_{mot}), & T_{mot} < 0 \end{cases} \tag{6.2.6}$$

$$T_{mot} = \frac{1}{fd} \cdot T_{wh} \tag{6.2.7}$$

$$\omega_{mot} = fd \cdot \omega_{wh} \tag{6.2.8}$$

Battery

The equivalent circuit approach is adopted to model the battery pack. The battery current I_{batt} can be derived from Ohm's law, which can be rearranged into Eq. (6.2.9). V_{oc} and R denote the battery open-circuit voltage and internal resistance, respectively, both of which are a function of battery SOC. P_{batt} denotes the battery power, which is provided to the traction motor together with the APU power, as expressed in Eq. (6.2.10).

$$I_{batt}(t) = \frac{V_{oc}(SOC) - \sqrt{V_{oc}(SOC)^2 - 4 \cdot R(SOC) \cdot P_{batt}}}{2 \cdot R(SOC)} \tag{6.2.9}$$

$$P_{batt} = P_{mot,elec} - P_{APU} \tag{6.2.10}$$

Battery SOC can be calculated based on Eq. (6.2.11), where Q_{batt} and η denote the battery capacity and coulombic efficiency, respectively.

$$SOC(t) = SOC(t_0) - \frac{\eta}{Q_{batt}} \int_{t_0}^{t} I_{batt}(t)dt \tag{6.2.11}$$

Vehicle Longitudinal Dynamics

The vehicle speed can be derived from longitudinal vehicle dynamics, as given in Eq. (6.2.12):

$$v_{veh} = \frac{1}{m_{equiv}} \int \left(\frac{T_{wh}}{R_{wh}} - \mu_1 - \mu_2 \cdot v_{veh} - \mu_3 \cdot v_{veh}^2 \right) dt \tag{6.2.12}$$

where m_{equiv} is the equivalent mass of the vehicle, T_{wh} is the torque at wheels, R_{wh} is the wheel radius, and μ_1, μ_2, and μ_3 are the road load coefficients.

6.2.3 Optimal Control Problem

Based on the control-oriented HEV model described above, the optimal control problem is formulated aiming at fuel minimization while maintaining battery SOC over a drive cycle, as given in Eq. (6.2.13), where ζ is a large weighting factor.

$$u^* = \arg\min_u \left\{ \int_{t_0}^{t_f} \dot{m}_{fuel}(x,u)dt + \zeta \cdot [SOC(t_f) - SOC(t_0)] \right\} \tag{6.2.13}$$

Moreover, the following constraints are imposed to limit the powertrain components

within their physical limits:

$$\begin{cases} SOC_{min} \leq SOC(t) \leq SOC_{max} \\ P_{batt,min} \leq P_{batt}(t) \leq P_{batt,max} \\ I_{batt,min} \leq I_{batt}(t) \leq I_{batt,max} \\ T_{ICE,min} \leq T_{ICE}(t) \leq T_{ICE,max} \\ \omega_{ICE,min} \leq \omega_{ICE}(t) \leq \omega_{ICE,max} \\ T_{EMA,min} \leq T_{EMA}(t) \leq T_{EMA,max} \\ \omega_{EMA,min} \leq \omega_{EMA}(t) \leq \omega_{EMA,max} \\ T_{EMB,min} \leq T_{EMB}(t) \leq T_{EMB,max} \\ \omega_{EMB,min} \leq \omega_{EMB}(t) \leq \omega_{EMB,max} \end{cases} \tag{6.2.14}$$

6.3 Deep Reinforcement Learning-based Energy Management Strategy

This section proposes a DRL-based energy management strategy for the series HEV introduced in Section 6.2. The system diagram of the proposed strategy is illustrated in Fig. 6.5. As shown in the diagram, the development and implementation of the proposed strategy include three stages:

Stage 1: DRL in simulation. At this stage, the HEV EMS, which is represented by an RL agent, is trained off-line. In this work, the A3C algorithm is adopted to update control parameters in simulation based on state, action, and reward data through

interacting with the environment, i.e., the HEV model plus the drive cycle. It should be noted that, since the RL agent only requires feedback from the vehicle, training with a prior knowledge of the drive cycle is not conflicted with its capability of online application without the prior knowledge.

Stage 2: EMS downloading. Once the training gets converged, the trained RL agent is downloaded and saved as the HEV EMS.

Stage 3: Strategy online application. The derived EMS can be implemented in the HEV hybrid control program and then applied online. Vehicle control solutions can be obtained by mapping states to actions.

The research focus of this work lies in the first and third stages. In the following context, developing the DRL-based EMS as *Stage 1* is thoroughly explained first. Then testing the trained EMS for online application as *Stage 3* is provided.

6.3.1 State, Action, and Reward

State: In RL, the state variables should be able to fully represent the environment, which is the vehicle plant in HEV energy management problems. Since the A3C algorithm is free from the curse of dimensionality, more state variables are allowed, which helps the agent understand the environment. However, too many state variables may deteriorate the convergence performance or trap the optimal control into local optima. As a result, a five-dimensional continuous state space consisting of vehicle speed v_{veh}, vehicle acceleration acc_{veh}, APU power P_{APU}, battery SOC, and its deviation from

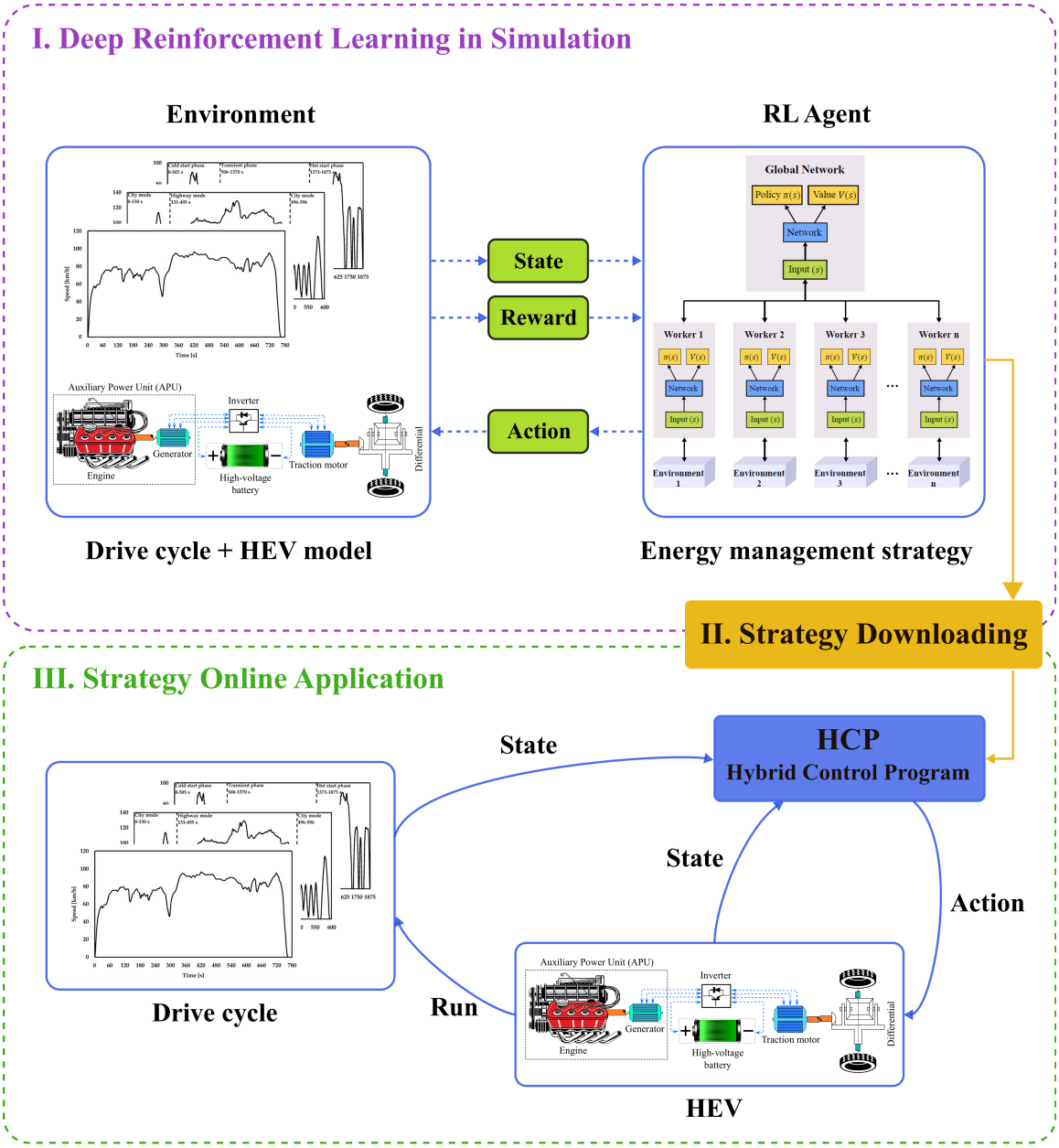

Figure 6.5: System diagram of DRL-based energy management for HEVs.

the reference value ΔSOC is defined as follows:

$$S = \{v_{veh}, acc_{veh}, P_{APU}, SOC, \Delta SOC\} \tag{6.3.1}$$

Action: According to Eq. (6.2.10), the APU and the battery together provide the requested power to the traction power to propel the vehicle. Therefore, given a vehicle power demand, the energy management problem is to optimally split the power between the APU and the battery.

Due to the randomness of RL, directly using P_{APU} as the action will lead to undesired abrupt changes in APU power. Instead, using power increment/decrement ΔP_{APU} will prevent the APU power from being arbitrary, ensuring better continuity. Furthermore, to alleviate the computational burden, a discrete action space is defined to enforce finite numbers of actions, as shown in Eq. (6.3.2), where there are 14 options: decrease 5 kW; decrease 2 kW; decrease 1 kW; stay unchanged; increase 1 kW; increase 2 kW; increase 3 kW; increase 4 kW; increase 5 kW; increase 6 kW; increase 7 kW; increase 8 kW; increase 9 kW; increase 10 kW.

$$A = \Delta P_{APU} = \{-5, -2, -1, 0, 1, 2, 3, 4, 5, 6, 7, 8, 9, 10\} \tag{6.3.2}$$

Reward: The reward function must be carefully designed since it directly affects the control performance. The HEV energy management in this work is to minimize the total fuel consumption over a drive cycle while achieving battery CS. Therefore, there are two indicators in the reward function: one is the instantaneous fuel mass

flow rate, and the other is the deviation of battery SOC from its reference value, which is the SOC at the beginning of the trip. Since the RL agent aims to maximize its return during the learning, a negative sign is assigned in the equation. The immediate reward function is formulated as Eq. (6.3.3), where α and β are two weighting factors. Through repeated tuning of these two parameters, a balance between fuel economy and battery CS performance can be achieved.

$$R = -tanh[\alpha \cdot \dot{m}_{fuel} + \beta \cdot |SOC(t) - SOC_{ref}|] \tag{6.3.3}$$

6.3.2 Design of Neural Networks

In DRL, neural networks are used as the universal function approximators. A neural work is a network of artificial neurons or nodes that are connected in some way to represent an input-to-output relationship. There is an input and an output layer, between which hidden layers transfer the information from input to output. The value of each node can be represented as a linear equation with weights and bias, and an activation function is applied after the linear operation to capture the non-linear features. In such a way, the neural network can represent any linear/nonlinear function.

There is no general way to determine the structure of a neural network. On the one hand, the structure should be complex enough to be able to approximate the function. On the other hand, it should not be too complex to make the training process extremely slow or even impossible. Based on the author's prior experience

and the reference from literature, the neural networks for the critic and actor in this work are designed as follows.

The critic network takes the state observations as the input and the state value function as the output. The input layer is a feature input layer with five neurons, one for each state variable. The output layer is a fully-connected layer with only one neuron representing a scalar value $V(s)$. Between the input and output layers are three fully-connected hidden layers with 100 neurons each. Each hidden layer is followed by a rectified linear unit (ReLU) activation function, which returns zero for negative values and keeps positive values unchanged, as given in Eq. (6.3.4):

$$f(x) = \begin{cases} 0, & x < 0 \\ x, & x \geq 0 \end{cases} \tag{6.3.4}$$

The actor network receives the state observations and outputs a stochastic policy, which is a probability distribution of the action space. The input and hidden layers have the same structure and activation functions as in the critic network. The output layer is a fully-connected layer with 14 neurons corresponding to each possible action. It is processed by a softmax activation function that calculates the probability of each action and ensures that all probabilities sum to 1, as given in Eq. (6.3.5). The softmax layer shares the same number of neurons as the output layer.

$$softmax(z_i) = \frac{e^{z_i}}{\sum_{j=1}^{K} e^{z_j}} \; for \; i = 1, ..., K \tag{6.3.5}$$

The architecture of the AC networks is illustrated in Fig. 6.6.

6.3.3 Data Normalization

One of the best practices in neural network training is to normalize the input to the neural networks. When the input variables are of the same scale, several benefits are enabled, such as speeding up the learning and convergence, preventing divergence, facilitating hyperparameter tuning, etc.

As stated in Section 6.3.2, the input to the critic and actor networks is the state observations. Therefore, the state variables defined in Section 6.3.1 are preprocessed as follows: vehicle speed v_{veh} and acceleration acc_{veh} are normalized by the z-score method, as illustrated in Eq. (6.3.6), where μ and σ are the mean and standard deviation of each data set, which are calculated based on the training driving cycle. P_{APU} is rescaled into [0, 1] by dividing the maximum value of APU power. Battery SOC belongs to [0, 1] inherently, and therefore ΔSOC falls between [-1, 1], both of which can be directly fed into the neural networks without further normalization.

$$Z = \frac{x - \mu}{\sigma} \tag{6.3.6}$$

On the other side, since the action space is discrete, each possible action is assigned a value of probability, so further normalization is unnecessary.

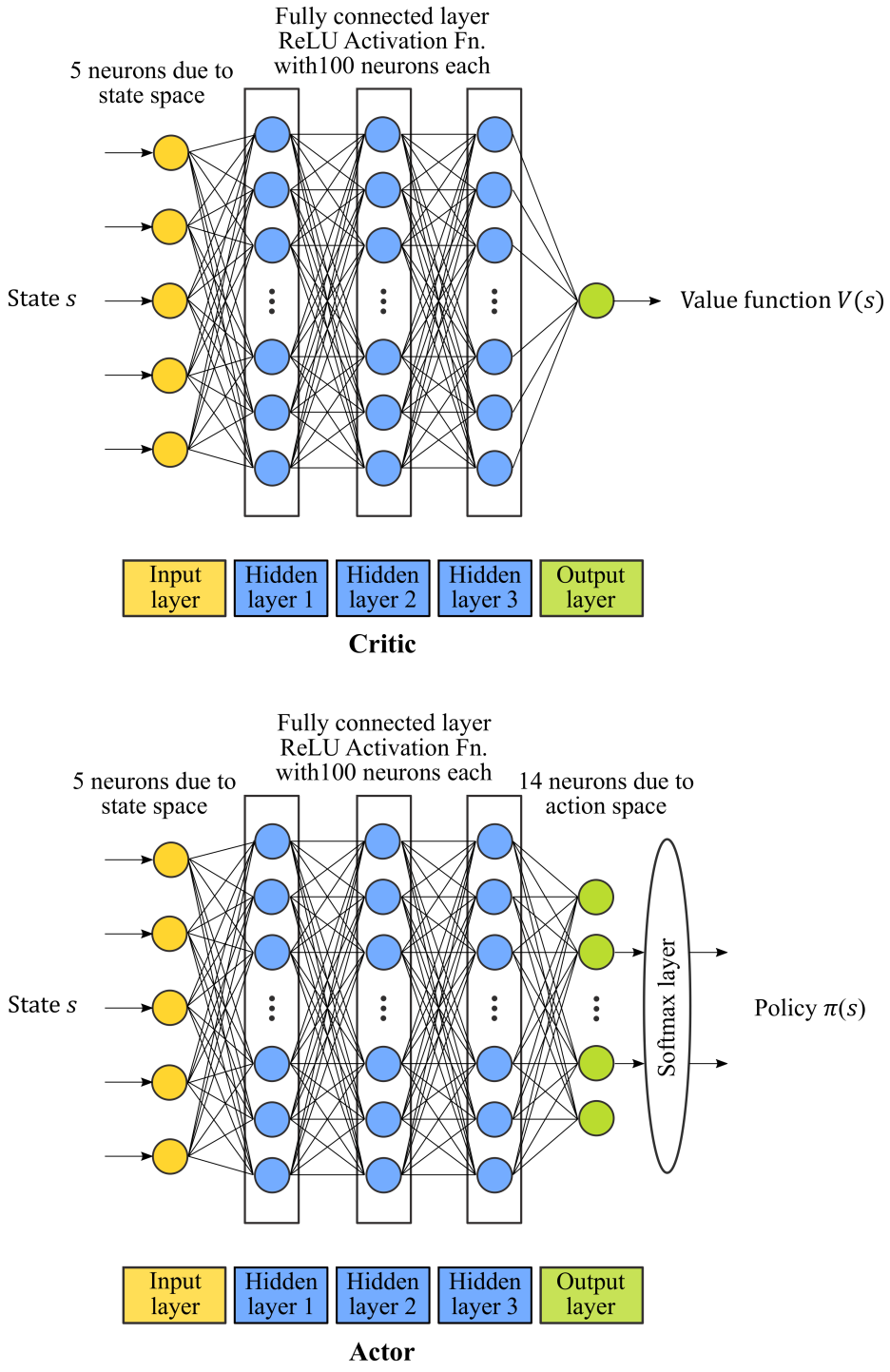

Figure 6.6: Illustration of the actor-critic networks.

6.3.4 Hyperparameters

Appropriate hyperparameters are essential to get desired results in DRL. In this section, the primary hyperparameters in the A3C algorithm are configured and summarized in Table 6.2.

Table 6.2: Hyperparameters in A3C.

Parameters	Symbol	Value
Learning rate for actor network	α_θ	$1e-4$
Learning rate for critic network	α_μ	$1e-4$
Optimizer	-	$Adam$
Discount factor	γ	0.95
Gradient threshold	-	1
Gradient threshold method	-	$L2norm$
Entropy loss weight	β	0.2
Sample time	T_s	$0.5s$
Step size of asynchronous update	N	100
Step size of each training episode	T	Length of training cycle/sample time
Number of training episodes	P	5000
Number of threads in CPU	n	4

Learning rate is considered the most critical hyperparameter in a neural network configuration. It controls how to nudge the old estimated value in the direction of the new estimation each time the network weights are updated. Choosing an appropriate learning rate is challenging since a low rate may result in a long training process, whereas a high rate may lead to suboptimal results or unstable learning. Through trial and error, a learning rate of 1e-4 is chosen for both actor and critic networks, i.e., $\alpha_\theta = 1e-4$ and $\alpha_\mu = 1e-4$. The Adam optimizer is adopted to train the neural

networks.

Without the prior knowledge of the future drive cycle, the A3C based optimal control can be seen as a continuing task since the terminal state is unknown. Therefore, a discount factor $\gamma = 0.95$ is defined to trade off the immediate and future rewards.

During the training, there might be a significant increase in the gradient, called exploding gradient, that may cause a significant update to the network parameters and thus leading to unstable learning. As a result, a gradient threshold is defined, beyond which the gradient will be clipped to prevent gradient explosion, called gradient clipping. This work defines a gradient threshold of 1 and adopts a norm-based gradient clipping method, "L2norm". If the L2 norm of a gradient is larger than the defined gradient threshold, the gradient will be scaled so that the L2 norm equals the defined gradient threshold.

In RL, entropy is used to encourage exploration to avoid being stuck in local optima. A higher entropy loss weight β will promote exploration by applying a penalty for taking an action that the agent already knows about, called exploitation. A balance between exploration and exploitation of the environment can be achieved by defining a proper entropy loss weight, which is set to 0.2 in this work.

In A3C, the independent local workers perform simulations against their own copies of the environment and send their data asynchronously to the host to update the global neural network after a certain amount of steps. Here, the step size of the asynchronous update N is set as 100, after which the local workers receive the updated parameters from the host and resume learning. The step size of each training episode T is given

by the length of the training cycle divided by the sample time.

6.3.5 A3C-based EMS Framework

Pseudo-code of the A3C algorithm is described in Algorithm 1, and the framework of the proposed A3C-based EMS is depicted in Fig. 6.7.

6.4 Results and Discussions

The proposed A3C-based EMS, including the hybrid powertrain model and RL configuration, is programmed in MATLAB® and Simulink®, where the Reinforcement Learning Toolbox™ is employed to construct the RL agent and deep neural networks. Simulation is conducted on a computer with the Intel® Core™ i7-6700 Processor with four cores @ 3.40 GHz and 32 GB of RAM.

6.4.1 Training Setup

In this section, the proposed A3C-based EMS is trained on HWFET, whose speed and acceleration profiles are shown in Fig. 6.8.

Based on the normalization methods introduced in Section 6.3.3, the training cycle is normalized as shown in Fig. 6.9.

The maximum number of training episodes in this work is set to 5000. Initial battery

Algorithm 1: Pseudo-code for A3C algorithm

Hyperparameters: Define hyperparameters α_θ, α_μ, β, γ, N, T, and P
Initialization: Initialize global shared actor and critic networks with weights θ and μ; thread-specific actor and critic networks with weights θ' and μ'; thread-specific time step $t \leftarrow 1$
/* For each of the n-threads, perform the following tasks */;
for $episode = 1, 2, ..., P$ **do**
  Reset environment;
  Reset thread-specific time step: $t \leftarrow 1$;
  repeat
    Reset gradients: $d\theta \leftarrow 0$ and $d\mu \leftarrow 0$;
    Synchronize thread-specific parameters with global shared parameters: $\theta' = \theta$ and $\mu' = \mu$;
    Reset starting time step of the N-step experiences: $t_{start} \leftarrow t$;
    Observe state $s_t = \{v_{veh}, acc_{veh}, P_{APU}, SOC, \Delta SOC\}_t$;
    /* Generate the N-step experiences */;
    repeat
      Choose action a_t according to policy $\pi(a_t|s_t;\theta')$;
      Perform action a_t, receive reward r_t, and change to state s_{t+1};
      Update time step $t \leftarrow t+1$;
    until $t - t_{start} == N$ **or** $s_t == s_T$;
    Initialize return estimation: $R = \begin{cases} V(s_t;\mu'), & s_t \neq s_T \\ 0, & s_t = s_T \end{cases}$;
    for $i = t-1, ..., t_{start}$ **do**
      Compute return through backward iterations: $R \leftarrow r_i + \gamma R$;
      Compute advantage: $A(a_i|s_i;\theta',\mu') = R - V(s_i;\mu')$;
      Compute entropy: $H(\pi(a_i|s_i;\theta')) = -\int \pi(a_i|s_i;\theta') \log \pi(a_i|s_i;\theta')$;
      Accumulate gradients w.r.t. θ':
      $d\theta \leftarrow d\theta + \nabla_{\theta'} \log \pi(a_i|s_i;\theta') A(a_i|s_i;\theta',\mu') + \beta \nabla_{\theta'} H(\pi(a_i|s_i;\theta'))$;
      Accumulate gradients w.r.t. μ':
      $d\mu \leftarrow d\mu + \partial (A(a_i|s_i;\theta',\mu'))^2 / \partial \mu'$;
    Perform asynchronous update of θ using $d\theta$: $\theta \leftarrow \theta + \alpha_\theta d\theta$;
    Perform asynchronous update of μ using $d\mu$: $\mu \leftarrow \mu + \alpha_\mu d\mu$;
  until $t == T$;

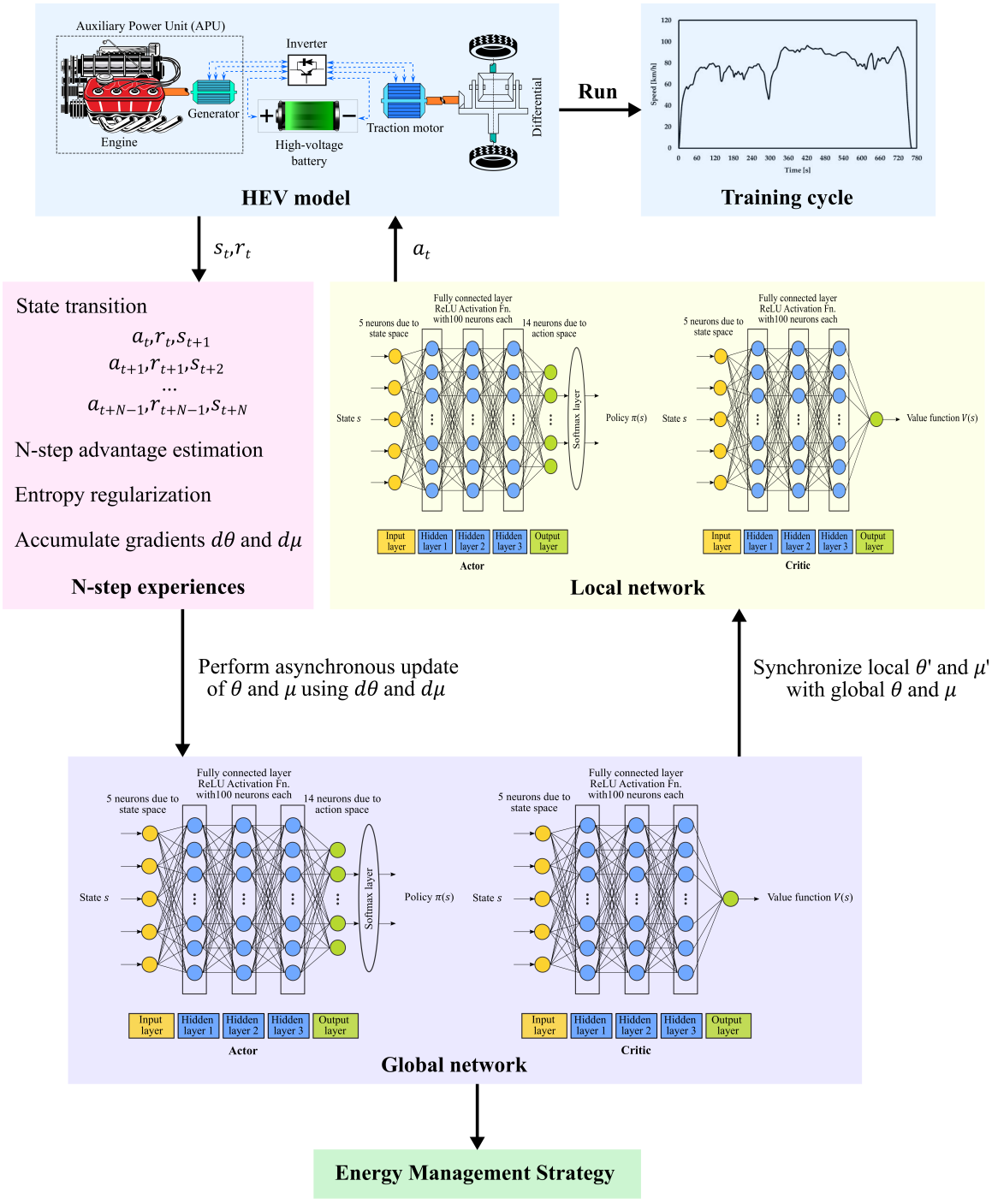

Figure 6.7: Schematic of A3C-based EMS for HEVs.

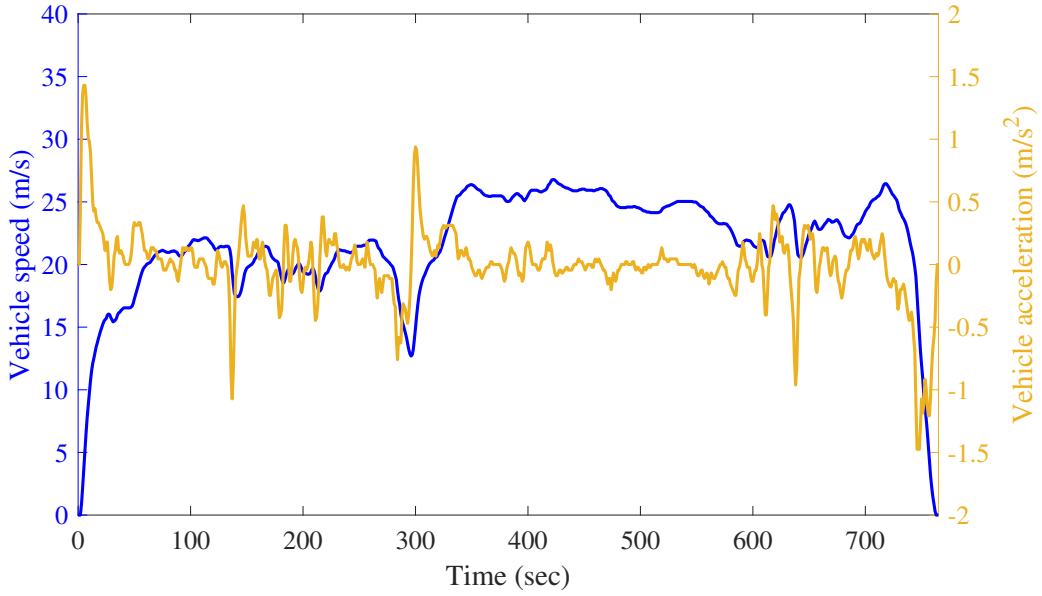

Figure 6.8: Vehicle speed and acceleration of the training drive cycle.

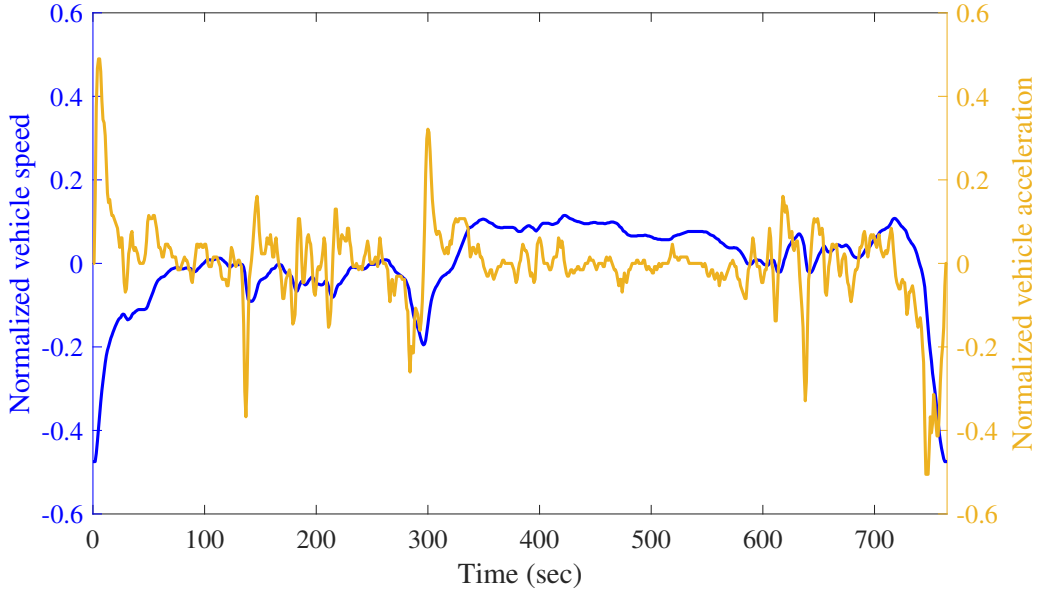

Figure 6.9: Normalized vehicle speed and acceleration of the training drive cycle.

SOC is set as 7%, and other state variables are initialized as 0.

6.4.2 Convergence

The main objective of RL algorithms is to train the agent toward higher rewards. Fig. 6.10 presents the trajectory of episodic reward during training, from where a gradually increasing trend can be observed, demonstrating the learning ability of the proposed strategy. After around 3500 episodes, the average episodic reward starts to stabilize, which indicates the convergence of the training.

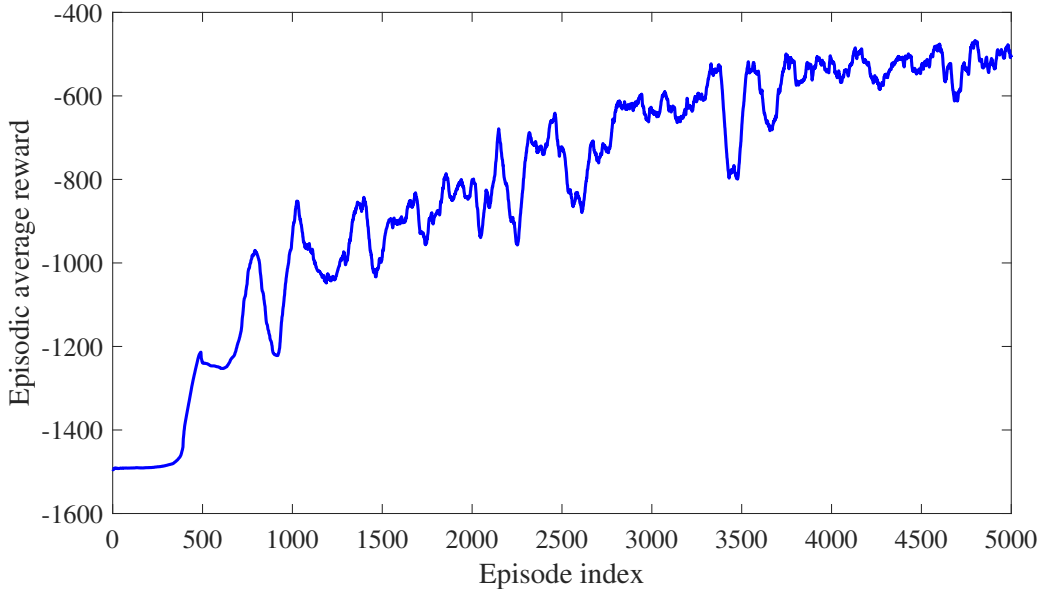

Figure 6.10: Trajectory of episodic reward during training.

6.4.3 Training Performance

To better evaluate the training performance of the proposed A3C-based strategy, a deterministic DP-based EMS is adopted as the benchmark, and an A-ECMS is also implemented for comparison.

Fig. 6.11 compares the battery SOC trajectories of the three control strategies. It can be observed that the three strategies follow different trajectories, but they are all capable of achieving CS under the training drive cycle. The largest ΔSOC is given by the A-ECMS, and the A3C-based strategy shows only 0.0246% ΔSOC. Moreover, although the trajectories are not identical, the A3C-based strategy exhibits similar trends to the DP-based EMS along the drive cycle. Compared to DP, the A3C-based EMS seems to discharge the battery more drastically. However, this can be mitigated by adding battery life consideration into the reward function.

Engine operating profiles of the three control strategies are depicted and compared in Fig. 6.12 to 6.14. Firstly, engine operating points in all three strategies always remain within engine speed and torque limits owing to the imposed constraints. In A3C-based strategy, all the operating points reside in the OOL since engine speed and torque are designed to be searched along this line for a given engine power. While in DP-based strategy, engine operating points locate mostly outside this line since engine speed and torque are controlled independently. Interestingly, operating points of the A-ECMS also fall on the OOL, as shown in Fig. 6.14.

Secondly, the engine tends to operate at medium speed and load points in both A3C-based and DP-based strategies, and lower-efficiency regions such as low speed/torque

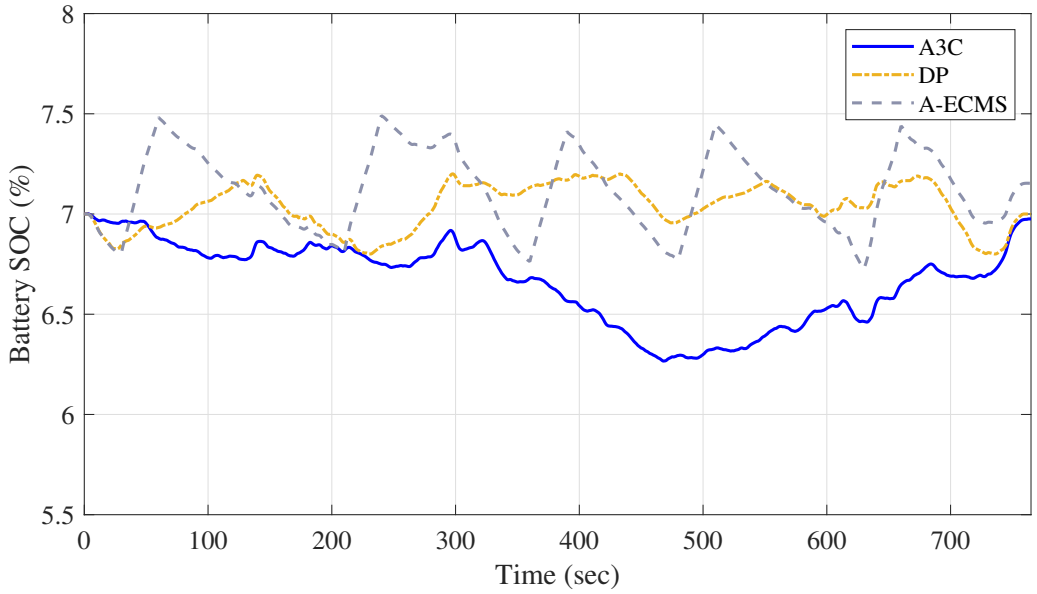

Figure 6.11: Comparison of SOC trajectories among A3C-based EMS, DP-based EMS, and A-ECMS under the training cycle.

points are discouraged, especially in DP, as reflected in the histograms. By contrast, the A-ECMS prefers to either run the engine at high loads or shut it down, which is the result of instantaneous optimization. Besides, engine operation distribution of the A3C-based EMS is more uniform than the DP-based EMS and the A-ECMS, and engine-off time is also much shorter.

Finally, the total fuel consumption of the three control strategies is corrected for SOC difference and then benchmarked by DP. A quantification of fuel optimality is given in Table 6.3. As can be seen, the proposed A3C-based EMS can achieve almost 89% fuel optimality with better fuel economy over the A-ECMS. Since DP-based strategies can only be used off-line, the superiority of the proposed A3C-based control strategy for online implementation has been demonstrated.

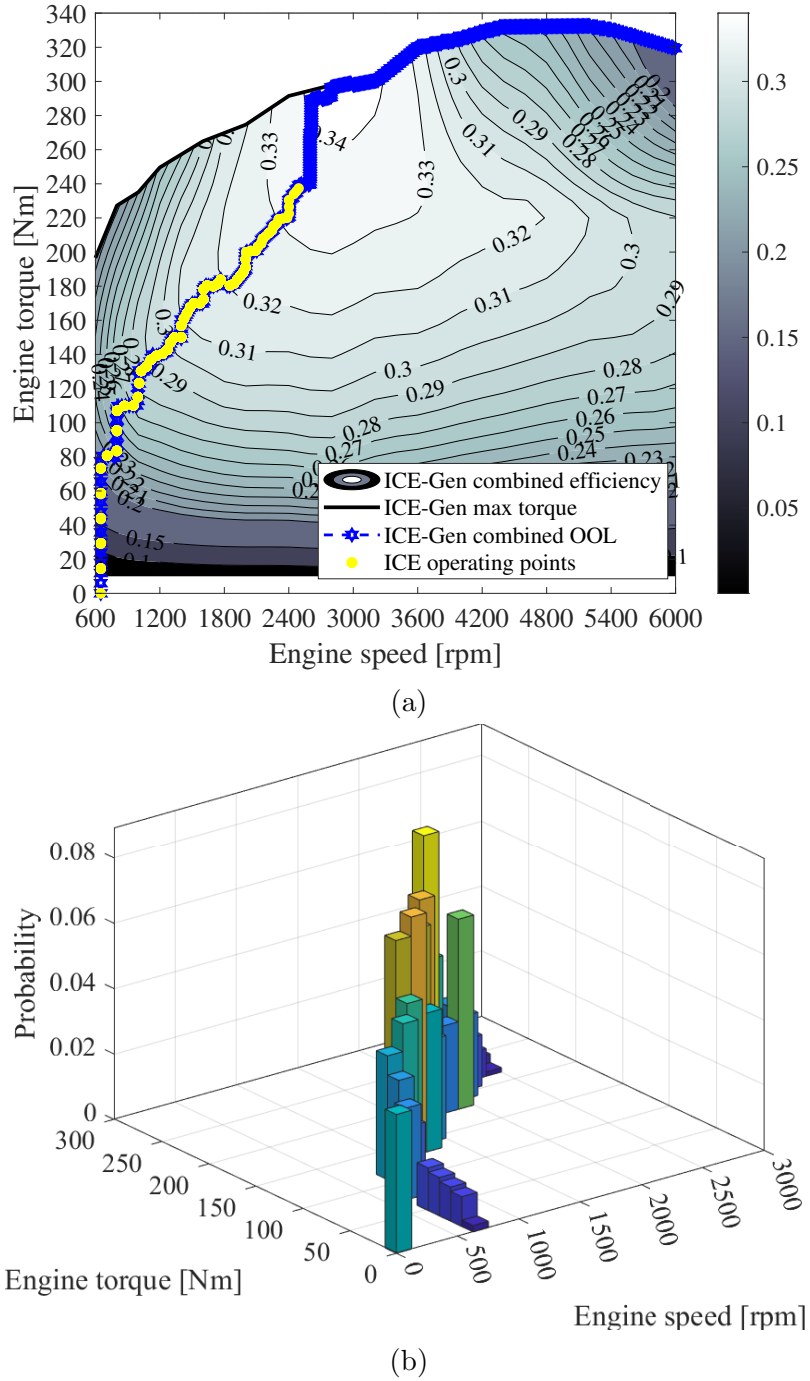

Figure 6.12: (a) Engine operating points; (b) Engine operation distribution in A3C under the training cycle.

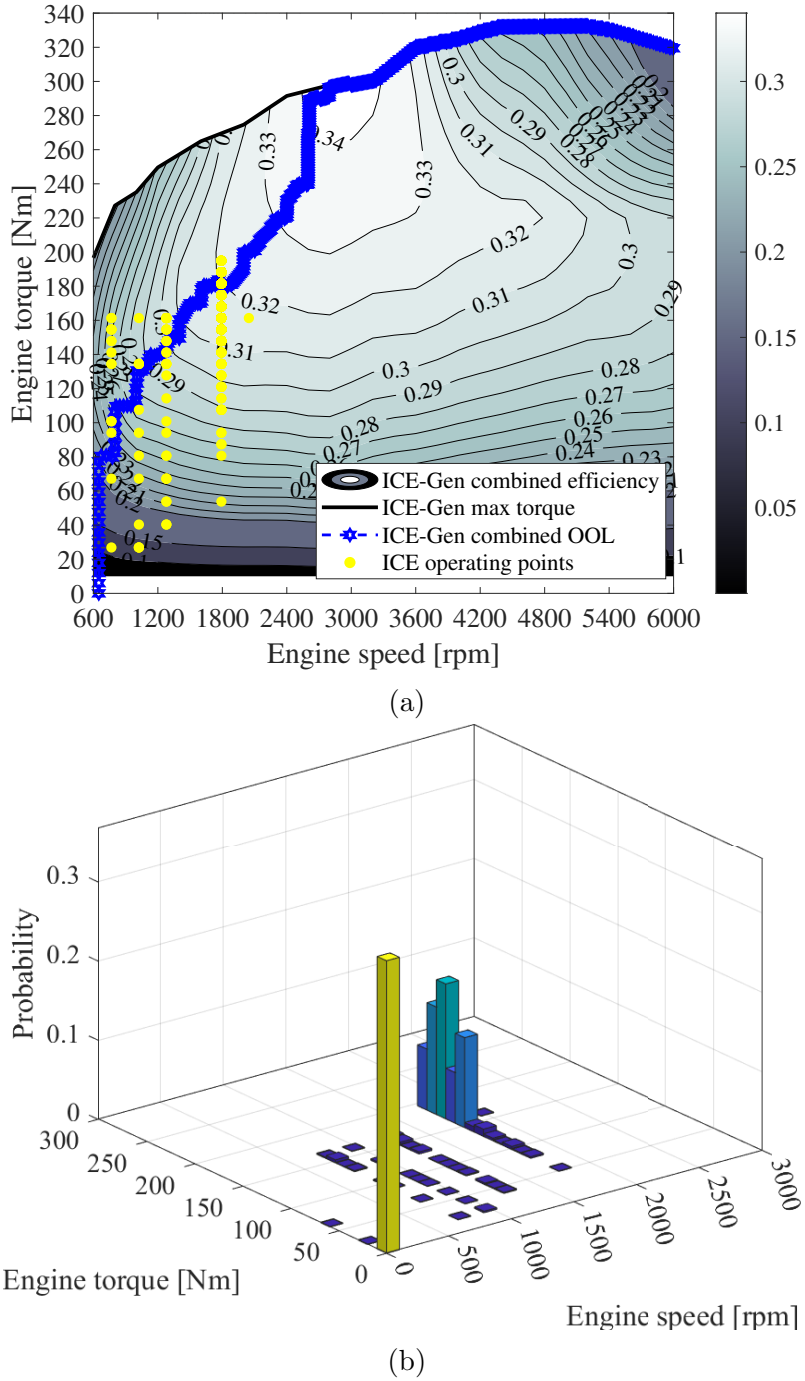

Figure 6.13: (a) Engine operating points; (b) Engine operation distribution in DP under the training cycle.

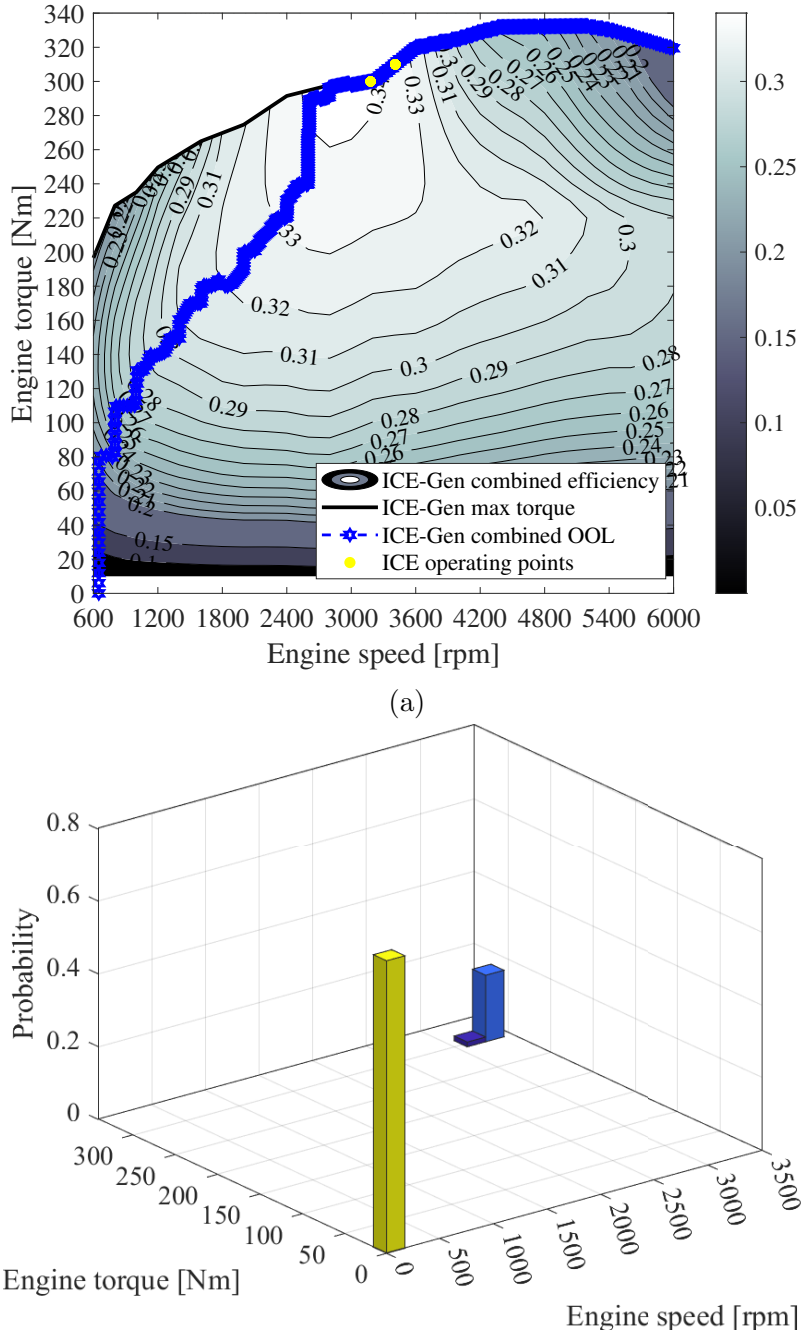

Figure 6.14: (a) Engine operating points; (b) Engine operation distribution in A-ECMS under the training cycle.

Table 6.3: Performance of DP, A3C, and A-ECMS under the training cycle.

Control strategy	Final SOC (%)	Fuel consumption (g)	Fuel optimality (%)
DP	7.0000	955.8208	100.0000
A3C	6.9754	1062.6188	88.8266
A-ECMS	7.1533	1082.4792	86.7487

6.4.4 Generalization Verification for Online Implementation

The generalization of the trained EMS to new drive cycles is extremely important for its online implementation. As a result, a long drive cycle mixed with the training cycle and several other new cycles is constructed to test the model's adaptability.

The testing cycle, as shown in Fig. 6.15, is composed of four consecutive drive cycles. Sequentially, they are US06, which is a high-acceleration aggressive cycle, HWFET, which is the training cycle, WLTP, which is a more representative cycle of real driving conditions covering urban, suburban, rural, and highway scenarios, and another US06 cycle. The normalized testing cycle is shown in Fig. 6.16.

Fig. 6.17 compares the SOC trajectories of the A3C-based EMS and the A-ECMS under the testing cycle. It can be seen that both strategies are capable of maintaining battery SOC with no dramatic deviations. Although the A3C-based strategy presents a larger SOC window, the overall SOC deviation is smaller, indicating better charge sustaining performance. Therefore, the proposed A3C-based EMS proves good ability of maintaining battery SOC for online implementation.

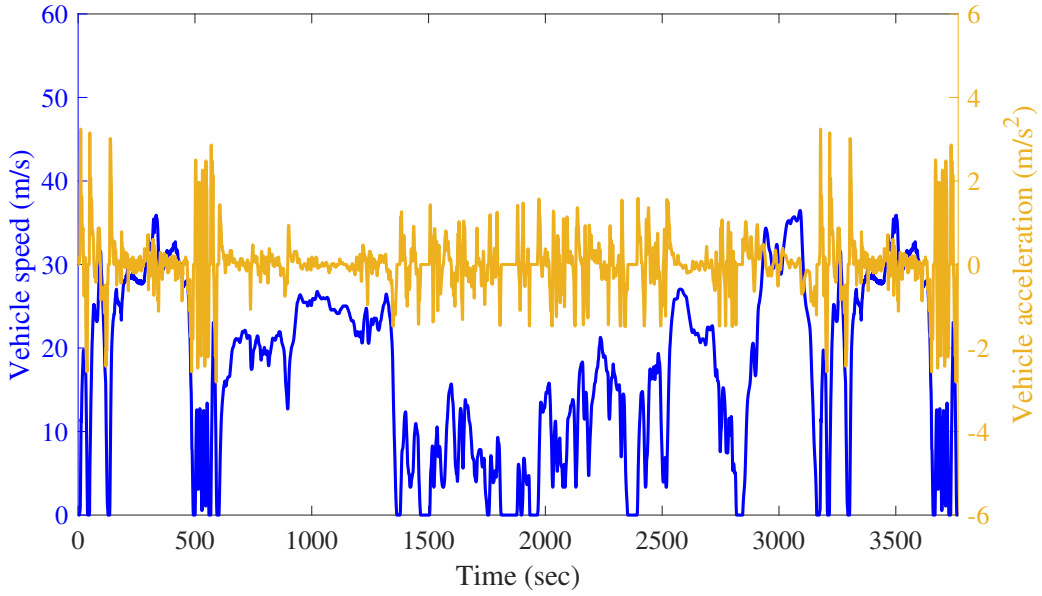

Figure 6.15: Vehicle speed and acceleration of the test driving cycle.

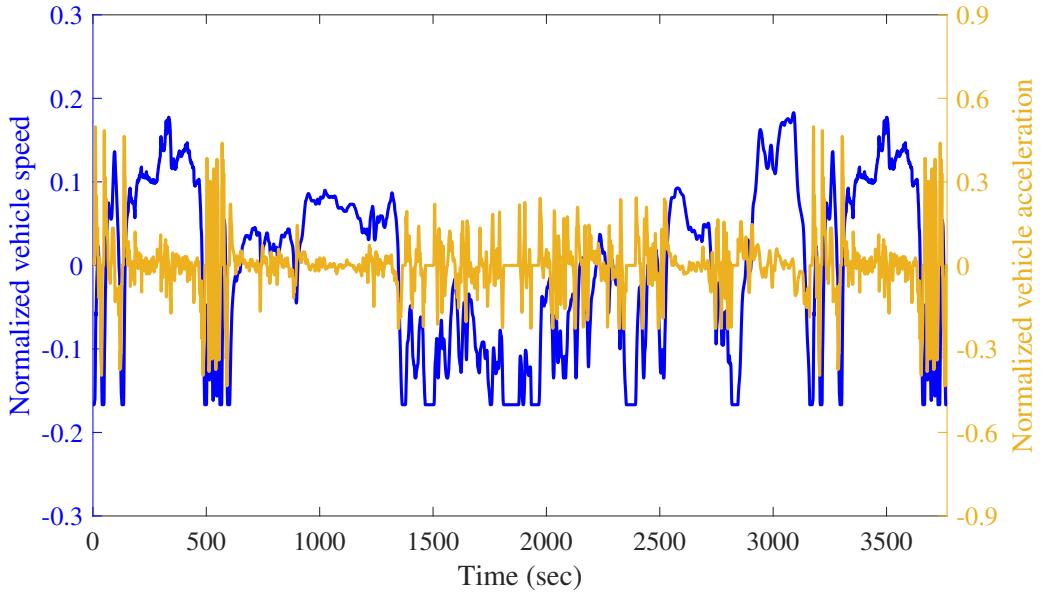

Figure 6.16: Normalized vehicle speed and acceleration of the test driving cycle.

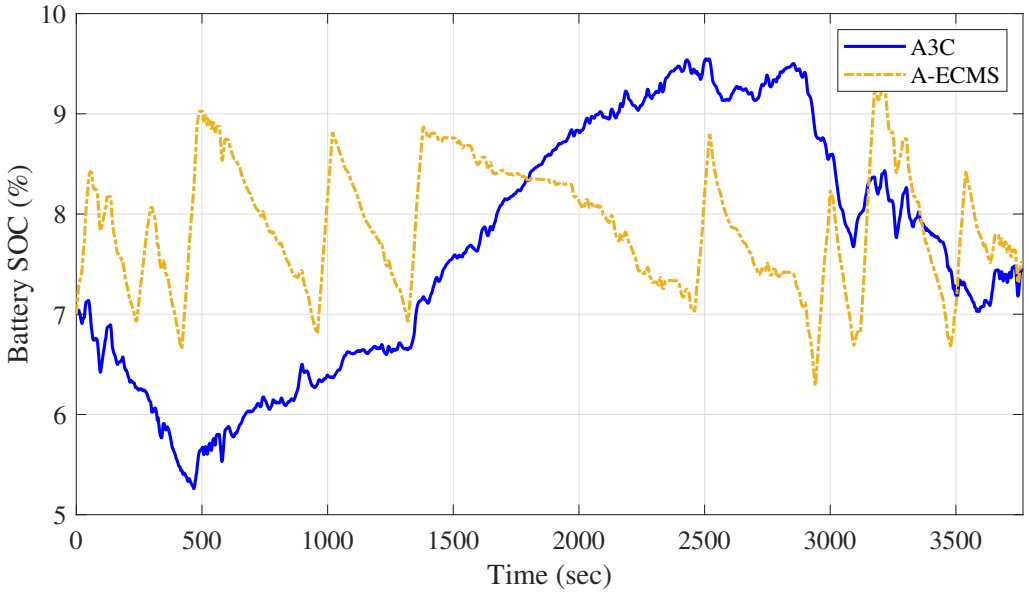

Figure 6.17: Comparison of SOC trajectories between A3C-based EMS and A-ECMS under the testing cycle.

Table 6.4 reports the fuel statistics of the two strategies with SOC correction. Compared to the A-ECMS, the A3C-based strategy presents better fuel economy, with approximately 11.62 % improvement. Therefore, the proposed A3C-based EMS demonstrates its fuel-efficiency-wise adaptability for online implementation.

Table 6.4: Performance of A3C-based EMS and A-ECMS under the testing cycle.

Control strategy	Final SOC (%)	Fuel consumption (g)
A3C	7.4411	5009.9272
A-ECMS	7.5211	5591.8703

As a summary, with excellent learning ability and good generalization performance, the proposed A3C-based EMS proves its great potential in real-time HEV control.

6.5 Summary

This chapter aims to improve the intelligence of HEV EMS by proposing a DRL-based control strategy with A3C algorithm. After reviewing the fundamentals of RL, a control-oriented model of a series HEV is introduced, based on which the A3C-based EMS is formulated. The proposed A3C-based strategy is then trained on HWFET, and training results are compared with DP benchmark and an A-ECMS constructed based on Chapter 5.

Training results indicate the great learning ability of the proposed A3C-based EMS with successful convergence, excellent charge sustenance, and good fuel optimality. Although a gap of fuel optimality still exists between the A3C-based EMS and DP, it shows better fuel economy and charge sustaining performance than the A-ECMS. Thus, its overall real-time performance can be demonstrated.

The trained EMS is then tested on a different long drive cycle to verify its generalization and adaptability. Results indicate that the proposed A3C-based EMS can achieve better fuel economy than the A-ECMS with a reasonable SOC deviation. Overall, the proposed A3C-based EMS exhibits great potential in real-time HEV control due to its good learning ability and adaptability.

Future research work can focus on improving the adaptability of the proposed strategy. One possible approach is to train the agent on more drive cycles with a variety of driving scenarios.

Chapter 7

Conclusions and Future Work

7.1 Conclusions

Hybrid electric vehicles (HEVs) offer a more renewable and efficient solution for transportation with higher fuel efficiency and reduced emissions. Aiming at narrowing the gap between HEVs and pure electric vehicles, further improvement in HEVs is demanded. Energy-efficient powertrain components and improved energy management strategies (EMSs) are two compelling methods to promote the potential of HEV systems.

As guidance for future explorations of energy-efficient powertrain components, a comprehensive review of hybrid electric vehicle specific engines is provided in Chapter 3. Discussed technologies include the over-expansion cycle, low temperature combustion mode, alternative fuels, and waste heat recovery techniques. Based on the benefits and challenges identified for each technological solution, specific recommendations are made for future research. Moreover, opportunities to simplify hybrid-optimized engines based on cost-effective trade-offs are also investigated.

As the main research focus of this thesis, Chapters 4 to 6 propose three improved HEV energy management strategies from a basic non-adaptive real-time approach to a state-of-the-art learning-based intelligent approach.

In real-world driving tasks where vehicles always run with dynamics, vehicle control strategies without considering powertrain inertial dynamics will lead to infeasible control solutions that deteriorate the vehicle drivability. Moreover, without accounting for the dynamics, fuel economy will be overestimated, causing a discrepancy between the predicted and actual fuel economy. To address these concerns and improve the

practicality of HEV EMS, a real-time equivalent consumption minimization strategy (ECMS) incorporating powertrain inertial dynamics is proposed in Chapter 4. Compared to the baseline ECMS, the proposed control strategy ensures the vehicle drivability and provides a more accurate prediction of fuel economy. It is concluded that the proposed dynamic ECMS offers a more convincing and better optimal solution for practical HEV control.

Although ECMS is an online strategy theoretically, the equivalence factor (EF) that maintains HEV charge sustainability relies on trial-and-error-based off-line tuning, which requires a prior knowledge of the drive cycle. To improve the real-time applicability of HEV EMS, a predictive adaptive ECMS (A-ECMS) with online EF calculation and instantaneous power distribution is proposed in Chapter 5. The proposed A-ECMS exhibits great charge sustaining capabilities under all studied drive cycles. With a real-time self-updating EF profile, control dependency on the drive cycle is reduced, and the need for manual tuning of the EF is also eliminated. It is concluded that the proposed A-ECMS overcomes the drawback of non-adaptive ECMS and becomes "real" real-time implementable with only slight sacrifice in fuel economy.

The A-ECMS in Chapter 5 achieves great improvement over the non-adaptive ECMS in real-time performance and shows intelligence by presenting a self-updating EF profile. It is pointed out in Chapter 6 that the employment of machine learning techniques offers the opportunity for further improvement of HEV EMS. As a result, a deep reinforcement learning (DRL)-based intelligent control strategy featuring the state-of-the-art asynchronous advantage actor-critic (A3C) algorithm is proposed in

Chapter 6. The proposed strategy exhibits great learning ability with successful convergence, excellent charge sustenance, and good fuel optimality. A generalization test is also conducted to evaluate its adaptability, where the A3C-based strategy presents better charge sustainability and fuel economy than the A-ECMS with a reasonable SOC deviation. It is concluded that the proposed A3C-based intelligent EMS has good real-time capabilities and thus great potential in real-time HEV control.

As a summary of the above conclusions, the control strategies proposed in this thesis achieve significant improvements in practicality, real-time applicability, adaptability, and intelligence of HEV EMS. These improved energy management strategies, together with the energy-efficient hybrid powertrain specific engines, will promote the development of hybrid electric vehicles.

7.2 Future Work

The following research topics are suggested for future work:

Powertrain inertial dynamics proposed in Chapter 4 could be incorporated into the A-ECMS presented in Chapter 5 and the DRL-based EMS presented in Chapter 6.

High-fidelity control-oriented HEV models are expected to integrate with EMS designs to fill the reality gap. Models of key powertrain components such as the internal combustion engine, battery, and electric motors, could be developed with more realistic considerations.

For the A-ECMS presented in Chapter 5, other enhanced algorithms for EF searching

that can improve computational accuracy and efficiency deserve further investigation. Examples of such algorithms are Brent's method and the Aberth method.

The control strategies developed in this thesis are based on model-in-the-loop (MIL) simulations. Software-in-the-loop (SIL), processor-in-the-loop (PIL), and hardware-in-the-loop (HIL) testings are desired to further validate the developed control strategies step by step.

7.3 Publications

7.3.1 Journal papers

(1) **Wang, Y.**, Biswas, A., Rodriguez, R., Keshavarz-Motamed, Z., and Emadi, A., "Hybrid electric vehicle specific engines: State-of-the-art review," *Energy Reports*, vol. 8, pp. 832-851, 2022, https://doi.org/10.1016/j.egyr.2021.11.265.

(2) **Wang, Y.**, Biswas, A., Keshavarz-Motamed, Z., and Emadi, A., "A real-time energy management strategy for power-split hybrid electric vehicles considering inertial dynamics of the powertrain." (To be submitted for journal publication)

7.3.2 Conference papers

(1) **Wang, Y.**, Biswas, A., Anselma, P., Rathore, A. et al., "Adaptive Real-Time Energy Management of a Multi-Mode Hybrid Electric Powertrain," *SAE Technical Paper* 2022-01-0676, 2022, https://doi.org/10.4271/2022-01-0676.

(2) Biswas, A., **Wang, Y.**, and Emadi, A., "Effect of immediate reward function on the performance of reinforcement learning-based energy management system," *2022 IEEE Transportation Electrification Conference & Expo (ITEC)*, 2022, pp. 1021-1026, https://doi.org/10.1109/ITEC53557.2022.9814050.

(3) Jamali, H., **Wang, Y.**, Yang, Y., Habibi, S., and Emadi, A., "Rule-Based Energy Management Strategy for a Power-Split Hybrid Electric Vehicle with LSTM Network Prediction Model," *2021 IEEE Energy Conversion Congress and Exposition (ECCE)*, 2021, pp. 1447-1453, https://doi.org/10.1109/ECCE47101.2021.9594926.

(4) Biswas, A., Rane, O., Rathore, A., Anselma, P., **Wang, Y.** et al., "Energy Management System for Input-Split Hybrid Electric Vehicle (Si-EVT) with Dynamic Coordinated Control and Mode-Transition Loss," *SAE Technical Paper* 2022-01-0674, 2022, https://doi.org/10.4271/2022-01-0674.

(5) Anselma, P., Rane, O., Biswas, A., Rathore, A., **Wang, Y.** et al., "A Computationally Lightweight Dynamic Programming Formulation for Hybrid Electric Vehicles," *SAE Technical Paper* 2022-01-0671, 2022, https://doi.org/10.4271/2022-01-0671.

References

[1] L. Horrein, A. Bouscayrol, Y. Cheng, C. Dumand, G. Colin, and Y. Chamaillard, "Influence of the heating system on the fuel consumption of a hybrid electric vehicle," *Energy Conversion and Management*, vol. 129, pp. 250–261, 2016, https://doi.org/10.1016/j.enconman.2016.10.030.

[2] International Energy Agency, "Energy Technology Perspectives 2014," International Energy Agency, Paris, France, Tech. Rep., Jun. 2014. [Online]. Available: https://www.iea.org/reports/energy-technology-perspectives-2014.

[3] J. Al Khoury and W. Bou Nader, "Design and simulation of turbogenerators for series hybrid electric vehicles," *Energy Conversion and Management*, vol. 236, p. 114078, 2021, https://doi.org/10.1016/j.enconman.2021.114078.

[4] M. Ehsani, Y. Gao, and J. M. Miller, "Hybrid electric vehicles: Architecture and motor drives," *Proceedings of the IEEE*, vol. 95, no. 4, pp. 719–728, 2007, https://doi.org/10.1109/JPROC.2007.892492.

[5] A. Emadi, *Advanced electric drive vehicles*. Boca Raton, FL: CRC Press, Oct. 2014, https://doi.org/10.1201/9781315215570.

[6] Y. M. Alkhulaifi, N. A. A. Qasem, and S. M. Zubair, "Improving the performance of thermal management system for electric and hybrid electric vehicles by adding an ejector," *Energy Conversion and Management*, vol. 201, p. 112133, 2019, https://doi.org/10.1016/j.enconman.2019.112133.

[7] M. F. M. Sabri, K. A. Danapalasingam, and M. F. Rahmat, "A review on hybrid electric vehicles architecture and energy management strategies," *Renewable and Sustainable Energy Reviews*, vol. 53, pp. 1433–1442, 2016, https://doi.org/10.1016/j.rser.2015.09.036.

[8] K. Çağatay Bayindir, M. A. Gözüküçük, and A. Teke, "A comprehensive overview of hybrid electric vehicle: Powertrain configurations, powertrain control techniques and electronic control units," *Energy Conversion and Management*, vol. 52, no. 2, pp. 1305–1313, 2011, https://doi.org/10.1016/j.enconman.2010.09.028.

[9] T. Banjac, F. Trenc, and T. Katrašnik, "Energy conversion efficiency of hybrid electric heavy-duty vehicles operating according to diverse drive cycles," *Energy Conversion and Management*, vol. 50, no. 12, pp. 2865–2878, 2009, https://doi.org/10.1016/j.enconman.2009.06.034.

[10] M. Fathi, O. Jahanian, and M. Shahbakhti, "Modeling and controller design architecture for cycle-by-cycle combustion control of homogeneous charge compression ignition (HCCI) engines – A comprehensive review," *Energy Conversion and Management*, vol. 139, pp. 1–19, 2017, https://doi.org/10.1016/j.enconman.2017.02.038.

[11] Z.-G. Shen, L.-L. Tian, and X. Liu, "Automotive exhaust thermoelectric generators: Current status, challenges and future prospects," *Energy Conversion and Management*, vol. 195, pp. 1138–1173, 2019, https://doi.org/10.1016/j.enconman.2019.05.087.

[12] K. Rahbar, S. Mahmoud, R. K. Al-Dadah, N. Moazami, and S. A. Mirhadizadeh, "Review of organic Rankine cycle for small-scale applications," *Energy Conversion and Management*, vol. 134, pp. 135–155, 2017, https://doi.org/10.1016/j.enconman.2016.12.023.

[13] Y. Wang, A. Biswas, R. Rodriguez, Z. Keshavarz-Motamed, and A. Emadi, "Hybrid electric vehicle specific engines: State-of-the-art review," *Energy Reports*, vol. 8, pp. 832–851, 2022, https://doi.org/10.1016/j.egyr.2021.11.265.

[14] A. Biswas and A. Emadi, "Energy Management Systems for Electrified Powertrains: State-of-the-Art Review and Future Trends," *IEEE Transactions on Vehicular Technology*, vol. 68, no. 7, pp. 6453–6467, 2019, https://doi.org/10.1109/TVT.2019.2914457.

[15] J. Van Mierlo, G. Maggetto, and P. Lataire, "Which energy source for road transport in the future? A comparison of battery, hybrid and fuel cell vehicles," *Energy Conversion and Management*, vol. 47, no. 17, pp. 2748–2760, 2006, https://doi.org/10.1016/j.enconman.2006.02.004.

[16] H. Guo, X. Wang, and L. Li, "State-of-charge-constraint-based energy management strategy of plug-in hybrid electric vehicle with bus route," *Energy Conversion and Management*, vol. 199, p. 111972, 2019, https://doi.org/10.1016/j.enconman.2019.111972.

[17] B. Xiao, J. Ruan, W. Yang, P. Walker, and N. Zhang, "A review of pivotal energy management strategies for extended range electric vehicles," *Renewable and Sustainable Energy Reviews*, vol. 149, p. 111194, 2021, https://doi.org/10.1016/j.rser.2021.111194.

[18] W. Enang and C. Bannister, "Modelling and control of hybrid electric vehicles (A comprehensive review)," *Renewable and Sustainable Energy Reviews*, vol. 74, pp. 1210–1239, 2017, https://doi.org/10.1016/j.rser.2017.01.075.

[19] "Mild Hybrid Electric Vehicle (MHEV) – architectures." [Online]. Available: https://x-engineer.org/automotive-engineering/vehicle/hybrid/mild-hybrid-electric-vehicle-mhev-architectures/.

[20] Y. Yang, X. Hu, H. Pei, and Z. Peng, "Comparison of power-split and parallel hybrid powertrain architectures with a single electric machine: Dynamic programming approach," *Applied Energy*, vol. 168, pp. 683–690, 2016, https://doi.org/10.1016/j.apenergy.2016.02.023.

[21] X. Tian, Y. Cai, X. Sun, Z. Zhu, and Y. Xu, "An adaptive ECMS with driving style recognition for energy optimization of parallel hybrid electric buses," *Energy*, vol. 189, p. 116151, 2019, https://doi.org/10.1016/j.energy.2019.116151.

[22] M. Joševski and D. Abel, "Energy Management of Parallel Hybrid Electric Vehicles based on Stochastic Model Predictive Control," *IFAC Proceedings Volumes*, vol. 47, no. 3, pp. 2132–2137, 2014, https://doi.org/10.3182/20140824-6-ZA-1003.01329.

[23] J. Du, F. Yang, Y. Cai, L. Du, and M. Ouyang, "Testing and Analysis of the Control Strategy of Honda Accord Plug-in HEV," *IFAC-PapersOnLine*, vol. 49, no. 11, pp. 153–159, 2016, https://doi.org/10.1016/j.ifacol.2016.08.024.

[24] T. M. Grewe, B. M. Conlon, and A. G. Holmes, "Defining the General Motors 2-Mode Hybrid Transmission," in *SAE World Congress & Exhibition*. SAE International, Apr. 2007, https://doi.org/10.4271/2007-01-0273.

[25] M. Pittel and D. Martin, "eFlite Dedicated Hybrid Transmission for Chrysler Pacifica," in *WCX World Congress Experience*. SAE International, Apr. 2018, https://doi.org/10.4271/2018-01-0396.

[26] A. Biswas, P. G. Anselma, A. Rathore, and A. Emadi, "Effect of co-ordinated control on real-time optimal mode selection for multi-mode hybrid electric powertrain," *Applied Energy*, vol. 289, p. 116695, 2021, https://doi.org/10.1016/j.apenergy.2021.116695.

[27] W. Geng, D. Lou, C. Wang, and T. Zhang, "A cascaded energy management optimization method of multimode power-split hybrid electric vehicles," *Energy*, vol. 199, p. 117224, 2020, https://doi.org/10.1016/j.energy.2020.117224.

[28] T. J. Böhme and B. Frank, *Hybrid Systems, Optimal Control and Hybrid Vehicles*, ser. Advances in Industrial Control. Cham: Springer, 2017, https://doi.org/10.1007/978-3-319-51317-1.

[29] S. Onori, L. Serrao, and G. Rizzoni, *Hybrid electric vehicles*, ser. SpringerBriefs in Electrical and Computer Engineering. London: Springer, 2016, https://doi.org/10.1007/978-1-4471-6781-5.

[30] L. Eriksson and L. Nielsen, *Mean Value Engine Modeling*. John Wiley & Sons, Ltd, 2014, ch. 7, pp. 143–210, https://doi.org/10.1002/9781118536186.ch7.

[31] A. Shukla, "Modelling and Simulation of Hybrid Electric Vehicles," PhD Thesis, Imperial College London, 2012, https://doi.org/10.25560/9761.

[32] "GT-POWER Engine Simulation Software." [Online]. Available: https://www.gtisoft.com/gt-suite-applications/propulsion-systems/gt-power-engine-simulation-software/.

[33] "Simcenter Amesim." [Online]. Available: https://www.plm.automation.siemens.com/global/en/products/simcenter/simcenter-amesim.html.

[34] C. Zheng, G. Xu, K. Xu, Z. Pan, and Q. Liang, "An energy management approach of hybrid vehicles using traffic preview information for energy saving," *Energy Conversion and Management*, vol. 105, pp. 462–470, 2015, https://doi.org/10.1016/j.enconman.2015.07.061.

[35] P. G. Anselma, A. Biswas, G. Belingardi, and A. Emadi, "Rapid assessment of the fuel economy capability of parallel and series-parallel hybrid electric vehicles," *Applied Energy*, vol. 275, p. 115319, 2020, https://doi.org/10.1016/j.apenergy.2020.115319.

[36] X. Hu, X. Zhang, X. Tang, and X. Lin, "Model predictive control of hybrid electric vehicles for fuel economy, emission reductions, and inter-vehicle safety in car-following scenarios," *Energy*, vol. 196, p. 117101, 2020, https://doi.org/10.1016/j.energy.2020.117101.

[37] S. Filgueira da Silva, J. J. Eckert, F. L. Silva, L. C. A. Silva, and F. G. Dedini, "Multi-objective optimization design and control of plug-in hybrid electric vehicle powertrain for minimization of energy consumption, exhaust emissions and battery degradation," *Energy Conversion and Management*, vol. 234, p. 113909, 2021, https://doi.org/10.1016/j.enconman.2021.113909.

[38] P. G. Anselma, P. Kollmeyer, J. Lempert, Z. Zhao, G. Belingardi, and A. Emadi, "Battery state-of-health sensitive energy management of hybrid electric vehicles: Lifetime prediction and ageing experimental validation," *Applied Energy*, vol. 285, p. 116440, 2021, https://doi.org/10.1016/j.apenergy.2021.116440.

[39] F. Zhang, L. Xiao, S. Coskun, H. Pang, S. Xie, K. Liu, and Y. Cui, "Comparative study of energy management in parallel hybrid electric vehicles considering battery ageing," *Energy*, p. 123219, 2022, https://doi.org/10.1016/j.energy.2022.123219.

[40] P. Saiteja and B. Ashok, "Critical review on structural architecture, energy control strategies and development process towards optimal energy management in hybrid vehicles," *Renewable and Sustainable Energy Reviews*, vol. 157, p. 112038, 2022, https://doi.org/10.1016/j.rser.2021.112038.

[41] H. Li, A. Ravey, A. N'Diaye, and A. Djerdir, "Online adaptive equivalent consumption minimization strategy for fuel cell hybrid electric vehicle considering power sources degradation," *Energy Conversion and Management*, vol. 192, pp. 133–149, 2019, https://doi.org/10.1016/j.enconman.2019.03.090.

[42] D.-D. Tran, M. Vafaeipour, M. El Baghdadi, R. Barrero, J. Van Mierlo, and O. Hegazy, "Thorough state-of-the-art analysis of electric and hybrid

vehicle powertrains: Topologies and integrated energy management strategies," *Renewable and Sustainable Energy Reviews*, vol. 119, p. 109596, 2020, https://doi.org/10.1016/j.rser.2019.109596.

[43] S. Bai and C. Liu, "Overview of energy harvesting and emission reduction technologies in hybrid electric vehicles," *Renewable and Sustainable Energy Reviews*, vol. 147, p. 111188, 2021, https://doi.org/10.1016/j.rser.2021.111188.

[44] S. Zhang and R. Xiong, "Adaptive energy management of a plug-in hybrid electric vehicle based on driving pattern recognition and dynamic programming," *Applied Energy*, vol. 155, pp. 68–78, 2015, https://doi.org/10.1016/j.apenergy.2015.06.003.

[45] Z. Chen, C. C. Mi, B. Xia, and C. You, "Energy management of power-split plug-in hybrid electric vehicles based on simulated annealing and Pontryagin's minimum principle," *Journal of Power Sources*, vol. 272, pp. 160–168, 2014, https://doi.org/10.1016/j.jpowsour.2014.08.057.

[46] S.-Y. Chen, Y.-H. Hung, C.-H. Wu, and S.-T. Huang, "Optimal energy management of a hybrid electric powertrain system using improved particle swarm optimization," *Applied Energy*, vol. 160, pp. 132–145, 2015, https://doi.org/10.1016/j.apenergy.2015.09.047.

[47] M. Wieczorek and M. Lewandowski, "A mathematical representation of an energy management strategy for hybrid energy storage system in electric vehicle and real time optimization using a genetic algorithm," *Applied Energy*, vol. 192, pp. 222–233, 2017, https://doi.org/10.1016/j.apenergy.2017.02.022.

[48] P. Zhang, F. Yan, and C. Du, "A comprehensive analysis of energy management strategies for hybrid electric vehicles based on bibliometrics," *Renewable and Sustainable Energy Reviews*, vol. 48, pp. 88–104, 2015, https://doi.org/10.1016/j.rser.2015.03.093.

[49] Z. Chen, C. C. Mi, R. Xiong, J. Xu, and C. You, "Energy management of a power-split plug-in hybrid electric vehicle based on genetic algorithm and quadratic programming," *Journal of Power Sources*, vol. 248, pp. 416–426, 2014, https://doi.org/10.1016/j.jpowsour.2013.09.085.

[50] P. G. Anselma, "Computationally efficient evaluation of fuel and electrical energy economy of plug-in hybrid electric vehicles with smooth driving constraints," *Applied Energy*, vol. 307, p. 118247, 2022, https://doi.org/10.1016/j.apenergy.2021.118247.

[51] L. Hao, Y. Wang, Y. Bai, and Q. Zhou, "Energy management strategy on a parallel mild hybrid electric vehicle based on breadth first search algorithm," *Energy Conversion and Management*, vol. 243, p. 114408, 2021, https://doi.org/10.1016/j.enconman.2021.114408.

[52] Z. Chen, Y. Liu, M. Ye, Y. Zhang, Z. Chen, and G. Li, "A survey on key techniques and development perspectives of equivalent consumption minimisation strategy for hybrid electric vehicles," *Renewable and Sustainable Energy Reviews*, vol. 151, p. 111607, 2021, https://doi.org/10.1016/j.rser.2021.111607.

[53] Z. Lei, D. Qin, L. Hou, J. Peng, Y. Liu, and Z. Chen, "An adaptive equivalent consumption minimization strategy for plug-in hybrid electric vehicles based on traffic information," *Energy*, vol. 190, p. 116409, 2020,

https://doi.org/10.1016/j.energy.2019.116409.

[54] H. Wang, Y. Huang, A. Khajepour, and Q. Song, "Model predictive control-based energy management strategy for a series hybrid electric tracked vehicle," *Applied Energy*, vol. 182, pp. 105–114, 2016, https://doi.org/10.1016/j.apenergy.2016.08.085.

[55] T. Liu, W. Tan, X. Tang, J. Zhang, Y. Xing, and D. Cao, "Driving conditions-driven energy management strategies for hybrid electric vehicles: A review," *Renewable and Sustainable Energy Reviews*, vol. 151, p. 111521, 2021, https://doi.org/10.1016/j.rser.2021.111521.

[56] A. H. Ganesh and B. Xu, "A review of reinforcement learning based energy management systems for electrified powertrains: Progress, challenge, and potential solution," *Renewable and Sustainable Energy Reviews*, vol. 154, p. 111833, 2022, https://doi.org/10.1016/j.rser.2021.111833.

[57] G. Du, Y. Zou, X. Zhang, L. Guo, and N. Guo, "Energy management for a hybrid electric vehicle based on prioritized deep reinforcement learning framework," *Energy*, vol. 241, p. 122523, 2022, https://doi.org/10.1016/j.energy.2021.122523.

[58] J. Zhou, S. Xue, Y. Xue, Y. Liao, J. Liu, and W. Zhao, "A novel energy management strategy of hybrid electric vehicle via an improved TD3 deep reinforcement learning," *Energy*, vol. 224, p. 120118, 2021, https://doi.org/10.1016/j.energy.2021.120118.

[59] A. Biswas, P. G. Anselma, and A. Emadi, "Real-Time Optimal Energy Management of Multimode Hybrid Electric Powertrain With Online Trainable Asynchronous Advantage Actor-Critic Algorithm," *IEEE Transactions on Transportation Electrification*, vol. 8, no. 2, pp. 2676–2694, 2022, https://doi.org/10.1109/TTE.2021.3138330.

[60] Y. Li, H. He, J. Peng, and H. Zhang, "Power Management for a Plug-in Hybrid Electric Vehicle Based on Reinforcement Learning with Continuous State and Action Spaces," *Energy Procedia*, vol. 142, pp. 2270–2275, 2017, https://doi.org/10.1016/j.egypro.2017.12.629.

[61] J. Zhao, "Research and application of over-expansion cycle (Atkinson and Miller) engines – A review," *Applied Energy*, vol. 185, pp. 300–319, 2017, https://doi.org/10.1016/j.apenergy.2016.10.063.

[62] A. M. K. P. Taylor, "Science review of internal combustion engines," *Energy Policy*, vol. 36, no. 12, pp. 4657–4667, 2008, https://doi.org/10.1016/j.enpol.2008.09.001.

[63] V. P. and D. Deshmukh, "A comprehensive review of waste heat recovery from a diesel engine using organic rankine cycle," *Energy Reports*, vol. 7, pp. 3951–3970, 2021, https://doi.org/10.1016/j.egyr.2021.06.081.

[64] R. T. Balmer, "Vapor and Gas Power Cycles," in *Modern Engineering Thermodynamics*, R. T. Balmer, Ed. Boston: Academic Press, 2011, ch. 13, pp. 447–534, https://doi.org/10.1016/B978-0-12-374996-3.00013-0.

[65] S.-S. Hou, "Comparison of performances of air standard Atkinson and Otto cycles with heat transfer considerations," *Energy Conversion and Management*, vol. 48, no. 5, pp. 1683–1690, 2007, https://doi.org/10.1016/j.enconman.2006.11.001.

[66] H. Hong, G. B. Parvate-Patil, and B. Gordon, "Review and analysis of variable valve timing strategies—eight ways to approach," *Proceedings of the Institution of Mechanical Engineers, Part D: Journal of Automobile Engineering*, vol. 218, no. 10, pp. 1179–1200, 2004, https://doi.org/10.1177/095440700421801013.

[67] "Advanced Light-Duty Powertrain and Hybrid Analysis (ALPHA) Tool." [Online]. Available: https://www.epa.gov/regulations-emissions-vehicles-and-engines/advanced-light-duty-powertrain-and-hybrid-analysis-alpha.

[68] N. Lutsey, D. Meszler, A. Isenstadt, J. German, and J. Miller, "Efficiency technology and cost assessment for U.S. 2025–2030 light-duty vehicles," International Council on Clean Transportation, Tech. Rep., Mar. 2017. [Online]. Available: https://theicct.org/publications/US-2030-technology-cost-assessment.

[69] M. D. Aaron Isenstadt, John German, "Naturally aspirated gasoline engines and cylinder deactivation," International Council on Clean Transportation, Tech. Rep., Jun. 2016. [Online]. Available: https://theicct.org/publications/naturally-aspirated-gasoline-engines-and-cylinder-deactivation.

[70] Office of Transportation and Air Quality U.S. Environmental Protection Agency, National Highway Traffic Safety Administration U.S.

Department of Transportation, and California Air Resources Board, "Draft Technical Assessment Report: Midterm Evaluation of Light-Duty Vehicle Greenhouse Gas Emission Standards and Corporate Average Fuel Economy Standards for Model Years 2022-2025," U.S. Environmental Protection Agency, Tech. Rep., Jul. 2016. [Online]. Available: https://www.epa.gov/regulations-emissions-vehicles-and-engines/midterm-evaluation-light-duty-vehicle-greenhouse-gas.

[71] J. Kargul, M. Stuhldreher, D. Barba, C. Schenk, S. Bohac, J. McDonald, P. Dekraker, and J. Alden, "Benchmarking a 2018 Toyota Camry 2.5-Liter Atkinson Cycle Engine with Cooled-EGR," *SAE International Journal of Advances and Current Practices in Mobility*, vol. 1, no. 2, pp. 601–638, 2019, https://doi.org/10.4271/2019-01-0249.

[72] "How things work: OMEGA modeling case study based on the 2018 Toyota Camry." [Online]. Available: https://theicct.org/publications/how-things-work-omega-modeling-case-study-based-2018-toyota-camry.

[73] D. Takahashi, K. Nakata, Y. Yoshihara, Y. Ohta, and H. Nishiura, "Combustion Development to Achieve Engine Thermal Efficiency of 40% for Hybrid Vehicles," in *SAE 2015 World Congress & Exhibition*. SAE International, Apr. 2015, https://doi.org/10.4271/2015-01-1254.

[74] Y. Li, S. Wang, X. Duan, S. Liu, J. Liu, and S. Hu, "Multi-objective energy management for Atkinson cycle engine and series hybrid electric vehicle based on evolutionary NSGA-II algorithm using digital twins," *Energy Conversion and Management*, vol. 230, p. 113788, 2021,

https://doi.org/10.1016/j.enconman.2020.113788.

[75] J. Ribau, C. Silva, F. P. Brito, and J. Martins, "Analysis of four-stroke, Wankel, and microturbine based range extenders for electric vehicles," *Energy Conversion and Management*, vol. 58, pp. 120–133, 2012, https://doi.org/10.1016/j.enconman.2012.01.011.

[76] A. K. Agarwal, A. P. Singh, and R. K. Maurya, "Evolution, challenges and path forward for low temperature combustion engines," *Progress in Energy and Combustion Science*, vol. 61, pp. 1–56, 2017, https://doi.org/10.1016/j.pecs.2017.02.001.

[77] K. D. Cung, S. A. Ciatti, S. Tanov, and Ö. Andersson, "Low-Temperature Combustion of High Octane Fuels in a Gasoline Compression Ignition Engine," *Frontiers in Mechanical Engineering*, vol. 3, p. 22, 2017, https://doi.org/10.3389/fmech.2017.00022.

[78] D. K. Srivastava, A. K. Agarwal, A. Datta, and R. K. Maurya, *Advances in Internal Combustion Engine Research*, ser. Energy, Environment, and Sustainability. Singapore: Springer, 2018, https://doi.org/10.1007/978-981-10-7575-9.

[79] T. Pachiannan, W. Zhong, S. Rajkumar, Z. He, X. Leng, and Q. Wang, "A literature review of fuel effects on performance and emission characteristics of low-temperature combustion strategies," *Applied Energy*, vol. 251, p. 113380, 2019, https://doi.org/10.1016/j.apenergy.2019.113380.

[80] M. Yao, Z. Zheng, and H. Liu, "Progress and recent trends in homogeneous charge compression ignition (HCCI) engines," *Progress in*

Energy and Combustion Science, vol. 35, no. 5, pp. 398–437, 2009, https://doi.org/10.1016/j.pecs.2009.05.001.

[81] Y. Yang, J. E. Dec, N. Dronniou, and M. Sjöberg, "Tailoring HCCI heat-release rates with partial fuel stratification: Comparison of two-stage and single-stage-ignition fuels," *Proceedings of the Combustion Institute*, vol. 33, no. 2, pp. 3047–3055, 2011, https://doi.org/10.1016/j.proci.2010.06.114.

[82] G. T. Kalghatgi, "Auto-Ignition Quality of Practical Fuels and Implications for Fuel Requirements of Future SI and HCCI Engines," in *SAE 2005 World Congress & Exhibition*. SAE International, Apr. 2005, https://doi.org/10.4271/2005-01-0239.

[83] I. Sakata, K. Inagaki, T. Fuyuto, K. Nishikawa, and K. Nakakita, "Dual-Fuel PCI Combustion Controlled by In-Cylinder Stratification of Ignitability," in *SAE 2006 World Congress & Exhibition*. SAE International, Apr. 2006, https://doi.org/10.4271/2006-01-0028.

[84] J. Benajes, A. García, J. Monsalve-Serrano, I. Balloul, and G. Pradel, "Evaluating the reactivity controlled compression ignition operating range limits in a high-compression ratio medium-duty diesel engine fueled with biodiesel and ethanol," *International Journal of Engine Research*, vol. 18, no. 1-2, pp. 66–80, 2017, https://doi.org/10.1177/1468087416678500.

[85] A. García, J. Monsalve-Serrano, V. Rückert Roso, and M. E. Santos Martins, "Evaluating the emissions and performance of two dual-mode RCCI combustion strategies under the World Harmonized Vehicle Cycle

(WHVC)," *Energy Conversion and Management*, vol. 149, pp. 263–274, 2017, https://doi.org/10.1016/j.enconman.2017.07.034.

[86] J. Benajes, A. García, J. Monsalve-Serrano, and D. Villalta, "Exploring the limits of the reactivity controlled compression ignition combustion concept in a light-duty diesel engine and the influence of the direct-injected fuel properties," *Energy Conversion and Management*, vol. 157, pp. 277–287, 2018, https://doi.org/10.1016/j.enconman.2017.12.028.

[87] J. Benajes, A. García, J. Monsalve-Serrano, I. Balloul, and G. Pradel, "An assessment of the dual-mode reactivity controlled compression ignition/conventional diesel combustion capabilities in a EURO VI medium-duty diesel engine fueled with an intermediate ethanol-gasoline blend and biodiesel," *Energy Conversion and Management*, vol. 123, pp. 381–391, 2016, https://doi.org/10.1016/j.enconman.2016.06.059.

[88] S. J. Curran, R. M. Hanson, and R. M. Wagner, "Reactivity controlled compression ignition combustion on a multi-cylinder light-duty diesel engine," *International Journal of Engine Research*, vol. 13, no. 3, pp. 216–225, 2012, https://doi.org/10.1177/1468087412442324.

[89] A. B. Dempsey, S. J. Curran, and R. M. Wagner, "A perspective on the range of gasoline compression ignition combustion strategies for high engine efficiency and low NOx and soot emissions: Effects of in-cylinder fuel stratification," *International Journal of Engine Research*, vol. 17, no. 8, pp. 897–917, 2016, https://doi.org/10.1177/1468087415621805.

[90] A. Delorme, A. Rousseau, T. Wallner, E. Ortiz-Soto, A. Babajimopoulos, and D. Assanis, "Evaluation of Homogeneous Charge Compression Ignition (HCCI) Engine Fuel Savings for Various Electric Drive Powertrains," in *The 25th World Battery, Hybrid and Fuel Cell Electric Vehicle Symposium & Exhibition*, Shenzhen, China, Nov. 2010.

[91] A. Solouk, M. Shahbakhti, and M. J. Mahjoob, "Energy management and control of a hybrid electric vehicle with an integrated low temperature combustion (LTC) engine," in *Proceedings of the ASME 2014 Dynamic Systems and Control Conference*, vol. 2, San Antonio, Texas, USA, Oct. 2014, https://doi.org/10.1115/DSCC2014-6286.

[92] A. Solouk and M. Shahbakhti, "Modeling and Energy Management of an HCCI based Powertrain for Series Hybrid and Extended Range Electric Vehicles," *International Journal of Powertrains*, vol. 6, no. 3, p. 226, 2017, https://doi.org/10.1504/ijpt.2017.10001761.

[93] Z. Gao, S. J. Curran, J. E. Parks, D. E. Smith, R. M. Wagner, C. S. Daw, K. D. Edwards, and J. F. Thomas, "Drive cycle simulation of high efficiency combustions on fuel economy and exhaust properties in light-duty vehicles," *Applied Energy*, vol. 157, pp. 762–776, 2015, https://doi.org/10.1016/j.apenergy.2015.03.070.

[94] A. García and J. Monsalve-Serrano, "Analysis of a series hybrid vehicle concept that combines low temperature combustion and biofuels as power source," *Results in Engineering*, vol. 1, p. 100001, 2019, https://doi.org/10.1016/j.rineng.2019.01.001.

[95] A. García, J. Monsalve-Serrano, S. Martinez-Boggio, P. Gaillard, O. Poussin, and A. A. Amer, "Dual fuel combustion and hybrid electric powertrains as potential solution to achieve 2025 emissions targets in medium duty trucks sector," *Energy Conversion and Management*, vol. 224, p. 113320, 2020, https://doi.org/10.1016/j.enconman.2020.113320.

[96] A. Solouk and M. Shahbakhti, "Energy Optimization and Fuel Economy Investigation of a Series Hybrid Electric Vehicle Integrated with Diesel/RCCI Engines," *Energies*, vol. 9, no. 12, pp. 1–23, 2016, https://doi.org/10.3390/en9121020.

[97] S. Nüesch and A. G. Stefanopoulou, "Multimode combustion in a mild hybrid electric vehicle. Part 2: Three-way catalyst considerations," *Control Engineering Practice*, vol. 58, pp. 107–116, 2017, https://doi.org/10.1016/j.conengprac.2016.10.007.

[98] S. Nüesch and A. G. Stefanopoulou, "Multimode combustion in a mild hybrid electric vehicle. Part 1: Supervisory control," *Control Engineering Practice*, vol. 57, pp. 99–110, 2016, https://doi.org/10.1016/j.conengprac.2016.09.002.

[99] K. Ahn, J. Whitefoot, A. Babajimopoulos, E. Ortiz-Soto, and P. Y. Papalambros, "Homogeneous charge compression ignition technology implemented in a hybrid electric vehicle: System optimal design and benefit analysis for a power-split architecture," *Proceedings of the Institution of Mechanical Engineers, Part D: Journal of Automobile Engineering*, vol. 227, no. 1, pp. 87–98, 2013, https://doi.org/10.1177/0954407012453237.

[100] A. Solouk, J. Tripp, M. Shakiba-Herfeh, and M. Shahbakhti, "Fuel consumption assessment of a multi-mode low temperature combustion engine as range extender for an electric vehicle," *Energy Conversion and Management*, vol. 148, pp. 1478–1496, 2017, https://doi.org/10.1016/j.enconman.2017.06.090.

[101] A. Solouk, M. Shakiba-herfeh, K. Kannan, H. Solmaz, P. Dice, M. Bidarvatan, N. N. T. Kondipati, and M. Shahbakhti, "Fuel Economy Benefits of Integrating a Multi-Mode Low Temperature Combustion (LTC) Engine in a Series Extended Range Electric Powertrain," in *SAE 2016 International Powertrains, Fuels & Lubricants Meeting*. SAE International, Oct. 2016.

[102] M. Shakiba-herfeh, A. Solouk, and M. Shahbakhti, "Analysis and Control of a Torque Blended Hybrid Electric Powertrain with a Multi-Mode LTC-SI Engine," *SAE International Journal of Alternative Powertrains*, vol. 6, no. 1, pp. 54–67, 2017, https://doi.org/10.4271/2017-01-1153.

[103] S. Yeh, "An empirical analysis on the adoption of alternative fuel vehicles: The case of natural gas vehicles," *Energy Policy*, vol. 35, no. 11, pp. 5865–5875, 2007, https://doi.org/10.1016/j.enpol.2007.06.012.

[104] L. Mohammed, E. Niesten, and D. Gagliardi, "Adoption of alternative fuel vehicle fleets – A theoretical framework of barriers and enablers," *Transportation Research Part D: Transport and Environment*, vol. 88, p. 102558, 2020, https://doi.org/10.1016/j.trd.2020.102558.

[105] B. Lane, B. Shaffer, and S. Samuelsen, "A comparison of alternative vehicle fueling infrastructure scenarios," *Applied Energy*, vol. 259, p. 114128, 2020, https://doi.org/10.1016/j.apenergy.2019.114128.

[106] I. Dincer, "Environmental and sustainability aspects of hydrogen and fuel cell systems," *International Journal of Energy Research*, vol. 31, no. 1, pp. 29–55, 2007, https://doi.org/10.1002/er.1226.

[107] K. Mazloomi and C. Gomes, "Hydrogen as an energy carrier: Prospects and challenges," *Renewable and Sustainable Energy Reviews*, vol. 16, no. 5, pp. 3024–3033, 2012, https://doi.org/10.1016/j.rser.2012.02.028.

[108] H. T. Arat, "Alternative fuelled hybrid electric vehicle (AF-HEV) with hydrogen enriched internal combustion engine," *International Journal of Hydrogen Energy*, vol. 44, no. 34, pp. 19 005–19 016, 2019, https://doi.org/10.1016/j.ijhydene.2018.12.219.

[109] T. Wallner, H. Lohse-Busch, S. Gurski, M. Duoba, W. Thiel, D. Martin, and T. Korn, "Fuel economy and emissions evaluation of BMW Hydrogen 7 Mono-Fuel demonstration vehicles," *International Journal of Hydrogen Energy*, vol. 33, no. 24, pp. 7607–7618, 2008, https://doi.org/10.1016/j.ijhydene.2008.08.067.

[110] "Hydrogen Vehicle." [Online]. Available: https://www.mazda.com/en/innovation/technology/env/hre/.

[111] "Aston Martin to Race World-First Hybrid Hydrogen Rapide S." [Online]. Available: https://www2.astonmartin.com/en/live/news/2013/04/12/aston-martin-to-race-world-first-hybrid-hydrogen-rapide-s.

[112] H. An, W. M. Yang, A. Maghbouli, J. Li, S. K. Chou, and K. J. Chua, "A numerical study on a hydrogen assisted diesel engine," *International Journal of Hydrogen Energy*, vol. 38, no. 6, pp. 2919–2928, 2013, https://doi.org/10.1016/j.ijhydene.2012.12.062.

[113] S. Wang, C. Ji, J. Zhang, and B. Zhang, "Comparison of the performance of a spark-ignited gasoline engine blended with hydrogen and hydrogen–oxygen mixtures," *Energy*, vol. 36, no. 10, pp. 5832–5837, 2011, https://doi.org/10.1016/j.energy.2011.08.042.

[114] T. Su, C. Ji, S. Wang, X. Cong, and L. Shi, "Improving performance of a gasoline Wankel rotary by hydrogen enrichment at different conditions," *Energy Conversion and Management*, vol. 171, pp. 721–728, 2018, https://doi.org/10.1016/j.enconman.2018.06.030.

[115] C. Ji, H. Wang, C. Shi, S. Wang, and J. Yang, "Multi-objective optimization of operating parameters for a gasoline Wankel rotary engine by hydrogen enrichment," *Energy Conversion and Management*, vol. 229, p. 113732, 2021, https://doi.org/10.1016/j.enconman.2020.113732.

[116] P. Dimitriou, T. Tsujimura, and Y. Suzuki, "Low-load hydrogen-diesel dual-fuel engine operation – A combustion efficiency improvement approach," *International Journal of Hydrogen Energy*, vol. 44, no. 31, pp. 17 048–17 060, 2019, https://doi.org/10.1016/j.ijhydene.2019.04.203.

[117] A. K. Jaura, W. Ortmann, R. Stuntz, B. Natkin, and T. Grabowski, "Ford's H2RV: An Industry First HEV Propelled with a H2 Fueled Engine - A Fuel Efficient and Clean Solution for Sustainable Mobility," in

SAE 2004 World Congress & Exhibition. SAE International, Mar. 2004, https://doi.org/10.4271/2004-01-0058.

[118] X. He, T. Maxwell, and M. E. Parten, "Development of a Hybrid Electric Vehicle With a Hydrogen-Fueled IC Engine," *IEEE Transactions on Vehicular Technology*, vol. 55, no. 6, pp. 1693–1703, 2006, https://doi.org/10.1109/TVT.2006.878609.

[119] H. T. Arat, "Simulation of diesel hybrid electric vehicle containing hydrogen enriched CI engine," *International Journal of Hydrogen Energy*, vol. 44, no. 20, pp. 10 139–10 146, 2019, https://doi.org/10.1016/j.ijhydene.2018.10.004.

[120] K. Turoń, "Hydrogen-powered vehicles in urban transport systems – current state and development," *Transportation Research Procedia*, vol. 45, pp. 835–841, 2020, https://doi.org/10.1016/j.trpro.2020.02.086.

[121] "Toyota Reveals World-First Flexible Fuel Hybrid Prototype in Brazil." [Online]. Available: https://global.toyota/en/newsroom/corporate/21633112.html?adid=ag478_mail&padid=ag478_mail.

[122] B. Albayrak Ceper and M. Yıldız, "Experimental investigation of performance and emissions of the SICAI-hybrid engine systems," *International Journal of Hydrogen Energy*, vol. 42, no. 40, pp. 25 791–25 800, 2017, https://doi.org/10.1016/j.ijhydene.2017.05.025.

[123] M. Ouyang, W. Zhang, E. Wang, F. Yang, J. Li, Z. Li, P. Yu, and X. Ye, "Performance analysis of a novel coaxial power-split hybrid powertrain using a

CNG engine and supercapacitors," *Applied Energy*, vol. 157, pp. 595–606, 2015, https://doi.org/10.1016/j.apenergy.2014.12.086.

[124] N. R. Council, *Transitions to Alternative Vehicles and Fuels*. Washington, DC: The National Academies Press, 2013, https://doi.org/10.17226/18264.

[125] T. Endo, S. Kawajiri, Y. Kojima, K. Takahashi, T. Baba, S. Ibaraki, T. Takahashi, and M. Shinohara, "Study on Maximizing Exergy in Automotive Engines," in *SAE World Congress & Exhibition*. SAE International, Apr. 2007, https://doi.org/10.4271/2007-01-0257.

[126] D. Champier, "Thermoelectric generators: A review of applications," *Energy Conversion and Management*, vol. 140, pp. 167–181, 2017, https://doi.org/10.1016/j.enconman.2017.02.070.

[127] T. Y. Kim and J. Kim, "Assessment of the energy recovery potential of a thermoelectric generator system for passenger vehicles under various drive cycles," *Energy*, vol. 143, pp. 363–371, 2018, https://doi.org/10.1016/j.energy.2017.10.137.

[128] N. Jaziri, A. Boughamoura, J. Müller, B. Mezghani, F. Tounsi, and M. Ismail, "A comprehensive review of Thermoelectric Generators: Technologies and common applications," *Energy Reports*, vol. 6, pp. 264–287, 2020, https://doi.org/10.1016/j.egyr.2019.12.011.

[129] C. Yu and K. Chau, "Thermoelectric automotive waste heat energy recovery using maximum power point tracking," *Energy Conversion and Management*, vol. 50, no. 6, pp. 1506–1512, 2009,

https://doi.org/10.1016/j.enconman.2009.02.015.

[130] B. Orr, A. Akbarzadeh, and P. Lappas, "An exhaust heat recovery system utilising thermoelectric generators and heat pipes," *Applied Thermal Engineering*, vol. 126, pp. 1185–1190, 2017, https://doi.org/10.1016/j.applthermaleng.2016.11.019.

[131] D. Crane, G. Jackson, and D. Holloway, "Towards Optimization of Automotive Waste Heat Recovery Using Thermoelectrics," in *SAE 2001 World Congress*. SAE International, Mar. 2001, https://doi.org/10.4271/2001-01-1021.

[132] Q. Cao, W. Luan, and T. Wang, "Performance enhancement of heat pipes assisted thermoelectric generator for automobile exhaust heat recovery," *Applied Thermal Engineering*, vol. 130, pp. 1472–1479, 2018, https://doi.org/10.1016/j.applthermaleng.2017.09.134.

[133] C. Liu, X. Pan, X. Zheng, Y. Yan, and W. Li, "An experimental study of a novel prototype for two-stage thermoelectric generator from vehicle exhaust," *Journal of the Energy Institute*, vol. 89, no. 2, pp. 271–281, 2016, https://doi.org/10.1016/j.joei.2015.01.019.

[134] F. P. Brito, N. Pacheco, R. Vieira, J. Martins, L. Martins, J. Teixeira, L. M. Goncalves, J. Oliveira, and M. J. Hall, "Efficiency improvement of vehicles using temperature controlled exhaust thermoelectric generators," *Energy Conversion and Management*, vol. 203, p. 112255, 2020, https://doi.org/10.1016/j.enconman.2019.112255.

[135] A. Marvão, P. J. Coelho, and H. C. Rodrigues, "Optimization of a thermoelectric generator for heavy-duty vehicles," *Energy Conversion and Management*, vol. 179, pp. 178–191, 2019, https://doi.org/10.1016/j.enconman.2018.10.045.

[136] Y. Choi, A. Negash, and T. Y. Kim, "Waste heat recovery of diesel engine using porous medium-assisted thermoelectric generator equipped with customized thermoelectric modules," *Energy Conversion and Management*, vol. 197, p. 111902, 2019, https://doi.org/10.1016/j.enconman.2019.111902.

[137] J. Liebl, S. Neugebauer, A. Eder, M. Linde, B. Mazar, and W. Stütz, "The thermoelectric generator from BMW is making use of waste heat," *MTZ worldwide*, vol. 70, no. 4, pp. 4–11, 2009, https://doi.org/10.1007/BF03226939.

[138] K. Shinohara, M. Kobayashi, K. Kushibiki, K. Furuya, M. Masayuki, and H. Komatsu, "Application of Thermoelectric Generator for Automobile," *Journal of the Japan Society of Powder and Powder Metallurgy*, vol. 46, no. 5, pp. 524–528, 1999, https://doi.org/10.2497/jjspm.46.524.

[139] T. Y. Kim, J. Kwak, and B. wook Kim, "Energy harvesting performance of hexagonal shaped thermoelectric generator for passenger vehicle applications: An experimental approach," *Energy Conversion and Management*, vol. 160, pp. 14–21, 2018, https://doi.org/10.1016/j.enconman.2018.01.032.

[140] Q. E. Hussain, D. R. Brigham, and C. W. Maranville, "Thermoelectric Exhaust Heat Recovery for Hybrid Vehicles," *SAE International Journal of Engines*, vol. 2, no. 1, pp. 1132–1142, 2009, https://doi.org/10.4271/2009-01-1327.

[141] M. Mori, T. Yamagami, M. Sorazawa, T. Miyabe, S. Takahashi, and T. Haraguchi, "Simulation of Fuel Economy Effectiveness of Exhaust Heat Recovery System Using Thermoelectric Generator in a Series Hybrid," *SAE International Journal of Materials and Manufacturing*, vol. 4, no. 1, pp. 1268–1276, 2011, https://doi.org/10.4271/2011-01-1335.

[142] K. Oetringer, M. Kober, and M. K. Altstedde, "Upgrading hybrid-vehicles with a Thermoelectric Generator," in *2014 Ninth International Conference on Ecological Vehicles and Renewable Energies (EVER)*, Mar. 2014, pp. 1–5, https://doi.org/10.1109/EVER.2014.6844021.

[143] R. Vijayagopal and A. Rousseau, "Impact of TEGs on the Fuel Economy of Conventional and Hybrid Vehicles," in *SAE 2015 World Congress & Exhibition*. SAE International, Apr. 2015, https://doi.org/10.4271/2015-01-1712.

[144] R. Wang, W. Yu, and X. Meng, "Performance investigation and energy optimization of a thermoelectric generator for a mild hybrid vehicle," *Energy*, vol. 162, pp. 1016–1028, 2018, https://doi.org/10.1016/j.energy.2018.08.103.

[145] S. Lan, R. Stobart, R. Chen, Z. Yang, and C. Rouaud, "The Potential of Thermoelectric Generator in Parallel Hybrid Vehicle Applications," in *WCX™ 17: SAE World Congress Experience*. SAE International, Mar. 2017, https://doi.org/10.4271/2017-01-0189.

[146] M. Kober, "The High Potential for Waste Heat Recovery in Hybrid Vehicles: A Comparison Between the Potential in Conventional and Hybrid Powertrains," *Journal of Electronic Materials*, vol. 49, no. 5, pp. 2928–2936, 2020, https://doi.org/10.1007/s11664-020-07991-5.

[147] F. P. Brito, J. Martins, L. Goncalves, and R. Sousa, "Modelling of thermoelectric generator with heat pipe assist for range extender application," in *IECON 2011 - 37th Annual Conference of the IEEE Industrial Electronics Society*, Nov. 2011, pp. 4589–4595, https://doi.org/10.1109/IECON.2011.6120066.

[148] M. S. B. Dzulkfli, A. Pesyridis, and D. Gohil, "Thermoelectric Generation in Hybrid Electric Vehicles," *Energies*, vol. 13, no. 14, 2020, https://doi.org/10.3390/en13143742.

[149] T. Y. Kim, J. Kwak, and B. wook Kim, "Application of compact thermoelectric generator to hybrid electric vehicle engine operating under real vehicle operating conditions," *Energy Conversion and Management*, vol. 201, p. 112150, 2019, https://doi.org/10.1016/j.enconman.2019.112150.

[150] N. Muralidhar, M. Himabindu, and R. V. Ravikrishna, "Modeling of a hybrid electric heavy duty vehicle to assess energy recovery using a thermoelectric generator," *Energy*, vol. 148, pp. 1046–1059, 2018, https://doi.org/10.1016/j.energy.2018.02.023.

[151] T. Caillat, J. P. Fleurial, G. J. Snyder, A. Zoltan, D. Zoltan, and A. Borshchevsky, "A New High Efficiency Segmented Thermoelectric Unicouple," in *34th Intersociety Energy Conversion Engineering Conference*. SAE International, Aug. 1999, https://doi.org/10.4271/1999-01-2567.

[152] F. Zhou, S. N. Joshi, R. Rhote-Vaney, and E. M. Dede, "A review and future application of Rankine Cycle to passenger vehicles for waste heat recovery," *Renewable and Sustainable Energy Reviews*, vol. 75, pp. 1008–1021, 2017, https://doi.org/10.1016/j.rser.2016.11.080.

[153] F. Mohammadkhani, M. Yari, and F. Ranjbar, "A zero-dimensional model for simulation of a Diesel engine and exergoeconomic analysis of waste heat recovery from its exhaust and coolant employing a high-temperature Kalina cycle," *Energy Conversion and Management*, vol. 198, p. 111782, 2019, https://doi.org/10.1016/j.enconman.2019.111782.

[154] A. E. Teo, M. S. Chiong, M. Yang, A. Romagnoli, R. F. Martinez-Botas, and S. Rajoo, "Performance evaluation of low-pressure turbine, turbo-compounding and air-Brayton cycle as engine waste heat recovery method," *Energy*, vol. 166, pp. 895–907, 2019, https://doi.org/10.1016/j.energy.2018.10.035.

[155] A. Mahmoudi, M. Fazli, and M. R. Morad, "A recent review of waste heat recovery by Organic Rankine Cycle," *Applied Thermal Engineering*, vol. 143, pp. 660–675, 2018, https://doi.org/10.1016/j.applthermaleng.2018.07.136.

[156] D. W. Stanton, "Systematic Development of Highly Efficient and Clean Engines to Meet Future Commercial Vehicle Greenhouse Gas Regulations," *SAE International Journal of Engines*, vol. 6, no. 3, pp. 1395–1480, 2013, https://doi.org/10.4271/2013-01-2421.

[157] D. Seher, T. Lengenfelder, J. Gerhardt, N. Eisenmenger, M. Hackner, and I. Krinn, "Waste Heat Recovery for Commercial Vehicles with a Rankine Process," in *21st Aachen Colloquium Automobile and Engine Technology*, Aachen, Germany, Oct. 2012. [Online]. Available: https://www.aachener-kolloquium.de/images/tagungsunterlagen/2012_21._ACK/E3.3_Seher_Bosch.pdf

[158] S. Subramanian, "Heavy Duty Roots Expander Heat Energy Recovery (HD-REHER)," U.S. Department of Energy (DOE) Office of Scientific and

Technical Information (OSTI), Tech. Rep., Oct. 2015. [Online]. Available: https://www.osti.gov/biblio/1337562.

[159] M. Glensvig, H. Schreier, M. Tizianel, H. Theissl, P. Krähenbühl, F. Cococcetta, and I. Calaon, "Testing of a Long Haul Demonstrator Vehicle with a Waste Heat Recovery System on Public Road," in *SAE 2016 Commercial Vehicle Engineering Congress*. SAE International, Sep. 2016, https://doi.org/10.4271/2016-01-8057.

[160] J. Ringler, M. Seifert, V. Guyotot, and W. Hübner, "Rankine Cycle for Waste Heat Recovery of IC Engines," *SAE International Journal of Engines*, vol. 2, no. 1, pp. 67–76, 2009, https://doi.org/10.4271/2009-01-0174.

[161] T. E. Briggs, R. Wagner, K. D. Edwards, S. Curran, and E. Nafziger, "A Waste Heat Recovery System for Light Duty Diesel Engines," in *SAE 2010 Powertrains Fuels & Lubricants Meeting*. SAE International, Oct. 2010, https://doi.org/10.4271/2010-01-2205.

[162] T. Chen, W. Zhuge, Y. Zhang, and L. Zhang, "A novel cascade organic Rankine cycle (ORC) system for waste heat recovery of truck diesel engines," *Energy Conversion and Management*, vol. 138, pp. 210–223, 2017, https://doi.org/10.1016/j.enconman.2017.01.056.

[163] A. S. Panesar, "An innovative Organic Rankine Cycle system for integrated cooling and heat recovery," *Applied Energy*, vol. 186, pp. 396–407, 2017, https://doi.org/10.1016/j.apenergy.2016.03.011.

[164] J. Li, Z. Yang, S. Hu, F. Yang, and Y. Duan, "Effects of shell-and-tube heat exchanger arranged forms on the thermo-economic performance of organic Rankine cycle systems using hydrocarbons," *Energy Conversion and Management*, vol. 203, p. 112248, 2020, https://doi.org/10.1016/j.enconman.2019.112248.

[165] X. Li, J. Song, G. Yu, Y. Liang, H. Tian, G. Shu, and C. N. Markides, "Organic Rankine cycle systems for engine waste-heat recovery: Heat exchanger design in space-constrained applications," *Energy Conversion and Management*, vol. 199, p. 111968, 2019, https://doi.org/10.1016/j.enconman.2019.111968.

[166] J. Bao and L. Zhao, "A review of working fluid and expander selections for organic Rankine cycle," *Renewable and Sustainable Energy Reviews*, vol. 24, pp. 325–342, 2013, https://doi.org/10.1016/j.rser.2013.03.040.

[167] A. W. Costall, A. Gonzalez Hernandez, P. J. Newton, and R. F. Martinez-Botas, "Design methodology for radial turbo expanders in mobile organic Rankine cycle applications," *Applied Energy*, vol. 157, pp. 729–743, 2015, https://doi.org/10.1016/j.apenergy.2015.02.072.

[168] G. Shu, Z. Yu, P. Liu, Z. Xu, and R. Sun, "Potential of a thermofluidic feed pump on performance improvement of the dual-loop Rankine cycle using for engine waste heat recovery," *Energy Conversion and Management*, vol. 171, pp. 1150–1162, 2018, https://doi.org/10.1016/j.enconman.2018.06.011.

[169] E. S. Richardson, "Thermodynamic performance of new thermofluidic feed pumps for Organic Rankine Cycle applications," *Applied Energy*, vol. 161, pp. 75–84, 2016, https://doi.org/10.1016/j.apenergy.2015.10.004.

[170] G. Shu, M. Zhao, H. Tian, Y. Huo, and W. Zhu, "Experimental comparison of R123 and R245fa as working fluids for waste heat recovery from heavy-duty diesel engine," *Energy*, vol. 115, pp. 756–769, 2016, https://doi.org/10.1016/j.energy.2016.09.082.

[171] Z. Wang, Y. Hu, X. Xia, Q. Zuo, B. Zhao, and Z. Li, "Thermo-economic selection criteria of working fluid used in dual-loop ORC for engine waste heat recovery by multi-objective optimization," *Energy*, vol. 197, p. 117053, 2020, https://doi.org/10.1016/j.energy.2020.117053.

[172] H. Tian, P. Liu, and G. Shu, "Challenges and opportunities of Rankine cycle for waste heat recovery from internal combustion engine," *Progress in Energy and Combustion Science*, vol. 84, p. 100906, 2021, https://doi.org/10.1016/j.pecs.2021.100906.

[173] H. Liu, H. Zhang, F. Yang, X. Hou, F. Yu, and S. Song, "Multi-objective optimization of fin-and-tube evaporator for a diesel engine-organic Rankine cycle (ORC) combined system using particle swarm optimization algorithm," *Energy Conversion and Management*, vol. 151, pp. 147–157, 2017, https://doi.org/10.1016/j.enconman.2017.08.081.

[174] E. Feru, B. de Jager, F. Willems, and M. Steinbuch, "Two-phase plate-fin heat exchanger modeling for waste heat recovery systems in diesel engines," *Applied Energy*, vol. 133, pp. 183–196, 2014, https://doi.org/10.1016/j.apenergy.2014.07.073.

[175] T. Chen, G. Shu, H. Tian, X. Ma, Y. Wang, and H. Yang, "Compact potential of exhaust heat exchangers for engine waste heat recovery using metal foams,"

International Journal of Energy Research, vol. 43, no. 4, pp. 1428–1443, 2019, https://doi.org/10.1002/er.4340.

[176] Y. Wang, G. Shu, G. Yu, H. Tian, X. Ma, and T. Chen, "Numerical analysis of forced convection of high-temperature exhaust gas around a metal-foam wrapped cylinder," *International Journal of Heat and Mass Transfer*, vol. 119, pp. 742–751, 2018, https://doi.org/10.1016/j.ijheatmasstransfer.2017.11.057.

[177] G. Qiu, H. Liu, and S. Riffat, "Expanders for micro-CHP systems with organic Rankine cycle," *Applied Thermal Engineering*, vol. 31, no. 16, pp. 3301–3307, 2011, https://doi.org/10.1016/j.applthermaleng.2011.06.008.

[178] S. Quoilin, M. V. D. Broek, S. Declaye, P. Dewallef, and V. Lemort, "Techno-economic survey of Organic Rankine Cycle (ORC) systems," *Renewable and Sustainable Energy Reviews*, vol. 22, pp. 168–186, 2013, https://doi.org/10.1016/j.rser.2013.01.028.

[179] F. Meng, H. Zhang, F. Yang, X. Hou, B. Lei, L. Zhang, Y. Wu, J. Wang, and Z. Shi, "Study of efficiency of a multistage centrifugal pump used in engine waste heat recovery application," *Applied Thermal Engineering*, vol. 110, pp. 779–786, 2017, https://doi.org/10.1016/j.applthermaleng.2016.08.226.

[180] U. Larsen, L. Pierobon, F. Haglind, and C. Gabrielii, "Design and optimisation of organic Rankine cycles for waste heat recovery in marine applications using the principles of natural selection," *Energy*, vol. 55, pp. 803–812, 2013, https://doi.org/10.1016/j.energy.2013.03.021.

[181] D. Jung, S. Park, and K. Min, "Selection of appropriate working fluids for Rankine cycles used for recovery of heat from exhaust gases of ICE in heavy-duty series hybrid electric vehicles," *Applied Thermal Engineering*, vol. 81, pp. 338–345, 2015, https://doi.org/10.1016/j.applthermaleng.2015.02.002.

[182] K. Kruijt, F. J. R. Verbruggen, M. F. M. Speetjens, and T. Hofman, "Modeling and control of a waste heat recovery system for integrated powertrain design optimization," *IFAC-PapersOnLine*, vol. 52, no. 5, pp. 598–603, 2019, https://doi.org/10.1016/j.ifacol.2019.09.095.

[183] Y. Gao, X. Wang, G. Shu, H. Tian, and X. Shi, "Applicability analysis of waste heat recovery technology and strategy exploration for hybrid electric vehicles under diverse road conditions," *Energy Conversion and Management*, vol. 230, p. 113780, 2021, https://doi.org/10.1016/j.enconman.2020.113780.

[184] C. Mansour, W. B. Nader, C. Dumand, and M. Nemer, "Waste heat recovery from engine coolant on mild hybrid vehicle using organic Rankine cycle," *Proceedings of the Institution of Mechanical Engineers, Part D: Journal of Automobile Engineering*, vol. 233, no. 10, pp. 2502–2517, 2019, https://doi.org/10.1177/0954407018797819.

[185] P. Skarke, S. Midlam-Mohler, and M. Canova, "Waste Heat Recovery From Internal Combustion Engines: Feasibility Study on an Organic Rankine Cycle With Application to the Ohio State EcoCAR PHEV," in *Proceedings of the ASME 2012 Internal Combustion Engine Division Fall Technical Conference*, Sep. 2012, pp. 609–615, https://doi.org/10.1115/ICEF2012-92018.

[186] M. Villani and L. Tribioli, "Comparison of different layouts for the integration of an organic Rankine cycle unit in electrified powertrains of heavy duty Diesel trucks," *Energy Conversion and Management*, vol. 187, pp. 248–261, 2019, https://doi.org/10.1016/j.enconman.2019.02.078.

[187] F. Galuppo, M. Nadri, P. Dufour, T. Reiche, and V. Lemort, "Evaluation of a Coupled Organic Rankine Cycle Mild Hybrid Architecture for Long-Haul Heavy-Duty Truck," *IFAC-PapersOnLine*, vol. 52, no. 5, pp. 478–483, 2019, https://doi.org/10.1016/j.ifacol.2019.09.076.

[188] A. M. Andwari, A. Pesiridis, A. Karvountzis-Kontakiotis, and V. Esfahanian, "Hybrid electric vehicle performance with organic rankine cycle waste heat recovery system," *Applied Sciences*, no. 5, 2017, https://doi.org/10.3390/app7050437.

[189] C. Mansour, W. B. Nader, C. Dumand, and M. Nemer, "Methodology for fuel saving assessment of a mild hybrid electric vehicle using organic Rankine cycle," in *Proceedings of the 31st International Conference on Efficiency, Cost, Optimization, Simulation and Environmental Impact of Energy Systems (ECOS 2018)*, Guimarães, Portugal, Jun. 2018.

[190] Y. Gao, X. Wang, H. Tian, J. Cai, and G. Shu, "Quantitative analysis of fuel-saving potential for waste heat recovery system integrated with hybrid electric vehicle," *International Journal of Energy Research*, vol. 44, no. 14, pp. 11 152–11 170, 2020, https://doi.org/10.1002/er.5675.

[191] A. Shabashevich, N. Richards, J. Hwang, and P. A. Erickson, "Analysis of powertrain design on effective waste heat recovery from conventional

and hybrid electric vehicles," *Applied Energy*, vol. 157, pp. 754–761, 2015, https://doi.org/10.1016/j.apenergy.2015.02.067.

[192] W. B. Nader, C. Mansour, C. Dumand, and M. Nemer, "Brayton cycles as waste heat recovery systems on series hybrid electric vehicles," *Energy Conversion and Management*, vol. 168, pp. 200–214, 2018, https://doi.org/10.1016/j.enconman.2018.05.004.

[193] R. Rodriguez, M. Preindl, J. S. Cotton, and A. Emadi, "Review and Trends of Thermoelectric Generator Heat Recovery in Automotive Applications," *IEEE Transactions on Vehicular Technology*, vol. 68, no. 6, pp. 5366–5378, 2019, https://doi.org/10.1109/TVT.2019.2908150.

[194] Z. Chen, Y. Liu, Y. Zhang, Z. Lei, Z. Chen, and G. Li, "A neural network-based ECMS for optimized energy management of plug-in hybrid electric vehicles," *Energy*, vol. 243, p. 122727, 2022, https://doi.org/10.1016/j.energy.2021.122727.

[195] C. Sun, F. Sun, and H. He, "Investigating adaptive-ECMS with velocity forecast ability for hybrid electric vehicles," *Applied Energy*, vol. 185, pp. 1644–1653, 2017, https://doi.org/10.1016/j.apenergy.2016.02.026.

[196] E. Rask, M. Duoba, H. Lohse-Busch, and D. Bocci, "Model year 2010 (Gen 3) Toyota Prius level 1 testing report," Argonne National Laboratory, United States, Tech. Rep., Jun. 2010. [Online]. Available: https://doi.org/10.2172/989465.

[197] T. A. Burress, S. L. Campbell, C. Coomer, C. W. Ayers, A. A. Wereszczak, J. P. Cunningham, L. D. Marlino, L. E. Seiber, and H.-T. Lin, "Evaluation of the 2010 Toyota Prius Hybrid Synergy Drive System," Oak Ridge National Laboratory, United States, Tech. Rep., Mar. 2011. [Online]. Available: https://doi.org/10.2172/1007833.

[198] Argonne National Laboratory, "Downloadable Dynamometer Database (D3)- Test Summary Sheet," U.S. Department of Energy (DOE), United States, Tech. Rep., Jul. 2013. [Online]. Available: https://www.anl.gov/es/energy-systems-d3-2010-toyota-prius.

[199] J. Li, Y. Liu, D. Qin, G. Li, and Z. Chen, "Research on Equivalent Factor Boundary of Equivalent Consumption Minimization Strategy for PHEVs," *IEEE Transactions on Vehicular Technology*, vol. 69, no. 6, pp. 6011–6024, 2020, https://doi.org/10.1109/TVT.2020.2986541.

[200] Y. Yang, Y. Zhang, J. Tian, and T. Li, "Adaptive real-time optimal energy management strategy for extender range electric vehicle," *Energy*, vol. 197, p. 117237, 2020, https://doi.org/10.1016/j.energy.2020.117237.

[201] J. Han, Y. Park, and D. Kum, "Optimal adaptation of equivalent factor of equivalent consumption minimization strategy for fuel cell hybrid electric vehicles under active state inequality constraints," *Journal of Power Sources*, vol. 267, pp. 491–502, 2014, https://doi.org/10.1016/j.jpowsour.2014.05.067.

[202] F. R. Salmasi, "Control Strategies for Hybrid Electric Vehicles: Evolution, Classification, Comparison, and Future Trends," *IEEE Transactions on Vehicular Technology*, vol. 56, no. 5, pp. 2393–2404, 2007,

https://doi.org/10.1109/TVT.2007.899933.

[203] H. Liu, C. Wang, X. Zhao, and C. Guo, "An Adaptive-Equivalent Consumption Minimum Strategy for an Extended-Range Electric Bus Based on Target Driving Cycle Generation," *Energies*, vol. 11, no. 7, p. 1805, 2018, https://doi.org/10.3390/en11071805.

[204] F. Tianheng, Y. Lin, G. Qing, H. Yanqing, Y. Ting, and Y. Bin, "A Supervisory Control Strategy for Plug-In Hybrid Electric Vehicles Based on Energy Demand Prediction and Route Preview," *IEEE Transactions on Vehicular Technology*, vol. 64, no. 5, pp. 1691–1700, 2015, https://doi.org/10.1109/TVT.2014.2336378.

[205] F. Zhang, J. Xi, and R. Langari, "Real-Time Energy Management Strategy Based on Velocity Forecasts Using V2V and V2I Communications," *IEEE Transactions on Intelligent Transportation Systems*, vol. 18, no. 2, pp. 416–430, 2017, https://doi.org/10.1109/TITS.2016.2580318.

[206] A. Demir, "Trisection method by k-Lucas numbers," *Applied Mathematics and Computation*, vol. 198, no. 1, pp. 339–345, 2008, https://doi.org/10.1016/j.amc.2007.08.039.

[207] C. Zhang, A. Vahidi, P. Pisu, X. Li, and K. Tennant, "Role of Terrain Preview in Energy Management of Hybrid Electric Vehicles," *IEEE Transactions on Vehicular Technology*, vol. 59, no. 3, pp. 1139–1147, 2010, https://doi.org/10.1109/TVT.2009.2038707.

[208] Z. Lei, D. Sun, J. Liu, D. Chen, Y. Liu, and Z. Chen, "Trip-oriented model predictive energy management strategy for plug-in hybrid electric vehicles," *IEEE Access*, vol. 7, pp. 113 771–113 785, 2019, https://doi.org/10.1109/ACCESS.2019.2933015.

[209] S. Suhaib Kamran, A. Haleem, S. Bahl, M. Javaid, C. Prakash, and D. Budhhi, "Artificial intelligence and advanced materials in automotive industry: Potential applications and perspectives," *Materials Today: Proceedings*, vol. 62, pp. 4207–4214, 2022, https://doi.org/10.1016/j.matpr.2022.04.727.

[210] R. Lian, J. Peng, Y. Wu, H. Tan, and H. Zhang, "Rule-interposing deep reinforcement learning based energy management strategy for power-split hybrid electric vehicle," *Energy*, vol. 197, p. 117297, 2020, https://doi.org/10.1016/j.energy.2020.117297.

[211] N. Parvez Farazi, B. Zou, T. Ahamed, and L. Barua, "Deep reinforcement learning in transportation research: A review," *Transportation Research Interdisciplinary Perspectives*, vol. 11, p. 100425, 2021, https://doi.org/10.1016/j.trip.2021.100425.

[212] Y. LeCun, Y. Bengio, and G. Hinton, "Deep learning," *Nature*, vol. 521, p. 436–444, 2015, https://doi.org/10.1038/nature14539.

[213] L. Buşoniu, T. de Bruin, D. Tolić, J. Kober, and I. Palunko, "Reinforcement learning for control: Performance, stability, and deep approximators," *Annual Reviews in Control*, vol. 46, pp. 8–28, 2018, https://doi.org/10.1016/j.arcontrol.2018.09.005.

[214] J. Zhou, Y. Xue, D. Xu, C. Li, and W. Zhao, "Self-learning energy management strategy for hybrid electric vehicle via curiosity-inspired asynchronous deep reinforcement learning," *Energy*, vol. 242, p. 122548, 2022, https://doi.org/10.1016/j.energy.2021.122548.

[215] C. Qi, Y. Zhu, C. Song, G. Yan, F. Xiao, Da wang, X. Zhang, J. Cao, and S. Song, "Hierarchical reinforcement learning based energy management strategy for hybrid electric vehicle," *Energy*, vol. 238, p. 121703, 2022, https://doi.org/10.1016/j.energy.2021.121703.

[216] I. Grondman, L. Busoniu, G. A. D. Lopes, and R. Babuska, "A Survey of Actor-Critic Reinforcement Learning: Standard and Natural Policy Gradients," *IEEE Transactions on Systems, Man, and Cybernetics, Part C (Applications and Reviews)*, vol. 42, no. 6, pp. 1291–1307, 2012, https://doi.org/10.1109/TSMCC.2012.2218595.

[217] F. A. Galatolo, M. G. Cimino, and G. Vaglini, "Solving the scalarization issues of Advantage-based Reinforcement Learning algorithms," *Computers & Electrical Engineering*, vol. 92, p. 107117, 2021, https://doi.org/10.1016/j.compeleceng.2021.107117.

[218] V. Mnih, A. P. Badia, M. Mirza, A. Graves, T. Lillicrap, T. Harley, D. Silver, and K. Kavukcuoglu, "Asynchronous Methods for Deep Reinforcement Learning," in *Proceedings of The 33rd International Conference on Machine Learning*, ser. Proceedings of Machine Learning Research, vol. 48. New York, New York, USA: PMLR, Jun. 2016, pp. 1928–1937. [Online]. Available: https://proceedings.mlr.press/v48/mniha16.html